Journal of Human Evolution 180 (2023) 103387

Contents lists available at ScienceDirect

Journal of Human Evolution

journal homepage: www.elsevier.com/locate/jhevol

Dental topography of the Oligocene anthropoids *Aegyptopithecus zeuxis* and *Apidium phiomense*: Paleodietary insights from analysis of wear series

Paul E. Morse [a, b, *], James D. Pampush [c, d], Richard F. Kay [e, f]

[a] Department of Cell and Developmental Biology, University of Colorado School of Medicine, Aurora, CO 80045, USA
[b] Florida Museum of Natural History, University of Florida, Gainesville, FL 32611, USA
[c] Department of Exercise Science, High Point University, High Point, NC 27260, USA
[d] Department of Physician Assistant Studies, High Point University, High Point, NC 27260, USA
[e] Department of Evolutionary Anthropology, Duke University, Durham, NC 27708, USA
[f] Division of Earth and Climate Sciences, Nicholas School, Duke University, Durham, NC 27708, USA

ARTICLE INFO

Article history:
Received 18 September 2022
Accepted 21 April 2023
Available online xxx

Keywords:
Diet
Tooth wear
Dental topography
DNE
Convex DNE
Enamel thickness

ABSTRACT

Fossil primate dietary inference is enhanced when ascertained through multiple, distinct proxies. Dental topography can be used to assess changes in occlusal morphology with macrowear, providing insight on tooth use and function across the lifespans of individuals. We measured convex Dirichlet normal energy—a dental topography metric reflecting occlusal sharpness of features such as cusps and crests—in macrowear series of the second mandibular molars of two African anthropoid taxa from ~30 Ma (*Aegyptopithecus zeuxis* and *Apidium phiomense*). Wear was quantified via three proxies: occlusal dentine exposure, inverse relief index, and inverse occlusal relief. The same measurements were calculated on macrowear series of four extant platyrrhine taxa (*Alouatta*, *Ateles*, *Plecturocebus*, and *Sapajus apella*) to provide an analogical framework for dietary inference in the fossil taxa. We predicted that *Ae. zeuxis* and *Ap. phiomense* would show similar patterns in topographic change with wear to one another and to extant platyrrhine frugivores like *Ateles* and *Plecturocebus*. The fossil taxa have similar distributions of convex Dirichlet normal energy to one another, and high amounts of concave Dirichlet normal energy 'noise' in unworn molars—a pattern shared with extant hominids that may distort dietary interpretations. Inverse relief index was the most useful wear proxy for comparison among the taxa in this study which possess disparate enamel thicknesses. Contrary to expectations, *Ae. zeuxis* and *Ap. phiomense* both resemble *S. apella* in exhibiting an initial decline in convex Dirichlet normal energy followed by an increase at the latest stages of wear as measured by inverse relief index, lending support to previous suggestions that hard-object feeding played a role in their dietary ecology. Based on these results and previous analyses of molar shearing quotients, microwear, and enamel microstructure, we suggest that *Ae. zeuxis* had a pitheciine-like strategy of seed predation, whereas *Ap. phiomense* potentially consumed berry-like compound fruits with hard seeds.

1. Introduction

Northern Africa remains the primary source of fossils documenting the early evolution of crown Anthropoidea (Simons, 1965; Kay et al., 1981; Seiffert et al., 2005; Seiffert, 2007; Jaeger et al., 2010). Specimens recovered from the late Eocene and early Oligocene of the Fayum Depression of northern Egypt have played outsized roles in shaping many of the hypotheses regarding early anthropoids, including their phylogeny and biogeography (Kay et al., 1981; Seiffert and Simons, 2001; Miller et al., 2005; Seiffert, 2012; Seiffert et al., 2020), brain and special sense evolution (Rasmussen and Simons, 1992; Simons, 1995, 2001; Kay and Kirk, 2000; Bush et al., 2004; Kirk and Kay, 2004), ontogeny (Kay and Simons, 1983; Miller et al., 2018), and dietary ecology (Kay and Simons, 1980a, 1980b; Teaford et al., 1996; Miller and Simons, 1997; Kirk and Simons, 2001). This lattermost topic remains of

* Corresponding author.
E-mail address: paul.morse@cuanschutz.edu (P.E. Morse).

https://doi.org/10.1016/j.jhevol.2023.103387
0047-2484/

particular interest to paleoanthropologists, as diet likely played a significant role in the origins and diversification of anthropoids—especially with regard to the specialized, 'bilophodont' molars of the Cercopithecoidea (Napier and Napier, 1970; Kay, 1977; Andrews, 1981; Temerin and Cant, 1983; Andrews and Aiello, 1984; Rasmussen and Simons, 1992). The early anthropoids of the Fayum predate the oldest known occurrence of species with bilophodonty by up to 5 Ma (Stevens et al., 2013); thus, reconstructing their diets would provide essential ecological and morphological context for understanding the origins of this key anthropoid dental innovation. A greater understanding of the diets of the Fayum anthropoids can offer insight into their ecology and life history (Godfrey et al., 2001; Borries et al., 2011) during this important interval of anthropoid diversification that took place in a tropical deltaic coastal plain (Bown et al., 1982) under a climatic regime quite distinct from modern day (Zachos et al., 2001; Seiffert, 2007).

In reconstructing a behavior as multifaceted as diet, many have advocated a multimodal approach wherein different techniques can provide independent, complementary lines of evidence (e.g., Ungar and Sponheimer, 2011; Ungar, 2015; Davis and Pineda-Munoz, 2016). To date, researchers have advanced dietary interpretations for two of the most well-represented Fayum anthropoids—*Aegyptopithecus zeuxis* Simons (1965) and *Apidium phiomense* Osborn (1908)—from description of their unworn molar morphology, shearing quotients, microwear, and enamel microstructure. Based on shearing quotients and enamel thickness, Kay and Simons (1980b) and Fleagle and Kay (1985) concluded that both species were frugivorous, but based on its thick molar enamel they further concluded that *Ap. phiomense* may have concentrated on feeding on very hard foods. Based on their analysis of microwear and enamel microstructure, Teaford et al. (1996) agree that the primary dietary items in these two species were fruit, but suggested that hard-object feeding was less likely in *Ap. phiomense*. Here we offer an additional approach for inferring the diet of these taxa by analyzing changes in the apparent functional properties of their molars as these teeth wear.

1.1. Prior assessments of Fayum anthropoid diet

The prevailing view is that most Fayum anthropoids of the families Parapithecidae and Propliopithecidae were frugivores—a conclusion derived from a variety of quantitative and qualitative assessments of the low-crowned cheek teeth with blunt cusps exhibited by many of these taxa (Kay and Simons, 1980a, 1980b; Simons, 1987; Rasmussen and Simons, 1992; Teaford et al., 1996; Kirk and Simons, 2001). Kay and Simons (1980a, 1980b) found the relative lengths of second mandibular molar (M_2) shearing crests (adjusted for tooth size and referred to as the shearing quotient, or SQ) of all Fayum anthropoids to be comparable to those of the extant frugivorous hominoids *Hylobates*, *Pongo*, and *Pan*, and the platyrrhine *Cebus*. Kay and Simons (1980a, 1980b) did not single out hard-object feeding as a dietary strategy of any Fayum primate, but Fleagle and Kay (1985) suggested that the particularly thick enamel of *Apidium* would have enabled it to feed on hard objects. Among the fossil taxa measured by Kay and Simons (1980a, 1980b), only *Parapithecus grangeri* Simons (1974) (hereafter referred to as *Simonsius grangeri* Gingerich 1978) possessed more developed shearing crests and taller molar crowns, which the authors suggested might indicate greater leaf consumption and/or more habitual terrestriality relative to other Fayum anthropoids. Still, the SQ of *S. grangeri* did not approach that of the more folivorous extant taxa in their sample (gorillas, siamangs, and the platyrrhine *Alouatta*). Kirk and Simons (2001) extended this work to additional Fayum taxa using a refined categorization of primate dietary strategies, parsing out gums and seeds as primary dietary items. These authors found evidence of broader dietary diversity within a more extensive Fayum primate sample that included strepsirrhines (Seiffert et al., 2010) and the stem anthropoid *Afrotarsius chatrathi* (Simons and Bown, 1985; Kay et al., 2004), with the strepsirrhines being more folivorous and *Afrotarsius* more insectivorous. Other Fayum anthropoids appeared to exhibit shearing crest lengths largely consistent with frugivory (with the only noted exceptions being *Oligopithecus savagei* Simons (1962) and *Qatrania wingi* Simons and Kay (1983), which displayed SQ values low enough to potentially indicate seed predation or gummivory, though these results were interpreted with caution). Notably, the taxa examined by Kirk and Simons (2001) span a longer temporal interval encompassing climatic and biotic shifts from the late Eocene to early Oligocene (Seiffert, 2006, 2007), and thus do not represent a single primate community.

In an alternative approach, Teaford et al. (1996) assessed trace evidence of tooth use through measurement of dental microwear and combined this with the histological examination of enamel microstructure of the common Fayum anthropoid taxa *Ae. zeuxis*, *Ap. phiomense*, and *S. grangeri* of the upper levels of the Jebel Qatrani Formation (Fm.). Microwear analysis as implemented at that time involved categorizing, counting, and measuring the microscopic scratches and pits on enamel wear facets, which are presumably generated during mastication (Teaford, 1994; Ungar, 1995; Grine et al., 2002). Shapes and proportions of these pits and scratches are thought to reflect the material properties of recently consumed foods, since such features have been observed to turnover during in vivo feeding experiments (Teaford and Oyen, 1989a; Teaford et al., 2020). Teaford et al. (1996) reported similar proportions of pits to scratches on *Ae. zeuxis* and *Ap. phiomense* molar facets, broadly overlapping the distribution of frugivores and hard-object feeders in their reference sample of extant anthropoids. Concerning *Ap. phiomense*, these authors further noted that while it exhibited similar percentages of microscopic enamel pits to extant anthropoid mixed- and hard-object feeders, these pits tended to be small, regular indentations unlike the larger, more stochastically-shaped pits that are supposed to reflect hard-object feeding (e.g., Teaford, 1985; Scott et al., 2006; Scott et al., 2012; Ungar, 2015; Teaford et al., 2020; Teaford et al., 2021). The pitting dimensions and incidence in *Simonsius grangeri* more closely resembled modern frugivores.

Teaford et al. (1996) further reported significant distinctions in enamel thickness and microstructure among these Fayum anthropoids. The molar enamel of *Ap. phiomense*, in addition to being relatively thicker than that of any other Fayum taxon, is characterized by non-decussating, radial enamel prisms. The interprismatic enamel crystallites at the cusp tips are parallel with the radial prisms, aligned to the occlusal surface in approximately the same direction as that expected by masticatory forces during puncture-crushing (Teaford et al., 1996). This finding is at odds with apical interprismatic crystallite orientation reported for *Ae. zeuxis* or *S. grangeri*—as well as for a variety of modern primates, in which these structures are typically oriented orthogonal to the expected force (i.e., parallel to the occlusal surface) in a functional arrangement that seems well suited for resisting compressive loads during puncture-crushing, but is less resistant to shearing abrasion (Maas, 1993; Maas and Dumont, 1999). Lacking this arrangement, in concert with radial, non-decussating prisms, makes enamel more prone to radial crack propagation originating at the enamel-dentine junction (EDJ), increasing the likelihood of catastrophic enamel failure (Maas and Dumont, 1999; Rensberger, 2000). Finding this enamel arrangement in *Ap. phiomense* led Teaford et al. (1996) to argue that this taxon was poorly adapted to the high occlusal forces encountered during hard-object feeding. In light of the apparently discrepant signals conveyed by the surface anatomy

(as measured by SQ), microwear (pits and scratches), enamel thickness, and microstructural pattern of enamel crystallites, additional indicators of diet should be investigated. Change in occlusal form with macroscopic tooth wear is one such signal.

1.2. Dental topography and the analysis of worn primate teeth

Functional dental morphology as assessed with metrics like SQ provides a useful perspective on adaptive dental form and therefore the evolutionary history of a species and insight into its masticatory capabilities (Kay, 1975). An approach that considers how teeth are altered during the lifespan of an organism, on the other hand, supplies evidence of the ways in which teeth have actually been used in life, potentially offering a more direct link with the physical properties of consumed foods (Ungar, 2015). Microwear, with its rapid surface-feature turnover produced through contacts that occur during chewing, reflects oral processing shortly before time of death, with the rate of formation of these features influenced by the material properties of the chewed items (Teaford and Oyen, 1989a, 1989b; Scott et al., 2012; Teaford et al., 2017, 2021). This record of recent interactions between enamel and food may produce a signal that differs from dietary interpretations inferred from (presumed adaptive) dental morphology. Confounding signals may indicate a morphological-ecological mismatch as is often observed between animal teeth and diet (Robinson and Wilson, 1998; Grine and Daegling, 2017), and elevate the value of dietary insights derived through documentation of the direct use of teeth, rather than relying on adaptive inference (Hespenheide, 1973). Macrowear—the summed total of dental tissue loss due to attrition and abrasion (Galbany et al., 2020)—offers an intermediate scale for dietary investigation (Harty et al., 2022) between that of evolutionary adaptation and that of tooth use near the end of life. Macrowear patterns reflect the interaction between the unworn dental morphology produced through evolutionary processes, and the oral behaviors and environment a tooth was subjected to over its lifespan. These produce a window into the dietary behavior of an individual over the lifetime of a tooth, thereby straddling the temporal and processual scales of dental functional morphology and microwear (Davis and Pineda-Munoz, 2016). While differentially worn primate teeth have been linked to diet by many authors (Teaford, 1982; Janis, 1984; Dennis et al., 2004; Elgart, 2010; Galbany et al., 2011; Morse et al., 2013; Glowacka et al., 2016), efforts to document and compare these wear-induced changes have been impeded by the lack of homologously comparable structures throughout wear series, since macrowear obliterates and/or transforms dental features. Quantitatively assessing differences among teeth at various stages of wear has required the development of new techniques that measure dental morphology as a continuous, landmark-free surface (Zuccotti et al., 1998; Jernvall and Selänne, 1999; Ungar and Williamson, 2000)—a set of methods now united under the field of dental topography.

Tooth enamel is remarkable for being the hardest tissue in the body and being incapable of remodeling, which preserves both a record of how the tissue develops in its microstructure (Maas and Dumont, 1999; Macho, 2001; Polly and Mock, 2018), and—importantly—how its surface modifies with use. While researchers have long recognized this as a potential signal conveying information about mammalian diet or ecology (among both extant and extinct groups; Janis, 1984; Fortelius, 1985; Janis and Fortelius, 1988), the fact that tooth wear may remove recognizable occlusal features meant that quantitative approaches to comparing among individuals or taxa were elusive until relatively recently (Fortelius and Solounias, 2000; Ungar and Williamson, 2000).

The construction of digital models of dental surfaces (Jernvall and Selänne, 1999) and the application of methods to evaluate those surfaces using the tools of geographic information systems (Zuccotti et al., 1998; Ungar and Williamson, 2000) permits the measurement of continuous occlusal topography without the need for homologous landmarks (such as cusp tips). These dental topographic (DT) metrics have since shown promise in multiple ways. For instance, several methods, when applied to unworn molars, have shown favorable correspondence with earlier linear measurements like SQ and shearing ratio that align with broad heuristic diet categories such as 'insectivory,' 'frugivory,' and 'folivory,' among primates (Boyer, 2008; Bunn and Ungar, 2009; Bunn et al., 2011; Godfrey et al., 2012; Winchester et al., 2014; Pampush et al., 2022), which supports their utility for making dietary inferences about extinct primate species. In addition, the omission of homologous occlusal features in deriving the measurement permits broader comparisons of taxa with widely disparate morphologies wherein determination of homology could prove challenging—or even impossible as in the case with some highly-derived rodents and extinct clades (Evans et al., 2007; Wilson et al., 2012; Prufrock et al., 2016a; Selig et al., 2021). This latter quality additionally enables comparison between specimens with differential wear, granting information about how the tooth crown is modified with use over the lifespan (M'Kirera and Ungar, 2003; Ungar and M'Kirera, 2003; Ungar, 2004; Pampush et al., 2016a, 2018; Li et al., 2020).

Many DT metrics have been proposed. Among the earliest created and most frequently used are slope (average surface inclination; M'Kirera and Ungar, 2003), angularity (average change in slope across the surface; Ungar and M'Kirera, 2003), and occlusal relief. This latter method was originally defined as the ratio of 3D surface area to 2D planometric area above the lowest point on the occlusal surface, and primarily applied to studies of hominids (Zuccotti et al., 1998; Ungar and M'Kirera, 2003; Ungar, 2004; Glowacka et al., 2016). When expanding the measurement of relief to a broader sample of euarchontan teeth with differential sidewall crown heights, Boyer (2008) moved the location of surface cropping to the enamel cervix and altered the calculation of the 3D area:2D area ratio. Boyer's (2008) adjusted approach is referred to as relief index (RFI) in most studies of euarchontan DT (e.g., Boyer, 2008; Winchester et al., 2014; Pampush et al., 2016b, 2018; Selig et al., 2021), with the simple 3D area:2D area ratio above the lowest point of the occlusal basin described by Ungar and colleagues retaining the term 'occlusal relief' (OR; Allen et al., 2015; Pampush et al., 2018), though other naming conventions have been proposed (Thiery et al., 2019).

Orientation patch count (OPC; Evans et al., 2007) is a DT metric in which the directionality of each component of a digitized tooth/tooth row surface is calculated (analogous to aspect in geographic information systems) and assigned to a particular bin according to its cardinal directionality, with 8 bins in total. Contiguous surface components in the same directional bin are grouped into a 'patch,' and the number of patches is summed to provide the OPC value of the surface. This value has been argued to represent a measurement of surficial complexity or the total number of food breakage 'tools' on a given specimen (Evans et al., 2007; Evans and Janis, 2014). While earlier implementations of OPC utilized rasterized representations of surface height to calculate aspect (Evans et al., 2007; Wilson et al., 2012; Evans and Janis, 2014; Winchester et al., 2014), more recent studies have calculated the metric using fully 3D surfaces that more accurately reflect dental morphology (Winchester, 2016; Pampush et al., 2016b, 2019; Melstrom and Wistort, 2021; Selig et al., 2021). However, application of OPC to primate teeth has so far yielded little insight into diet or occlusal function. Linear discriminant analyses that attempt to classify teeth of primate species with known diets based on their DT routinely result in OPC being the worst performing among the employed DT metrics

(Winchester et al., 2014; Berthaume et al., 2019), and patterns of how OPC relates to diet are inconsistent across primate clades (Winchester et al., 2014). Given these findings, it seems that OPC is not well-suited to evaluate the generally conservative, bunodont molars of primates and is better applied to clades that exhibit a broader range of occlusal morphologies (e.g., from sectorial to lophodont) or among herbivores wherein crest development and complexity is more reliably related to the number of 'breakage-sites' on a dental surface (Evans and Janis, 2014; Pineda-Munoz et al., 2017).

Another DT metric gaining widespread use is Dirichlet normal energy (DNE; Bunn et al., 2011). Dirichlet normal energy is a measure of surface sharpness that effectively represents a surface-wide application of the radius of curvature measurement previously used to quantify the sharpness of dental cusps and crests (Popowics and Fortelius, 1997; Evans and Sanson, 1998; Evans et al., 2005; Berthaume, 2014). It has proven to be generally effective at sorting euarchontan molars into heuristic categories of known diet (Bunn et al., 2011; Winchester et al., 2014; Pampush et al., 2018; Selig et al., 2019). This success is likely because it quantifies occlusal curvature in such a way that places greatest emphasis on the sharpest features (Bunn et al., 2011; Pampush et al., 2016a; Berthaume et al., 2020), and sharpness is a property considered to be relevant to how teeth interact with food materials (Bunn et al., 2011; Pampush et al., 2022).

The closeness of the relationship between DT metrics and dental performance has not yet been experimentally tested—indeed, this persists as a challenging yet important step in fully validating the use and interpretation of these measures, especially when deployed in studies of functional morphology. Rather, headway in this area has relied primarily on comparative approaches whereby a metric is evaluated in terms of its success at classifying molar surfaces into broad dietary categories (e.g., Evans et al., 2007; Winchester et al., 2014). High DNE values on primate molars have been associated with diets comprised of tough materials that require shearing for comminution, such as those of folivores and insectivores (Bunn et al., 2011; Winchester et al., 2014; Pampush et al., 2018). When most DT investigators measure a high DNE value on a molar, the typical functional inference is an adaptive morphology for shearing of tough materials, even if the molar morphology appears blunt and would lead other researchers to intuit a different dental function. For instance, Berthaume et al. (2018, 23) noted, "The relatively higher DNE values in *H. naledi*, *A. africanus*, and *P. robustus* imply their diets required higher shear forces, for eating substances such as plant fiber and/or muscle fiber…"

While all DT metrics represent abstractions of dental morphology, one of the core benefits of DNE is that beyond having shown success at classifying dental surfaces into dietary categories, the foundation of the measurement (squared radii of osculating circles) has been correlated with a performance measurement—the penetrating ability of knives (Hainsworth et al., 2008)—and the regions of highest DNE usually (see below) correspond to the regions of the tooth surface making a penetrating or shearing contact with food or other teeth during occlusion (Pampush et al., 2022).[1]

Within this context, a potential drawback of the way DNE was originally designed and implemented was that it treated occlusal sharpness contributed by cusps and crests equally to that contributed by furrows and grooves. Without orientational sorting, this metric may score sharpness identically from regions of the tooth crown that must function quite differently during mastication (e.g., cusp apices vs. sulcal nadirs). Comingling these sources of sharpness invites functional misinterpretation. During intraspecific comparisons, similarities in occlusal anatomies will likely prevent meaningful variation in concave- vs. convex-sourced DNE, meaning that researchers will be making like-for-like comparisons of DNE values between individuals. However, orientation blindness creates a particularly acute interpretive challenge when teeth from two or more taxa have similar DNE values yet present distinctively different molar anatomies with variable ratios of concave- to convex-sourced DNE (Fig. 1). For instance, the M_2 of the small insectivorous Calabar angwantibo *Arctocebus calabarensis* possesses an occlusal surface with tall, sharp crests interposed with broad, gently sloping basins and has a high DNE value that is largely derived from these sharp convex features. The M_2 of *Gorilla gorilla*, in contrast, has an occlusal surface with broad, gently sloping cusps between which are interposed deep, sharp sulci and a DNE that is

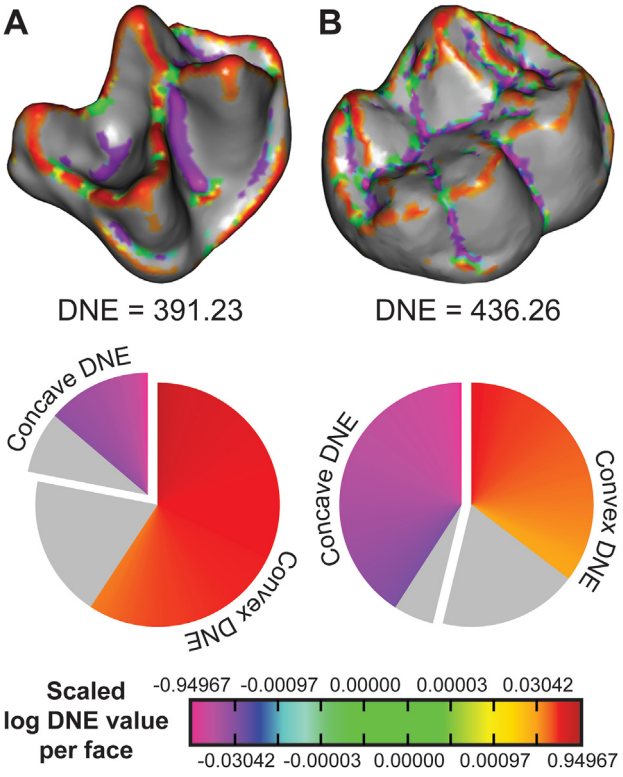

Figure 1. Distribution of the top quartile of Dirichlet normal energy (DNE) values across two primate molar surfaces with contrasting morphologies. Note that due to the exponential nature of the underlying DNE calculation (Bunn et al., 2011; Pampush et al., 2016a), the top quartile of values typically contributes a majority of the total surface DNE. Top row: three-dimensional digital surface models of lightly-worn second mandibular molars (not to scale), with only the top quartile colored, of A) right M_2 of AMNH 207949, *Arctocebus calabarensis* (an insectivore), and B) left M_2 (reflected) of ZMB 31435, *Gorilla gorilla* (a frugivore). Bottom row: Pie charts distinguishing convex and concave contributions to total surface DNE, with contribution from the top quartile of DNE values colored (contribution from the bottom three quartiles in gray). Color scale differentiates sharp convex features (in red) from sharp concave features (in magenta). Note that the top quartile of DNE in (A) is mostly convex (as is the majority of the total surface DNE), with the concentration of red and orange values on crests and cusp tips making a large contribution to the total DNE. In contrast, the surface in (B) has a higher DNE (and is thus a 'sharper' tooth), but much of the top quartile of values are concentrated in occlusal furrows, with cusp tips and crests generally blunter compared to (A). Coloration is scaled consistently across both surfaces and natural log-transformed to improve visualization. Models obtained from Pampush et al. (2022, supplementary file 4). AMNH = American Museum of Natural History, New York, NY, USA; ZMB = Museum für Naturkunde, Berlin, Germany. (For interpretation of the references to color in this figure legend, the reader is referred to the Web version of this article).

[1] See Pampush et al. (2022) for a detailed background on the strengths of DNE as a DT metric that is likely to convey functional meaning.

largely derived from these sharp concave features (Fig. 1). Surprisingly, the DNE values of the surfaces illustrated in Figure 1 indicates that the gorilla tooth is sharper than that of the angwantibo, though the majority of this sharpness is derived from narrow fissures between the cusps. In the context of assessing dental sharpness as it relates to shearing ability during mastication—which DNE has been traditionally interpreted to reflect—this concave sharpness obscures the intended functional estimate of DNE, and has thus been suggested to constitute measurement 'noise' that should be eliminated (Pampush et al., 2022).

Occlusal sulci might play a role as architectural 'sinks' for compressive stresses experienced by enamel (Benazzi et al., 2013), or in generating enamel crenulations that possibly increase food contact during hard-object crushing (Kinzey, 1992; Vogel et al., 2008) or stabilize slippery foods (Lucas and Teaford, 1994). These functions—while potentially of importance during mastication—are clearly distinct from shearing and are likely not best evaluated using DNE. In the first case, a parabolic shape optimally resists high compressive loads, while such morphologies generate low DNE values. Dirichlet normal energy might be effective at measuring the likelihood a fissure will experience an enamel cap fracture during high load, since sharp occlusal fissures concentrate tensile stresses (Zelentsov et al., 2023) that can induce enamel spread—driving a crown-to-dentine crack into the tooth. In the second case, researchers should carefully construct their functional scenarios prior to applying DNE to crenulation curvature. Berthaume et al. (2020) speculated that crenulated enamel in primates could represent an adaptation for cutting fiber (distinct from the above proposed functions) since it is associated with higher DNE. However, the benefit of surface crenulations has yet to be incorporated into, or meaningfully tested, in models of dental shearing function and Berthaume et al.'s (2020) conjecture fails to consider whether the greater contribution to increased sharpness is realized by the convex crenulations themselves or the concave fissures that separate them.

Pampush et al. (2022) introduced a useful modification of the DNE calculation to bring it into better alignment with the functional expectations of the measurement, by separating the total DNE of a tooth into the signal contributions made by the convex portions of the surface (cusps and crests) from those made by the concave portions (sulci). Given that the convex portions of the tooth are expected to contact and aid in the breakdown of food materials, the sharpness of these components is functionally relevant for considering how DNE reflects the ability of an occlusal surface to tear apart tough, crack-arresting materials (Pampush et al., 2022). For instance, the total, surface-wide molar DNE of the extant hominids *Pan* and *Pongo* is much higher than would be expected (Berthaume and Schroer, 2017) given how rarely these taxa ingest tough items like leaves. Rather, each of these taxa exhibits a preference for ripe fruit over other foods in the wild (Wrangham et al., 1991; Vogel et al., 2008, 2014; Watts et al., 2012), with the fruit parts consumed by *Pongo* being more resistant to deformation and fracture than those eaten by *Pan* (Vogel et al., 2008). In contrast, when DNE is limited to only their convex dental features such as cusps and crests (vexDNE), these taxa exhibit values similar to those of other primate frugivores and omnivores (Pampush et al., 2022). Thus, vexDNE as an approach for assessing dental sharpness in a dietary context (for breakdown of tough food items) aligns better with observational data of extant primate dietary habits than does the original DNE measurement, at least for some taxa. Additionally, vexDNE has been shown to be influenced very little by differences in scanning resolution as long as consistent protocols for producing surfaces for analysis are followed, since scanning- and processing-related surface artifacts tend to be concentrated in the concave crevices of digitized dental surfaces (Pampush et al., 2022, their supplementary file 5).

Application of DT metrics to primate molar wear series offers an opportunity to infer how occlusal functional properties change with—or are maintained despite—wear (Ungar and Williamson, 2000; Ungar and M'Kirera, 2003). Many early studies focused primarily on hominids and measured variables such as OR, slope, and angularity (Zuccotti et al., 1998; Ungar and Williamson, 2000; M'Kirera and Ungar, 2003; Ungar and M'Kirera, 2003; Ungar, 2004). These studies document that hominid OR and slope typically decline with wear, whereas angularity remains stable until the most extreme wear stages (cf. Klukkert et al., 2012; Glowacka et al., 2016). Similar findings are reported in ring-tailed lemurs (Cuozzo et al., 2014), platyrrhines (Dennis et al., 2004), and cercopithecoids (Bunn and Ungar, 2009; Galbany et al., 2011), with the totality of this evidence leading Ungar (2015) to put forward that primates with more folivorous diets adaptively maintain their occlusal shearing (as expressed by angularity). Ungar (2015) referred to this proposed phenomenon as 'enamel sculpting,' a concept that has since been re-termed 'dental sculpting' by Pampush and colleagues (2016a, 2018). Although angularity has been purported to measure occlusal cutting ability (Ungar and M'Kirera, 2003), it does not correlate with DNE among a wide sample of platyrrhine primates (Pampush et al., 2019), despite DNE being a more direct measurement of surface sharpness (Pampush et al., 2022). The root of this difference lies in the distinct ways in which their values express occlusal shape: Surface DNE is a summative value of surface curvature in which sharper regions make exponentially greater contributions and thus have the greatest impact on determining the overall surface DNE value. In contrast, angularity is an average value of change in slope across the entire surface, which may result in a signal dampened by the proportion of the occlusal surface with very low angularity.

Data on how DNE changes with wear remains scant. Distinct from prior results on angularity, Pampush et al. (2016a) found that DNE increases in thinly enameled, folivorous mantled howling monkeys (*Alouatta palliata*). *Alouatta* was found to conform to the basic expectations of dental sculpting (i.e., maintenance of dental function despite wear), and is an example of a primate that exhibits what Fortelius (1985) has described as 'secondary morphology,' in which tooth wear results in an apparent improvement in some measure of dental function (in this case, shearing). A follow-up study by Pampush et al. (2018) found that for the closely-related, frugivorous, and relatively more thickly enameled spider monkey *Ateles* spp., DNE is maintained but does not increase with wear. These authors took these findings to mean that dental sculpting is at work in *Alouatta* and could result from selection caused by the more folivorous diet of *Alouatta* compared to *Ateles*, potentially achieved through a relatively thinner enamel cap (Olejniczak et al., 2008). Additional work by Li et al. (2020) measured DNE across a wear series in the omnivorous platyrrhine titi monkey *Callicebus* (*Plecturocebus*) spp., and produced similar results to those found for *Ateles*.

In summary, while few extant taxa have been assessed as yet for changes in DNE with wear, the current evidence suggests that there are taxon-specific wear modalities that may be associated with distinct dietary strategies, dental construction (e.g., enamel thickness and distribution), or a combination of the two (Pampush et al., 2018). This approach thus represents an opportunity to assess how properties such as vexDNE (Pampush et al., 2022) that are thought to reflect dental function are altered by actual tooth use (Ungar, 2015), adding a source of dietary insight that is ripe for application to the primate fossil record (Ungar, 2004; Li et al., 2020).

1.3. An analogical framework for Fayum anthropoid dental topography

In this study we investigate changes in vexDNE with wear within and between *Ae. zeuxis* and *Ap. phiomense*. These taxa are of interest in part because complementary methods have already been applied to their paleodietary reconstruction. Moreover, they are represented by sufficiently large numbers of dental specimens to document teeth worn to various stages that are free of post-mortem damage. Both taxa are common at penecontemporaneous Egyptian Fayum Quarries I and M, dated to the early Oligocene at 30.2–29.5 Ma (Seiffert, 2006, 2007). Phylogenetic hypotheses regularly support *Ae. zeuxis* (a propliopithecid) as a stem catarrhine (Kay et al., 1981; Seiffert et al., 2005, 2010), and *Ap. phiomense* (a parapithecid) as a stem anthropoid (Fleagle and Kay, 1987; Seiffert et al., 2005, 2010, 2020). The estimated body mass for *Ae. zeuxis* ranges from ~5 to 8 kg based on dental, cranial, and postcranial elements, with differences among contemporaneous specimens suggesting it was highly sexually dimorphic (Fleagle et al., 1980; Kay and Simons, 1980b; Conroy, 1987; Simons et al., 2007; Perry et al., 2018). *Apidium phiomense* is considerably smaller, with dental and postcranial estimates suggesting a body mass between ~1 and 1.5 kg (Conroy, 1987; Perry et al., 2018). The two taxa have been inferred to have largely overlapping frugivorous diets and to have both been arboreal (Kay and Simons, 1980b). *Aegyptopithecus* has been reconstructed as a slow-moving, above-branch arboreal quadruped moving on flexed limbs, with multiple studies suggesting *Alouatta* as an extant analog for its locomotor behavior (e.g., Fleagle et al., 1975; Fleagle and Simons, 1982; Almécija et al., 2019). *Apidium* is inferred to have been an arboreal quadruped well adapted to leaping, expressing limb morphology like that of a small platyrrhine such as the squirrel monkey *Saimiri* (Fleagle and Simons, 1995).

Determining an appropriate modern analog for primates that have been extinct for many millions of years is challenging, but those extant platyrrhine taxa that have already been analyzed for changes in DNE with wear (*Alouatta*, *Ateles*, and *Plecturocebus*) make for appropriate models: The atelids *Alouatta* and *Ateles* have body masses that approximately encompass the range estimated for *Ae. zeuxis* (Smith and Jungers, 1997) and encompass a broad dietary range from more folivorous (*Alouatta*) to feeding primarily on fleshy fruits (*Ateles*: Anapol and Lee, 1994; González-Zamora et al., 2009). These taxa can thus be argued to provide insight into *Ae. zeuxis* ecology. The titi monkey *Plecturocebus* (for taxonomic review, see Byrne et al., 2016) occasionally consumes seeds, but has a broader diet that primarily emphasizes other fruit parts, leaves, and arthropods (Kinzey, 1992), as well as a body size like that estimated for *Ap. phiomense*. Seed ingestion in *Plecturocebus* appears to most commonly occur without mastication, when the seeds are small and embedded in fleshy pulp (DeLuycker, 2021). While these modern platyrrhines are phylogenetically remote from the fossil taxa under investigation (Kay et al., 2004; Seiffert et al., 2010, 2020), the form-function relationship between their teeth and diets of varying material properties provides a useful analogical framework for applying to interpretation of diet in *Ae. zeuxis* and *Ap. phiomense*, as has been done in past studies (e.g., Kay and Simons, 1980a, 1980b; Teaford et al., 1996; Kirk and Simons, 2001).

The molars of *Ap. phiomense* are unusual for exhibiting very thick enamel (Kay and Simons, 1983; Teaford et al., 1996), indicating that inclusion of an additional comparative modern taxon is warranted. The tufted capuchin, *Sapajus apella*, is a small-bodied platyrrhine (although not as small as *Ap. phiomense*). It primarily consumes fruits, but is a seed predator sensu Janzen (1970) that chews up fruits and their contained hard seeds (Fragaszy et al., 2004) rather than passing them whole through the digestive tract as do *Ateles* and *Plecturocebus*. Seed predation is more pronounced in *S. apella* individuals occupying dry environments or during the dry season (Peres, 1991; Galetti and Pedroni, 1994). *Sapajus apella* also exhibits very thick enamel and a robust mandibular corpus relative to frugivorous atelids as well as other capuchins (Daegling, 1992; Wright, 2005), traits that presumably represent adaptations for seed predation (Kay et al., 2013). Thick enamel is a hallmark of durophagous adaptation (Kay, 1981), and it has been suggested that *Ap. phiomense*'s thick enamel played an analogous role to that in *S. apella* (Fleagle and Kay, 1985). Thus, in the present analysis we also include a wear series of *S. apella* as representative of an extant, thick-enameled, small-bodied hard object feeder.

1.4. Choice of wear variable

Occlusal wear is the gradual loss of dental tissue, which may result from tooth–tooth contact (i.e., attrition), tooth contact with foreign material (dietary or otherwise, i.e., abrasion), or acidic erosion. Cross-sectional studies of wear series that benefit from samples of known age have utilized individual age as an independent variable against which to measure changes in DT metrics (Dennis et al., 2004; King et al., 2005; Cuozzo et al., 2014; Glowacka et al., 2016; Cuesta-Torralvo et al., 2021). This option is unavailable in the study of fossil organisms, in which assumptions must be made that an amassed sample of differentially worn individuals is representative of the pattern of wear exhibited by a particular species, and wear itself forms the independent variable against which to measure changes in topography. The most popular approaches for assessing degree of wear on primate molars have been ordinal scoring methods formulated by Molnar (1971) and Scott (1979), with the latter employed in several studies of DT change with wear (M'Kirera and Ungar, 2003; Ungar and M'Kirera, 2003; Ungar, 2004; Klukkert et al., 2012). These scoring methods visually identify and ordinate degree of enamel loss, particularly through dentine exposure (Scott, 1979). Other DT studies (including all that have measured DNE against wear) have quantified wear as a continuous variable by measuring the areas of exposed dentine against total occlusal area (Pampush et al., 2016a, 2018; Li et al., 2020). Known as the dentine exposure ratio (DER), this method has been applied in many studies of primate teeth to quantify wear, regardless of whether individual chronologic age is known (Kay and Cant, 1988; Elgart, 2010; Morse et al., 2013; Galbany et al., 2014, 2016).

However, methods reliant on dentine exposure for tooth wear quantification may not effectively capture degree of wear in thick-enameled taxa such as *S. apella* (Martin et al., 2003; Wright, 2005) and *Ap. phiomense* (Kay and Simons, 1983; Teaford et al., 1996), whose dental morphology can sustain considerable surface tissue loss without exposing the underlying dentine (Molnar and Gantt, 1977). Some previous studies have normalized DER values within taxa to account for species-level differences in DER distribution, essentially creating comparable wear series in taxa exhibiting differing rates and levels of dental wear (Pampush et al., 2016a, 2018; Li et al., 2020). However, these studies have focused on comparisons between taxa that exhibit generally similar relative enamel thickness. When DER is employed among taxa with highly disparate relative enamel thicknesses, it may mistakenly imply both a reduced sample of 'worn' thickly enameled specimens in comparison with thinner-enameled taxa, as well as calling into question the general comparability of wear series (i.e., a *S. apella* M_2 with considerable wear as indicated by the rounding and lowering of cusps may yet have a DER of 0 because the enamel is not perforated and no dentine is exposed). Therefore, in addition to DER, two other metrics were considered here as potential alternatives to wear quantification.

As described above, both RFI and OR represent ways of quantifying a ratio of the 3D area to 2D planometric area (sometimes called footprint area; Pampush et al., 2016b, 2018) of a digitized dental surface. Given that dental wear results from tissue loss that typically begins at the apex of occlusal features, it is reasonable to predict that wear will result in a reduction in 3D surface area while the 2D footprint area is little effected. Thus, both of these DT metrics should decline with tooth wear. Indeed, they have been shown to decline in nearly all past DT analyses of wear series, where they have been negatively correlated with either ordinal scoring based on Scott's (1979) method or DER (e.g., M'Kirera and Ungar, 2003; Ungar and M'Kirera, 2003; Ungar, 2004; Pampush et al., 2016a, 2018; Li et al., 2020; Cuesta-Torralvo et al., 2021). This indicates that these metrics—which do not rely on dentine exposure—may provide an alternative approach for assessing degree of wear in thick-enameled taxa that can experience wear modification to the occlusal surface prior to dentine exposure. However, it should be noted that these methods cannot be assumed to be consistent, simple reflections of dental wear. Some studies that include OR have found a potential effect of diet, in that more folivorous primate taxa appear to maintain OR despite wear compared to non-folivores (M'Kirera and Ungar, 2003; Ungar, 2015; Ungar et al., 2018). Pampush et al. (2018) made a similar finding in a wear series of *Alouatta* spp. compared to *Ateles* spp. and noted that since 2D planometric footprint of the OR calculation is defined by the lowest point on the occlusal surface, enamel perforation in the talonid basin causes this point (and, therefore, 2D area) to become unfixed. Thus, while RFI and OR make for good potential alternatives to DER in terms of wear proxy, we are wary of the potential confounding effects of diet and/or enamel thickness that may influence how these measurements are altered in a wear series.

Given the current state of knowledge about how DT changes with wear, and previous hypotheses of the diets of *Ae. zeuxis* and *Ap. phiomense*, we predict that these taxa will both resemble the trends exhibited by the modern frugivores *Ateles* and *Plecturocebus* in terms of change in vexDNE with wear. Consistent with past analyses comparing DNE to wear in *Ateles* and *Plecturocebus*, we predict that there will be no change in vexDNE of the lower molars of *Ae. zeuxis* or *Ap. phiomense* as they wear. Implicit in this prediction is the additional prediction that these Oligocene anthropoids will resemble one another in terms of overall dental sharpness and how it relates to wear, despite previous studies indicating differences in their dental traits that may relate to feeding ecology.

2. Materials and methods

2.1. Specimen scanning and segmentation

Scan data of mandibular specimens of *Ae. zeuxis* and *Ap. phiomense* collected and uploaded to MorphoSource.org (Boyer et al., 2016) by the Duke Lemur Center Museum of Natural History were downloaded as TIFF stacks. Each specimen was visualized as a volume rendering using Avizo v. 2021.1 (FEI, Thermo Fisher Scientific, Waltham, MA) to determine suitability of the M_2 for topographic analysis (i.e., that the tooth was free from significant damage). Based on these visualizations, 21 specimens of *Ae. zeuxis* and 32 specimens of *Ap. phiomense* were selected for further analysis. New scan data were acquired from originals of variably worn mandibular specimens of *S. apella* ($n = 22$) at Duke University's Shared Materials Instrumentation Facility on a Nikon XT H 225 ST micro x-ray computed tomography (μCT) scanner. Scans of *S. apella* mandibles were collected using parameters tailored for their geometric size, including 2800 projections with two frames per projection, with energy settings of 175–180 kV and 74–80 μA within a cubic voxel range of 23.3–32.2 μm. The resulting reconstructed volumes were exported as 16-bit TIFF stacks for segmentation in Avizo. For specimens containing both M_2 antimeres, the side with the least amount of visible postmortem damage (i.e., cracks and chips) was selected for further processing and analysis.

Three-dimensional digital models representing the M_2 surfaces of *Ae. zeuxis*, *Ap. phiomense*, and *S. apella* specimens were segmented in Avizo following the protocols of Boyer (2008) and Prufrock et al. (2016b) and exported as PLY files. See Supplementary Online Material (SOM) methods for a detailed description of the procedure used to generate digital surface models. This sample was supplemented with previously published PLY-format files representing primate dental wear series downloaded from MorphoSource.org, including the lower first molars (M_1) of specimens of *Alouatta* spp. ($n = 20$) and *Ateles* spp. ($n = 16$) originally published by Pampush et al. (2018) and those of *Plecturocebus* spp. ($n = 13$) originally published by Li et al. (2020). The decision to use M_1 or M_2 was based on available materials and the similar unworn morphology of these tooth positions in the investigated extant taxa. While cercopithecine M_1s have been suggested to show a different pattern between wear and topography than M_2s (Bunn and Ungar, 2009), there has been no such finding for platyrrhines. To maintain consistent alignment and retriangulation procedures, only those meshes representing the full, non-retriangulated surfaces were used. See SOM Table S1 for a list of all study specimens.

2.2. Mesh preparation, alignment, and retriangulation

Multiple studies have indicated that DT metrics are significantly influenced by mesh alignment and retriangulation (which includes simplification and smoothing) procedures (Boyer et al., 2015; Pampush et al., 2016b; Prufrock et al., 2016b; Spradley et al., 2017; Berthaume et al., 2019). To align the 124 PLY meshes analyzed in this study, we developed a novel approach utilizing custom code written in R v. 4.1.3 (R Core Team, 2022) and MeshLab v. 2020.06 (Cignoni et al., 2008). This method resulted in each surface being aligned with the enamel cervix approximately even with the plane defined by the x- and y-axes, centered at the origin, and with the occlusal surface projecting in the positive z direction (see SOM for a detailed description).

Once aligned, all surfaces were subjected to identical retriangulation steps following the recommended protocol of Spradley et al. (2017). A Tcl script was written for Avizo that would apply the following steps to each surface and save the output as a new PLY: Each surface was 1) simplified to 20,000 faces using the Simplification Editor, 2) remeshed using the 'Remesh Surface' module to 51% original face count (Pampush et al., 2018), 3) simplified to 10,000 faces, and 4) smoothed 20 iterations using the 'Smooth Surface' module with a default lambda value of 0.6. This protocol ensures that specimens are not overly smoothed, which may lead to a poor reflection of the original morphology or introduce errors (Pampush et al., 2016b; Spradley et al., 2017). This approach further agrees with a methodological study indicating that consistent face count among surfaces should be prioritized (Berthaume et al., 2019) and with numerous past studies that have found that the target face count (10,000) is appropriate for capturing functionally relevant morphological details on primate molars (e.g., Bunn et al., 2011; Winchester et al., 2014; Pampush et al., 2016b; Spradley et al., 2017). A preliminary methodological study (Morse et al., 2019) additionally found that a mesh face count of 10,000 produced consistent DNE values in a specimen scanned at multiple different resolutions (voxel sizes). This suggests that this face count is appropriate in the present study for comparing DNE among specimens that were scanned at different resolutions (primarily due to differences in overall specimen size).

Measurement of OR requires elimination of the digital surface portions corresponding to the dental sidewalls below the lowest point on the occlusal surface (M'Kirera and Ungar, 2003). To prepare surfaces for OR measurement, each aligned surface was cut by an xy plane intersecting the lowest point on the occlusal surface using the default arguments of the 'plyPlaneCut' function in molaR v. 5.2 (Pampush et al., 2016b, 2022), with the portion above this plane saved as a new PLY file. These new surfaces were subjected to the same retriangulation steps described above, so that a second copy of all 124 surfaces, each cropped to the lowest point on the occlusal surface, simplified to 10,000 faces, and smoothed 20 iterations in Avizo with a lambda of 0.6, was produced.

2.3. Dental topographic analyses

All dental topographic analyses were performed in molaR v. 5.2 using the 'molaR_Batch' function. Relief index and sign-oriented DNE (Pampush et al., 2022) were calculated on all 124 aligned, retriangulated surfaces with sidewalls. Sign-oriented DNE was calculated using the 'DNE' function with default arguments, including a kappa of 0 (Pampush et al., 2022), producing measurements of total surface DNE, convex DNE (vexDNE), concave DNE, and surface areas of the convex and concave portions of the surfaces. Relief index was calculated using the 'RFI' function with the findAlpha argument set to TRUE, so a unique, ideal alpha value was calculated for 2D planometric area estimation of each specimen, improving measurement accuracy (see Pampush et al., 2016b). Every resultant DNE-object (the output of the molaR 'DNE' function) was visually inspected using the 'DNE3d' function to confirm consistent specimen orientation and face quality resulting from the alignment and retriangulation steps described above. Occlusal relief was calculated using the 'RFI' function, again with findAlpha set to TRUE, on the set of surfaces with sidewalls removed. The 3D area and 2D area results returned by the 'RFI' function were used in a simple ratio to represent specimen OR. A digital R object containing the DNE-objects of all 124 specimens analyzed in this study—which includes the aligned, retriangulated, digitized surfaces—is provided as a separate SOM file.

2.4. Wear quantification

The dentine exposure ratio was calculated for specimens of *Ae. zeuxis*, *Ap. phiomense*, and *S. apella* 2D images of specimens using the image analysis software Fiji v. 1.53t (Schindelin et al., 2012). Specimens were placed in occlusal view with a scale bar oriented parallel to and level with the occlusal plane. Mandibles of *S. apella* were photographed using a Fein Optic FZ-6 trinocular microscope equipped with a 3DCxM20 camera at ~20× magnification. Specimens of *Ae. zeuxis* and *Ap. phiomense* were imaged as 3D volume renderings in Avizo oriented into occlusal view, with a scale bar module. Two-dimensional images for calculating areas were opened in Fiji and the image scale was defined based on a line tracing a known distance in the image along the scale bar. Areas were defined using the polygon tool and calculated using the 'Measure' function. Dentine exposure ratio was defined as [2D total exposed dentine area/2D occlusal surface area] in mm^2.

As described above, RFI and OR were also investigated as potential metrics for describing wear that may avoid the limitations of DER when applied to molars with thick enamel (i.e., when wear occurs before dentine is exposed). Unlike DER, which increases with wear as more dentine becomes exposed with greater enamel loss, RFI and OR have been shown to decline as dental tissue is shed with wear (resulting in loss of 3D surface area). Therefore, the inverses (RFI^{-1} and OR^{-1}, respectively) were employed here as wear proxies to make them more readily comparable with DER.

2.5. Statistical analyses

Dental topography studies incorporating DNE have frequently compared unworn specimens when investigating diet (e.g., Bunn et al., 2011; Winchester et al., 2014; Selig et al., 2019; Pampush et al., 2022). Thus, as a baseline for this study, to compare differences in the dietary inferences drawn from unworn DNE vs. vexDNE for the fossil taxa, a subsample (Table 1) comprising the least worn specimens of *Ae. zeuxis* ($n = 8$) and *Ap. phiomense* ($n = 9$) were compared with the values calculated for DNE and vexDNE by Pampush et al. (2022) from the unworn M_2s of extant prosimians ($n = 104$; Boyer, 2008) and platyrrhines ($n = 105$; Winchester et al., 2014) via analysis of variance (ANOVA). The least worn specimens of *Ae. zeuxis* were determined as those with a DER < 0.01 (i.e., less than 1% of the occlusal surface was comprised of exposed dentine). This approach was inadequate for determining the least worn *Ap. phiomense* specimens, as many specimens may be significantly worn despite lack of enamel perforation owing to the thick enamel in this taxon. Therefore, the least worn specimens of *Ap. phiomense* were determined to be those with both a DER < 0.01 as well as an OR > 1.5 (indicating relatively tall, unworn cusps above the lowest point on the occlusal basin), producing an unworn sample size comparable to that of *Ae. zeuxis*. The extant sample employed here (or a subset) has been used in several previous studies of fossil euarchontan DT for the purpose of dietary inference (e.g., Godfrey et al., 2012; Prufrock et al., 2016a; López-Torres et al., 2018; Fulwood et al., 2021). The aye—aye (*Daubentonia madagascariensis*) was removed from the extant dataset as its peculiar feeding ecology (Randimbiharinirina et al., 2018) and attendant dental morphology was deemed irrelevant for comparison with the Fayum taxa. While platyrrhine anthropoids are more suitable models for *Ae. zeuxis* and *Ap. phiomense*, given the frequent usage of the prosimian dataset in DT studies and its opportunity to provide an alternative line of evidence from the platyrrhine dataset, both groups were analyzed. Platyrrhine dietary categories included specialized hard seed predation (durophagy), frugivory, folivory, and insectivory (Winchester et al., 2014) while the prosimian dietary categories included frugivory, omnivory, folivory, and insectivory (Boyer, 2008). Samples within the ANOVAs were grouped by dietary category for extant taxa and by species for fossil taxa, with their means compared for the topographic metric of interest (either DNE or vexDNE). A Tukey's honestly significant difference (HSD) test using a 95% family-wise confidence level ($\alpha = 0.05$) was performed on significant ANOVA models to assess significance of difference between means among pairs of variables (diet category or fossil genus) while correcting for family-wise error rate. All ANOVAs and Tukey's HSD tests were performed in R using common stats functions. These and all subsequent statistical analyses were performed in R v. 4.1.3 (R Core Team, 2022).

To characterize and measure taxa for which wear series were available (*Alouatta* spp., *Ateles* spp., *Plecturocebus* spp., *S. apella*, *Ae. zeuxis*, and *Ap. phiomense*), each metric of interest (DNE, vexDNE, RFI, RFI^{-1}, OR, OR^{-1}, and DER) was assessed for normality using the Shapiro—Wilks test (Shapiro and Wilk, 1965) within each genus (SOM Table S2). Non-normally distributed variables were normalized using the ordered quantile transformation implemented in the R package bestNormalize v. 1.8.3 (Peterson and Cavanaugh, 2020). This approach guarantees normally distributed transformed values for all in-sample data that are free of ties (Peterson and Cavanaugh, 2020) and its results were employed in ordinary least-squares (OLS) analyses of change in vexDNE with wear (described below). As all variables with the exceptions of OR and OR^{-1} failed to exhibit normality across all six genera (four extant and two extinct), comparisons among them for DNE, vexDNE, RFI, OR, and DER were performed on the non-transformed data using Kruskal—Wallis tests

Table 1
Novel dental topographic data collected and analysed in this study. Tooth position is M_2 for all specimens. All analyzed surfaces are hosted on the digital repository MorphoSource as well as being available for download as a digital R object in SOM.

Taxon	Specimen	Side	DNE	vexDNE	DER	RFI	OR	MorphoSource ARK
Ae. zeuxis[a]	DPC 1027	L	101.739	82.085	0.067	0.405	1.246	ark:/87602/m4/M64066
Ae. zeuxis[a]	DPC 1028	L	134.455	102.886	0.065	0.454	1.306	ark:/87602/m4/M64067
Ae. zeuxis[a]	DPC 2332	L	118.273	89.896	0.019	0.411	1.287	ark:/87602/m4/M32996
Ae. zeuxis[a]	DPC 2806	L	144.308	108.236	0.038	0.412	1.359	ark:/87602/m4/M34904
Ae. zeuxis[a]	DPC 3835[b]	R	158.610	116.282	0.007	0.468	1.479	ark:/87602/m4/M34289
Ae. zeuxis[a]	DPC 3837[b]	L	165.462	114.398	0.009	0.459	1.430	ark:/87602/m4/M34902
Ae. zeuxis[a]	DPC 5258	R	166.210	138.983	0.485	0.424	1.496	ark:/87602/m4/M37075
Ae. zeuxis[a]	DPC 5391	R	116.376	86.415	0.038	0.437	1.355	ark:/87602/m4/M34912
Ae. zeuxis[a]	DPC 7247	R	124.183	95.169	0.024	0.434	1.315	ark:/87602/m4/M34299
Ae. zeuxis[a]	DPC 7258	L	99.855	76.017	0.066	0.381	1.214	ark:/87602/m4/M36985
Ae. zeuxis[a]	DPC 8797	L	115.294	93.522	0.107	0.427	1.312	ark:/87602/m4/M34910
Ae. zeuxis[a]	DPC 10375	L	110.608	86.836	0.177	0.425	1.397	ark:/87602/m4/M33960
Ae. zeuxis[a]	DPC 10691	R	134.92	104.177	0.011	0.435	1.367	ark:/87602/m4/M64070
Ae. zeuxis[a]	DPC 11265	L	141.606	102.622	0.027	0.404	1.372	ark:/87602/m4/M64071
Ae. zeuxis[a]	DPC 13599[b]	R	169.822	110.599	0.004	0.465	1.566	ark:/87602/m4/M35428
Ae. zeuxis[a]	DPC 14213[b]	L	120.076	87.228	0.006	0.475	1.434	ark:/87602/m4/M11541
Ae. zeuxis[a]	DPC 21012[b]	R	166.151	114.963	0	0.459	1.487	ark:/87602/m4/M34906
Ae. zeuxis[a]	DPC 21540[b]	L	178.564	131.316	0	0.480	1.568	ark:/87602/m4/M37083
Ae. zeuxis[a]	DPC 23231[b]	R	194.66	139.382	0	0.490	1.526	ark:/87602/m4/M35361
Ae. zeuxis[a]	DPC 23953[b]	L	145.054	100.667	0.008	0.450	1.418	ark:/87602/m4/M37340
Ae. zeuxis[a]	DPC 24208	L	147.524	131.668	0.714	0.321	1.656	ark:/87602/m4/M34000
Ap. phiomense[a]	DPC 1037	L	171.411	99.889	0.009	0.474	1.377	ark:/87602/m4/M28696
Ap. phiomense[a]	DPC 1041	L	174.241	156.651	0.634	0.339	1.832	ark:/87602/m4/M38283
Ap. phiomense[a]	DPC 1089	R	77.010	65.739	0.002	0.444	1.328	ark:/87602/m4/M40653
Ap. phiomense[a]	DPC 1102	R	203.951	109.743	0.019	0.508	1.599	ark:/87602/m4/M64803
Ap. phiomense[a]	DPC 1104	R	98.813	81.705	0.051	0.443	1.209	ark:/87602/m4/M64805
Ap. phiomense[a]	DPC 1115	L	95.401	81.624	0.223	0.387	1.143	ark:/87602/m4/M42507
Ap. phiomense[a]	DPC 1119	L	100.821	73.666	0.003	0.463	1.278	ark:/87602/m4/M35860
Ap. phiomense[a]	DPC 2059	R	95.369	74.556	0.026	0.406	1.152	ark:/87602/m4/M37187
Ap. phiomense[a]	DPC 2395	L	145.139	94.106	0	0.486	1.484	ark:/87602/m4/M40655
Ap. phiomense[a]	DPC 2401[b]	L	235.511	125.479	0	0.505	1.684	ark:/87602/m4/M44991
Ap. phiomense[a]	DPC 2412	R	114.924	81.225	0.003	0.398	1.233	ark:/87602/m4/M35839
Ap. phiomense[a]	DPC 2808[b]	L	176.812	99.409	0	0.509	1.576	ark:/87602/m4/M35841
Ap. phiomense[a]	DPC 2938	L	172.827	97.633	0.005	0.497	1.419	ark:/87602/m4/M44995
Ap. phiomense[a]	DPC 2943	L	150.529	89.251	0	0.49	1.458	ark:/87602/m4/M11571
Ap. phiomense[a]	DPC 3080	L	133.418	82.643	0.003	0.456	1.33	ark:/87602/m4/M35853
Ap. phiomense[a]	DPC 3133	L	89.547	67.657	0	0.427	1.159	ark:/87602/m4/M28701
Ap. phiomense[a]	DPC 3661	R	115.766	77.492	0	0.488	1.317	ark:/87602/m4/M38280
Ap. phiomense[a]	DPC 3871[b]	R	192.918	94.935	0	0.502	1.529	ark:/87602/m4/M37189
Ap. phiomense[a]	DPC 3900	L	169.896	98.720	0	0.441	1.468	ark:/87602/m4/M64804
Ap. phiomense[a]	DPC 3906	R	77.83	67.197	0.026	0.405	1.544	ark:/87602/m4/M33523
Ap. phiomense[a]	DPC 5046[b]	L	207.098	122.118	0	0.518	1.632	ark:/87602/m4/M35849
Ap. phiomense[a]	DPC 5276[b]	R	204.866	115.199	0	0.501	1.567	ark:/87602/m4/M35851
Ap. phiomense[a]	DPC 5673	L	124.34	106.739	0.486	0.399	1.358	ark:/87602/m4/M38270
Ap. phiomense[a]	DPC 6137[b]	R	225.153	121.665	0	0.516	1.651	ark:/87602/m4/M35843
Ap. phiomense[a]	DPC 6251	R	119.386	81.160	0	0.449	1.326	ark:/87602/m4/M33633
Ap. phiomense[a]	DPC 6253	R	106.058	78.384	0	0.466	1.306	ark:/87602/m4/M33638
Ap. phiomense[a]	DPC 8808[b]	L	285.96	146.258	0	0.523	1.736	ark:/87602/m4/M33853
Ap. phiomense[a]	DPC 12645[b]	L	245.565	127.342	0	0.522	1.668	ark:/87602/m4/M35869
Ap. phiomense[a]	DPC 13596	R	172.748	103.158	0	0.458	1.39	ark:/87602/m4/M11610
Ap. phiomense[a]	DPC 22916[b]	L	191.477	104.694	0	0.513	1.515	ark:/87602/m4/M45043
Ap. phiomense[a]	DPC 22972	L	259.02	136.878	0.007	0.511	1.631	ark:/87602/m4/M42521
Ap. phiomense[a]	DPC 24812	R	86.286	69.435	0	0.423	1.205	ark:/87602/m4/M45032
S. apella	AMNH 6319	R	106.493	96.903	0	0.440	1.350	ark:/87602/m4/513347
S. apella	AMNH 10571	L	169.059	129.946	0	0.546	1.818	ark:/87602/m4/513282
S. apella	AMNH 16721	R	131.689	124.029	0.190	0.401	1.351	ark:/87602/m4/513328
S. apella	AMNH 61786	L	143.876	108.229	0	0.507	1.576	ark:/87602/m4/513348
S. apella	AMNH 80048	L	134.603	108.223	0	0.523	1.670	ark:/87602/m4/513349
S. apella	AMNH 80403	R	111.733	98.341	0.018	0.444	1.423	ark:/87602/m4/513358
S. apella	AMNH 80404	R	142.464	108.716	0	0.509	1.584	ark:/87602/m4/513359
S. apella	AMNH 133578	R	175.699	148.068	0.413	0.403	1.883	ark:/87602/m4/513283
S. apella	AMNH 133586	L	135.490	116.325	0.040	0.436	1.373	ark:/87602/m4/513284
S. apella	AMNH 133600	R	121.847	112.322	0.131	0.402	1.525	ark:/87602/m4/513285
S. apella	AMNH 133604	L	108.035	92.796	0.006	0.451	1.335	ark:/87602/m4/513298
S. apella	AMNH 133614	L	104.254	92.676	0.010	0.464	1.336	ark:/87602/m4/513300
S. apella	AMNH 133616	R	126.875	102.225	0	0.478	1.569	ark:/87602/m4/513299
S. apella	AMNH 133825	R	115.668	103.958	0.002	0.454	1.321	ark:/87602/m4/513301
S. apella	AMNH 133837	L	131.444	114.146	0.191	0.435	1.599	ark:/87602/m4/513312
S. apella	AMNH 133840	R	96.857	91.705	0.024	0.443	1.356	ark:/87602/m4/513314
S. apella	AMNH 133878	R	142.007	113.702	0	0.494	1.473	ark:/87602/m4/513316
S. apella	AMNH 133887	L	138.738	120.463	0.021	0.429	1.695	ark:/87602/m4/513318
S. apella	AMNH 211578	R	120.745	111.419	0	0.461	1.366	ark:/87602/m4/513329

(*continued on next page*)

Table 1 (*continued*)

Taxon	Specimen	Side	DNE	vexDNE	DER	RFI	OR	MorphoSource ARK
S. apella	AMNH 211579	R	115.591	106.943	0.004	0.460	1.501	ark:/87602/m4/513330
S. apella	AMNH 245697	R	136.047	111.011	0	0.491	1.517	ark:/87602/m4/513336
S. apella	AMNH 247693	L	111.907	105.011	0.039	0.452	1.261	ark:/87602/m4/513345

Abbreviations: DNE = total surface Dirichlet normal energy; vexDNE = convex Dirichlet normal energy; DER = dentine exposure ratio; RFI = relief index; OR = occlusal relief; L = left; R = right.
[a] Extinct species.
[b] Unworn specimens of fossil anthropoids used in analysis comparing DNE and vexDNE to extant primates of known dietary category.

(Kruskal and Wallis, 1952). Significance was assessed with an α level of 0.05 for all analyses.

Dentine exposure ratio has typically been employed as the continuous metric of wear in DT studies, but two additional proxies of wear (RFI^{-1} and OR^{-1}) were added in this study. The motivation for adding these proxies was to include specimens that exhibit wear (loss of enamel tissue) but in which the enamel is not perforated and therefore have a DER = 0. This is a particularly important consideration given the inclusion of relatively thickly enameled taxa such as *S. apella* and *Ap. phiomense*. To test if RFI^{-1} and OR^{-1} conformed to expectations of increase with wear, OLS regressions were performed between untransformed RFI^{-1} and DER and between untransformed OR^{-1} and DER for those specimens with DER > 0. The exclusion of specimens with DER = 0 ensured that they would not influence the regression models by introducing variation in the response variable (either RFI^{-1} or OR^{-1}) at a single predictor (DER) value.

Ordinary least-squares regressions were used to compare vexDNE as a response to the three normalized wear metrics (DER, RFI^{-1}, and OR^{-1}). First, RFI^{-1} and OR^{-1} were used as predictors of vexDNE for the large sample of *S. apella* and *Ap. phiomense* specimens with DER = 0 ($n = 9$ and $n = 18$, respectively) in order to test if occlusal sharpness changes with these metrics prior to enamel perforation. Next, OLS regressions were performed to assess the relationships between vexDNE as the response variable and the three normalized wear metrics (DER, RFI^{-1}, and OR^{-1}) as the predictor variables across the entire wear series for each taxon. Utilization of the normalized wear metrics addresses distributional differences among these predictor variables. For instance, the average and maximal DER values of *Alouatta* spp. are greater than those of *Ateles* spp. or *Plecturocebus* spp. in the samples used here (Pampush et al., 2018; Li et al., 2020). To our knowledge, based on observations of wear severity at multiple institutions, this distribution of DER for *Alouatta* spp. is reflective of dental wear among adults of this genus (Pampush et al., 2018). Normalizing the wear metrics ensures that the minimally and maximally worn specimens for each taxon—despite differences in metric distributions—are compared during analyses. To test the differences in slopes among taxa for each normalized wear variable, an analysis of covariance (ANCOVA) model was designed using vexDNE as the dependent variable, genus as an independent factor, and wear as the continuous independent variable (covariate). Each pair of genera was subjected to ANCOVA for each wear variable, and the interaction term was assessed for significance. For those cases in which the interaction term was significant, the slopes of the two genera were interpreted as nonhomogeneous, i.e., as indicating significantly different relationships between vexDNE and wear.

3. Results

Results of DT analysis and calculation of DER for *Ae. zeuxis*, *Ap. phiomense*, and *S. apella* are presented in Table 1. Example surfaces displaying the distribution of DNE and sign-oriented DNE at various stages of wear for these three taxa are illustrated in Figure 2.

The results of all ANOVAs comparing the least worn specimens of *Ae. zeuxis* and *Ap. phiomense* (Table 1) with the extant unworn samples are significant ($p < 0.001$), indicating differences among means in the groups (SOM Table S3). Only the results for comparisons with extant platyrrhines are presented here, though the extant prosimian results show similar patterns. Results of all Tukey's HSD comparisons (including those that incorporated extant prosimians) are listed in SOM Table S4. Tukey's HSD tests show distinctive patterns when employing either DNE or vexDNE to compare the fossil taxa to extant platyrrhine dietary groups and each other: In the ANOVA of DNE, *Ap. phiomense* is indistinguishable from modern platyrrhine folivores (*Alouatta* and *Brachyteles*) and the insectivore *Saimiri*, whereas *Ae. zeuxis* is indistinguishable from frugivores (*Aotus*, *Ateles*, *Callicebus*, and *Lagothrix*) and specialized seed predators (*Cebus*, *Cacajao*, *Chiropotes*, *Pithecia*, and *Sapajus*; Table 2; Fig. 3A). The DNE of the least worn specimens of *Ae. zeuxis* and *Ap. phiomense* is significantly different (Table 2), a finding confirmed via Wilcoxon rank sum test for difference in mean DNE between these two species ($p < 0.001$). By contrast, the ANOVA of vexDNE in this sample finds no significant difference between *Ae. zeuxis* and *Ap. phiomense* (Table 2), additionally confirmed by Wilcoxon rank sum test ($p = 0.606$). For this variable, both Oligocene taxa group with extant platyrrhine seed predators to the exclusion of other dietary categories. Figure 4 illustrates the average convex and concave contributions to total surface DNE and total surface area in unworn to lightly worn *Ae. zeuxis* and *Ap. phiomense* specimens, as well as in each of the extant platyrrhine dietary categories.

The untransformed distributions of DNE, vexDNE, DER, RFI, and OR for all wear series (four extant platyrrhine and two Oligocene fossil taxa) are illustrated via violin plots in Figure 5, with summary statistics reported in Table 3. The results of Kruskal–Wallis tests for differences in the distributions within these metrics among the taxa are listed in Table 4. For each metric, the distribution in at least one taxon is significantly different from that of others ($p < 0.001$). *Alouatta* has the highest values of DNE and DER—both absolutely and on average—consistent with past studies (Pampush et al., 2016a, 2018; Li et al., 2020), as well as the highest average vexDNE (Fig. 5). The wear series distributions for the two fossil taxa generally fall within the range of the extant distributions, although both have surfaces with DNE, vexDNE, and OR values that are lower than any of those within the extant sample (Table 3, 'Min' column). The DER ranges exhibited by all taxa other than *Alouatta* trend toward being low, with many specimens tied at DER = 0. Notably, both *Ap. phiomense* and *S. apella* have median DER values of ~0 (Fig. 5), with a large number of specimens that exhibit no occlusal dentine exposure.

Three-dimensional renderings of a wear series of specimens of *Al. palliata* and *S. apella* including cross-sections through the protoconid and metaconid in oblique and coronal views are presented in Figure 6. These highlight differences in relative enamel thickness between these two extant taxa as well as differences in the rate and pattern at which that enamel is perforated to expose dentine. The corresponding measurements of DER, RFI^{-1}, and OR^{-1} for the

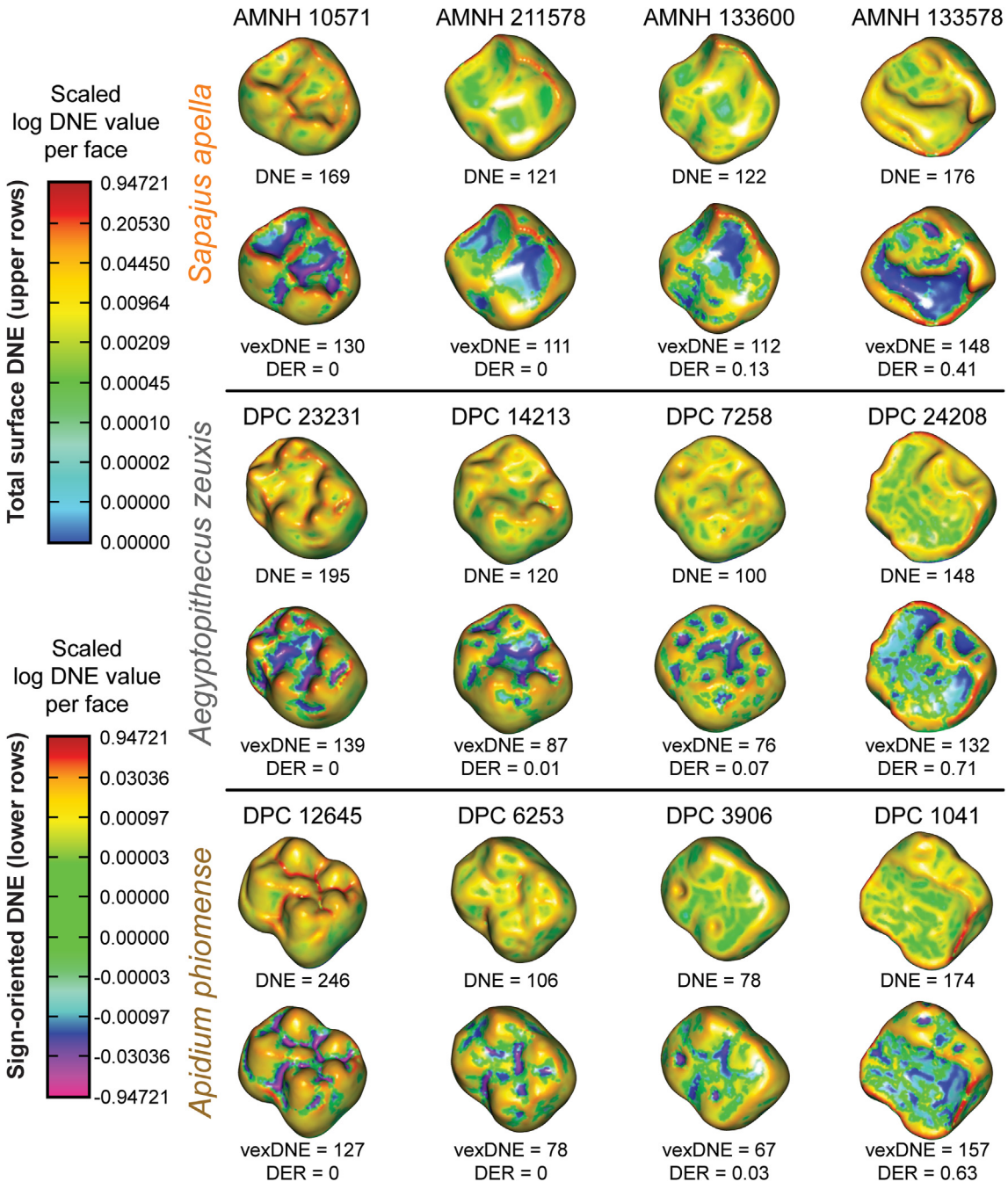

Figure 2. Three-dimensional digital surface models of second mandibular molars (not to scale) to illustrate distribution of Dirichlet normal energy (DNE) at various stages of wear for *S. apella*, *Ae. zeuxis*, and *Ap. phiomense*. Top rows for each taxon illustrate total surface DNE without reflecting sign orientation, while lower rows for each taxon illustrate sign-oriented DNE (Pampush et al., 2022). Dirichlet normal energy, convex DNE (vexDNE), and DER (wear) values are provided for each specimen. Color maps representing DNE values are scaled consistently across all surfaces and natural log-transformed to improve visualization. (For interpretation of the references to color in this figure legend, the reader is referred to the Web version of this article).

depicted specimens are also provided (Fig. 6C). Figure 7 includes 3D renderings in the same views of wear series of *Ae. zeuxis* and *Ap. phiomense* and supplies the measurements of DER, RFI^{-1}, and OR^{-1} for the illustrated specimens.

Outcomes of the OLS regression analyses comparing untransformed RFI^{-1} and OR^{-1} to DER for only those specimens with DER > 0 are presented in Table 5. For specimens that have dentine exposure, RFI^{-1} is significantly positively correlated with DER, as expected given the finding of a significant negative correlation between RFI and wear in past studies. Models of RFI^{-1} against DER result in r^2 values above 0.52 for all taxa, indicating a strong relationship between the two variables. The only significant positive correlations between OR^{-1} and DER are those for *Ateles* and *Plecturocebus* (Table 5). In contrast with these taxa, *Alouatta* has a nonsignificant relationship between these variables, with low r^2 and a coefficient of ~0, indicating that OR^{-1} does not change with DER, in agreement with past findings. A significant relationship exists between OR^{-1} and DER in *S. apella*; however, unlike the other extant taxa, this relationship is negative, indicating that OR^{-1} declines with increasing dentine exposure for this taxon. The fossil

Table 2
Significance values from Tukey's HSD tests of two analyses of variance (ANOVAs) that employ both extant platyrrhine diet and the fossil genera *Aegyptopithecus* and *Apidium* as grouping variables: 1) DNE; and 2) vexDNE. Significant *p*-values ($\alpha = 0.05$) are listed in bold. Only the results involving the fossil taxa are included; see SOM Table S3 for the complete list of all Tukey's HSD comparisons, including those for ANOVAs that incorporate extant prosimian diet as grouping variables.[a]

Topo. var.	Fossil genus	Diet cat.	Diff.	*p* adj.
DNE	*Aegyptopithecus*	Insectivory	−56.310	**<0.001**
		Folivory	−42.657	**0.002**
		Frugivory	−16.774	0.525
		Durophagy	10.788	0.875
	Apidium	Insectivory	−2.190	0.999
		Folivory	11.462	0.872
		Frugivory	37.345	**0.001**
		Durophagy	64.907	**<0.001**
	Aegyptopithecus:*Apidium*	–	54.120	**<0.001**
vexDNE	*Aegyptopithecus*	Insectivory	−52.335	**<0.001**
		Folivory	−39.666	**<0.001**
		Frugivory	−25.152	**0.003**
		Durophagy	−7.929	0.826
	Apidium	Insectivory	−49.123	**<0.001**
		Folivory	−36.454	**<0.001**
		Frugivory	−21.940	**0.008**
		Durophagy	−4.718	0.973
	Aegyptopithecus:*Apidium*	–	3.211	0.999

Abbreviations: Topo. var. = topographic variable; Diet cat. = extant dataset dietary category; Diff. = difference in the observed means; *p* adj. = *p*-value after adjustment for multiple comparisons by the 'TukeyHSD' function in R; DNE = total surface Dirichlet normal energy; vexDNE = convex Dirichlet normal energy.

[a] Rows marked *Aegyptopithecus*:*Apidium* compare the according topographic variable between these two genera and do not include a comparison with an extant dietary category.

taxa also have a negative relationship between OR^{-1} and DER, but it is only significant for *Ae. zeuxis* and both are characterized by low r^2 values (Table 5).

The OLS regression analysis results for comparison of vexDNE to RFI^{-1} and OR^{-1} that only include specimens of *S. apella* and *Ap. phiomense* with DER = 0 are presented in Table 6. Convex DNE trends negatively with each wear proxy and is significantly negatively correlated with RFI^{-1} in both taxa as well as with OR^{-1} in *Ap. phiomense*. High r^2 values in both correlations for the latter taxon indicate that the negative relationship between vexDNE and these proxies for wear is quite strong (Table 6). These negative trends are apparent when plotted, as is the trend in crown morphology toward lower, blunter cusps as RFI^{-1} and OR^{-1} increase prior to enamel perforation (Fig. 8).

Results of the OLS regression analyses comparing vexDNE with the three normalized wear metrics (DER, RFI^{-1}, and OR^{-1}) across the entire wear series for all six taxa are presented in Table 7. Both *Alouatta* and *Ateles* show a significant positive relationship between vexDNE and DER ($p < 0.001$ and $p = 0.015$ respectively), although a greater proportion of vexDNE variance is explained by DER for *Alouatta* (0.64) than for *Ateles* (0.36) and *Alouatta* is characterized by a steeper positive slope (Fig. 9). All other taxa have a very low proportion of variance in vexDNE explained by DER ($r^2 < 0.15$), especially *Ae. zeuxis* and *Ap. phiomense* (Table 7). The linear relationship between vexDNE and RFI^{-1} is significant only in *Alouatta* ($p = 0.013$) and *Ap. phiomense* ($p = 0.009$), though in the former it is positive while in the latter it is negative (Fig. 10). No taxon has a large proportion of variance in vexDNE explained by RFI^{-1}, with *Alouatta* exhibiting the greatest r^2 (0.30). In contrast, vexDNE displays a significant negative relationship with OR^{-1} for *S. apella*, *Ae. zeuxis*, and *Ap. phiomense* ($p = 0.001$, $p < 0.001$, and $p < 0.001$ respectively). These three taxa also exhibit a moderate to high proportion of variance explained (0.45, 0.66, and 0.72 respectively) compared to the other taxa, with $r^2 < 0.11$ (Table 7). However, given contrasting patterns of relationship between OR^{-1} and DER for specimens that have dentine exposure (Table 5), these results are viewed with caution. Plots of the relationship between vexDNE and OR^{-1} for all taxa are presented in SOM Figure S1.

Analysis of covariance models incorporating vexDNE as dependent variable, genus as independent factor and wear (measured as normalized DER, RFI^{-1}, or OR^{-1}) as covariate were used to make pairwise comparisons between taxa to test the differences in their slopes. The significance of the interaction term was used to assess if the vexDNE slopes of the two compared taxa were significantly different. Interaction term *p*-values for the pairwise ANCOVAs are listed in Table 8. Unsurprisingly given the differences in distribution between wear proxies (Fig. 5), the choice of wear variable impacts the pattern of interaction term significance, with DER and RFI^{-1} showing the greatest similarity. When comparing vexDNE to DER, a significant interaction term is found for the ANCOVAs between each extinct taxon and *Alouatta*, and additionally for the ANCOVA between *Ae. zeuxis* and *Ateles*. All other covariate pairs involving the fossil genera are nonsignificant, and therefore the homogeneity of slopes between them cannot be rejected. A similar pattern is recovered in the comparisons of vexDNE to RFI^{-1}, with the additional finding of a significant interaction term in the models for *Ap. phiomense* and *Ateles* and for *Ap. phiomense* and *S. apella* (Table 8). The interaction term significance results are quite different for the comparisons of vexDNE to OR^{-1}. Neither extinct taxon has a significant interaction term when included in an ANCOVA with *Alouatta*, but both are significant for ANCOVAs including *Ateles* and *Plecturocebus*, indicating statistical difference in the OLS regression slopes between vexDNE and OR^{-1} in the case of the latter two, but an inability to reject the homogeneity of slopes in the former. As in the case with RFI^{-1}, a significant interaction term is also recovered in the ANCOVA incorporating *Ap. phiomense* and *S. apella* (Table 8).

4. Discussion

4.1. Convex Dirichlet normal energy versus total surface Dirichlet normal energy

The utility of the DNE metric for making inferences about the diets of extinct taxa lies in its characterization of dental morphological properties relevant to how teeth interact with dietary materials: DNE is an effective measurement of surface-wide sharpness (Bunn et al., 2011; Pampush et al., 2022). This property is expected to positively correlate with ability of a tooth to triturate tough, crack-arresting materials, including such common primate foods as leaves or insect chitin (Kay, 1975; Lucas, 2006), and likely explains why DNE correlates well with relative shearing crest length measures like SQ (Winchester et al., 2014). However, occlusal sharpness is only a relevant measurement for understanding shearing in a dietary context insofar as it reflects actual interactions between teeth and food. Sharp, inward-facing occlusal sulci are unlikely to contact food materials during chewing and in the event that they do, they will not be splitting or slicing apart those materials, therefore these features contribute measurement noise when DNE is used to measure dental sharpness in the context of triturating tough food materials (see discussion in Pampush et al., 2022).

Pampush et al. (2022) introduced sign-oriented DNE to distinguish the DNE contributed by convex regions from that contributed by the concave portions of an occlusal surface. They illustrated that while most extant non-cercopithecoid primates express a ratio of concave DNE to convex DNE (DNE-R) that is relatively low (~0.2–0.3), nonhuman great ape molars are characterized by a far higher contribution from concave DNE (DNE-R = ~0.4–0.7). Figure 4 clearly shows that the same pattern of elevated concave DNE on unworn to lightly worn molars previously observed in extant hominids is also characteristic of the unworn M_2s of the

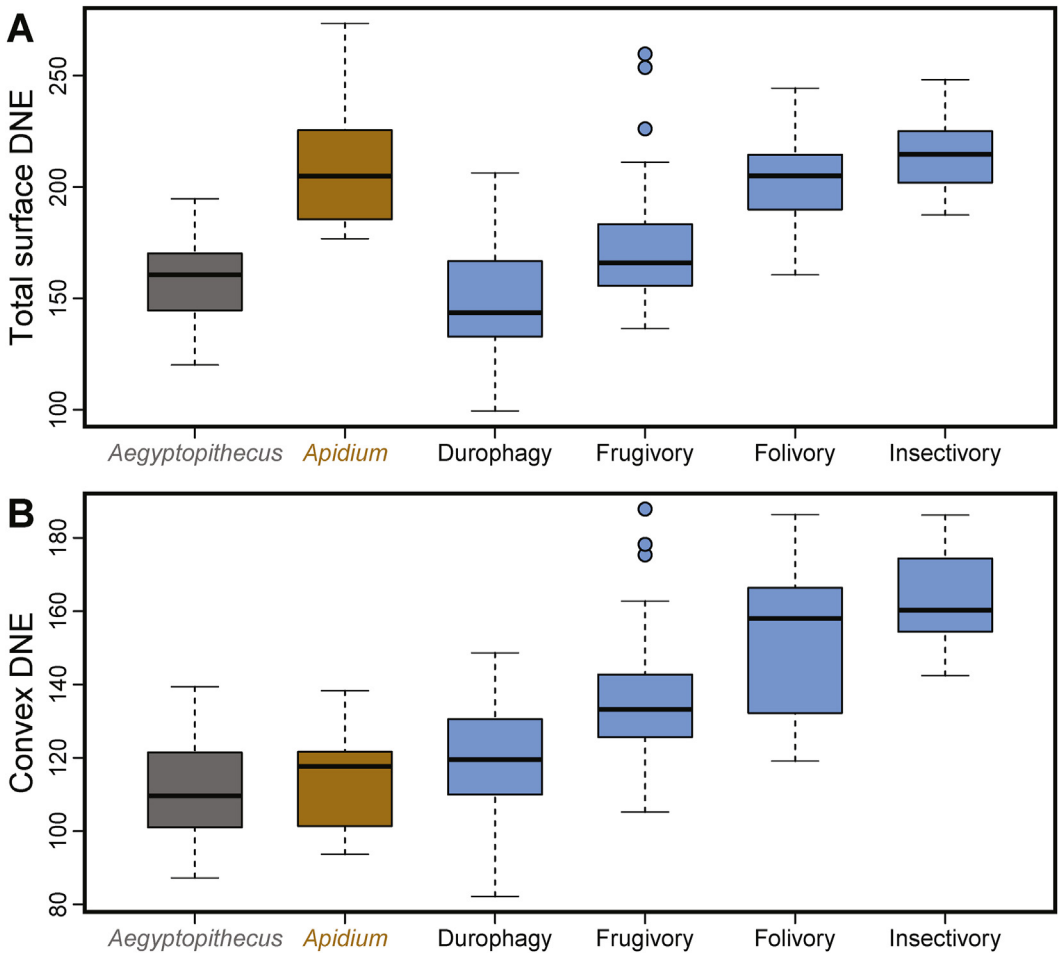

Figure 3. Boxplots of total surface Dirichlet normal energy (DNE; A) and convex DNE (B) values of unworn second mandibular molars of *Ae. zeuxis* and *Ap. phiomense* compared with those of extant platyrrhines (plotted in blue) sorted by diet following the categories of Winchester et al. (2014). Note that while the pattern of differences between extant platyrrhine dietary categories is quite similar for the two variables, the values of *Ae. zeuxis* and *Ap. phiomense* compared to the extant sample and to each other are highly dependent on the chosen variable. Box height denotes the interquartile range, with sample median indicated by the thick horizontal line in each box. Whiskers encompass the sample range within 1.5× the interquartile distance from the median; all observations farther from the sample median are denoted by points. (For interpretation of the references to color in this figure legend, the reader is referred to the Web version of this article).

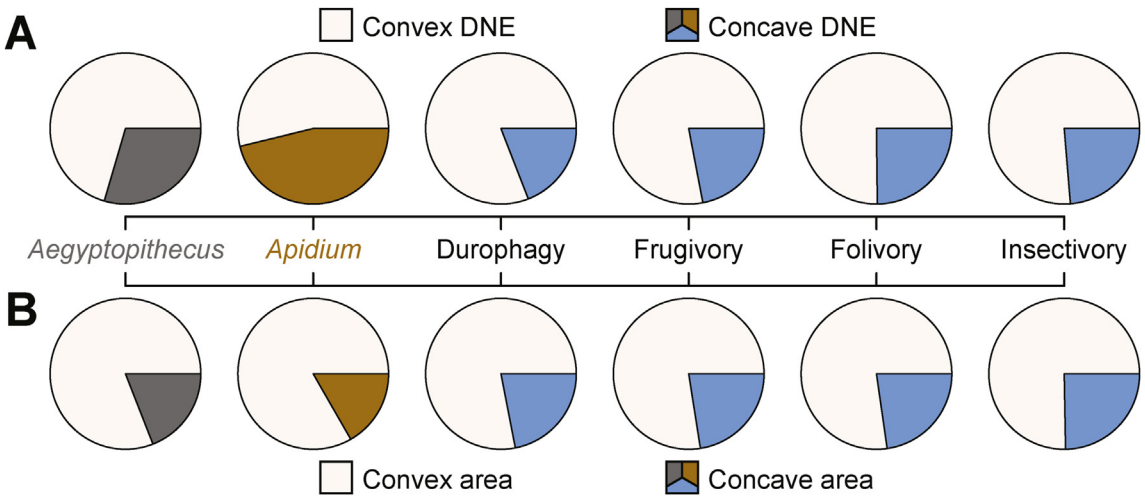

Figure 4. Pie charts illustrating average convex and concave contributions to unworn second mandibular molars of *Ae. zeuxis*, *Ap. phiomense*, and extant platyrrhines. Platyrrhines (plotted in blue) are sorted by diet following the categories of Winchester et al. (2014). (A) Average convex and concave portions of Dirichlet normal energy (DNE). (B) Average convex and concave portions of M_2 surface area. Note the greater contribution of concave DNE to the total DNE in the fossil anthropoids (upper two leftmost pie charts) despite their smaller percentage of concave surface area (bottom two leftmost pie charts) relative to the trends observed in extant platyrrhines. (For interpretation of the references to color in this figure legend, the reader is referred to the Web version of this article).

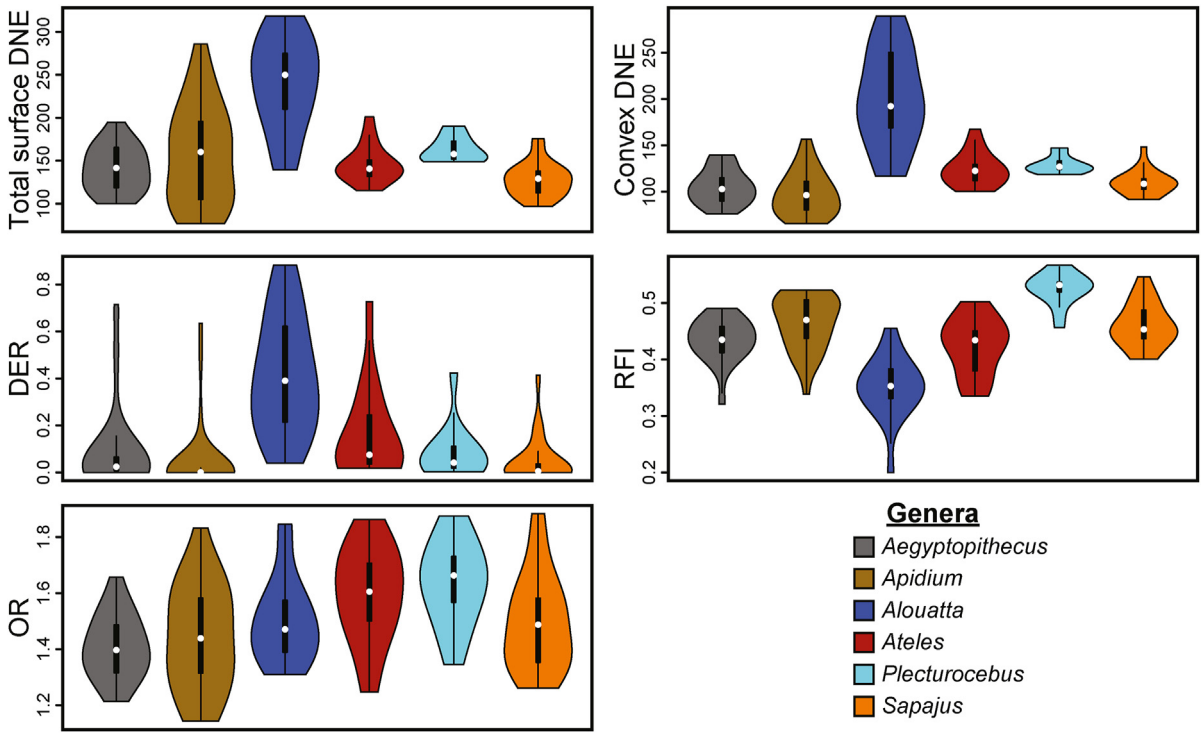

Figure 5. Violin plots of dental topography and wear measurements. The width of the colored area represents the density of the variable distribution, white dots indicate the distributional average, and black rectangles and lines illustrate interquartile distances. (For interpretation of the references to color in this figure legend, the reader is referred to the Web version of this article).

early Oligocene anthropoids *Ae. zeuxis* and *Ap. phiomense*. This follows from the distribution of curvature observed on their lightly-worn surfaces (Fig. 2). For the lightly worn specimens of *Ae. zeuxis*, the average DNE-R is 0.422, similar to that for extant *Pan troglodytes* (0.476), while for lightly worn specimens of *Ap. phiomense* the average ratio is 0.851—higher than that reported so far for any extant primate (Pampush et al., 2022: table 2). Indeed, one specimen of *Ap. phiomense*, Duke Lemur Center Museum of Natural History (DPC) 3871 (Fig. 11), has a majority of its total surface DNE contributed by the narrow, sharp furrows between cusps, producing a DNE-R in this specimen of 1.03. The implications for these findings are twofold: 1) Dietary inferences based on the total surface DNE of unworn M_2s for *Ae. zeuxis* and *Ap. phiomense* would—mistakenly—suggest that their teeth have relatively sharply projecting features and were perhaps well-suited to masticate tough items like leaves or insect chitin. This interpretation would be flawed due to the relatively high contributions of the concave portions of the tooth surface to DNE when compared to the extant reference sample. When considering only the convex regions of the occlusal surface, the teeth of the fossil taxa appear blunter, implying a non-folivorous/non-insectivorous diet (Fig. 3); and 2) The morphogenetic process speculated to produce deep occlusal sulci contributing to high DNE-R in great apes (Pampush et al., 2022) may have also characterized these two early anthropoids of the Fayum. This trait presumably evolved convergently in two different clades of anthropoids, one leading to catarrhines (including *Ae. zeuxis*), and the other to the stem anthropoid family Parapithecidae (including *Ap. phiomense*).

Inferring diet in extinct taxa from total surface Dirichlet normal energy versus convex Dirichlet normal energy. Aegyptopithecus zeuxis and *Ap. phiomense* are two added examples of primates in which concave DNE makes a large contribution to the DNE measurement (Fig. 4)—to the extent that the dietary signal derived from DNE is almost certainly a mischaracterization (Fig. 3). The DNE values of *Ae. zeuxis* are consistent with those of extant platyrrhine frugivores and/or seed predators (Table 2), in agreement with most prior dietary interpretations (Kay and Simons, 1980a, 1980b; Teaford et al., 1996) based on its low, blunt molar cusps (Figs. 2 and 7). In contrast, the DNE of *Ap. phiomense* more closely resembles that of extant platyrrhine insectivores or folivores (Table 2), a finding at odds with the low, blunt, thickly enameled morphology previously described for *Ap. phiomense* molars, which have been interpreted as indicative of frugivory (Kay and Simons, 1980a, 1980b; Teaford et al., 1996) or hard-object feeding (Fleagle and Kay, 1985). While the small body size of *Ap. phiomense* (Conroy, 1987; Perry et al., 2018) effectively rules out dedicated folivory (Kay and Simons, 1980b; Kay and Covert, 1984), researchers relying solely on the DNE of unworn M_2s would likely interpret this taxon as having a mixed frugivorous-insectivorous diet, out of step with prior quantitative analyses or visual inspection of their blunt molars. Indeed, as Figure 11 makes clear, specimens of *Ap. phiomense* with little wear, such as DPC 3871, have much higher DNE values concentrated in their inter-cuspal sulci than on their cusps or crests.

As with extant hominids (Pampush et al., 2022), analysis of vexDNE, i.e., with the contribution from concave portions of the surface removed, brings the measured sharpness of unworn *Ae. zeuxis* and *Ap. phiomense* molars more in line with that of extant frugivores and seed predators (Fig. 3; Table 2). Notably, while the DNE of unworn M_2s in the two Fayum species is significantly different, they possess similar average vexDNE (Fig. 3; Table 2). Notably, the large concave DNE values in *Ae. zeuxis* and *Ap. phiomense* do not arise from greater concave surface areas on their molars relative to extant platyrrhines (Fig. 4B)—rather, the fossil taxa have relatively lower concave proportions of their occlusal surface areas. While for many primate examples isolating vexDNE will lead to the same dietary interpretations as those reached with

total surface DNE (Pampush et al., 2022), the differences in these two metrics for the Fayum anthropoids analyzed here underscores the importance of using vexDNE for future analyses intending to reconstruct the diets of fossil primates.

Distribution of high concave Dirichlet normal energy in anthropoid primates. As Gregory (1916) noted, the so-called '*Dryopithecus*' pattern of molar occlusal morphology, characterized by the presence of deep sulci separating the cusps, is foreshadowed in the early Oligocene anthropoid *Propliopithecus* Schlosser, 1910.[2] This pattern also extends to its close relative *Aegyptopithecus* and encompasses the bunodont molar condition observed in Miocene to Recent non-cercopithecoid catarrhines (Gregory, 1916). The finding of high concave DNE values in the unworn to lightly-worn molars of *Ae. zeuxis* and *Ap. phiomense* (Figs. 3 and 4) is a metric expression of these deep sulci. This raises the question as to whether this pattern evolved just once in a catarrhine-parapithecoid ancestor or several times independently, which in turn hinges on the phylogenetic position of *Ap. phiomense* and other parapithecoids (e.g., *Simonsius* and *Parapithecus* Schlosser, 1910). The Parapithecoidea have been suggested by some researchers to be stem catarrhines (e.g., Simons, 1971; Jaeger et al., 1998), although subsequent analyses of more complete cranial and postcranial material led to an emerging consensus that they are stem anthropoids (Fleagle and Kay, 1987; Seiffert et al., 2005). A commonly held dental trait with extant hominids raises the possibility that *Ae. zeuxis* and *Ap. phiomense* are both catarrhines, counter to the results of recent phylogenetic analyses (Seiffert et al., 2010, 2020). However, further work is required to link the DT result of high concave DNE with the developmental processes that result in the positioning of cusps, crests, and sulci across the occlusal surface. Examining the taxonomic distribution of this dental pattern that emphasizes the presence of deep and narrow occlusal sulci should reveal whether or not it is a shared derived feature of parapithecoids and early catarrhines. For example, are deep molar sulci shared among all late Eocene and early Oligocene parapithecoids, or is it expressed by only a few taxa, indicating it evolved within the clade? Similarly, is the deep sulcus pattern widely distributed among early Miocene hominoids, or does it appear in only a few isolated lineages? In any event, the trait of sharp, inwardly oriented occlusal sulci is a commonality of this dental Bauplan, and not a unique acquisition of extant hominids. As such, the DNE values of Miocene-Recent non-cercopithecoid catarrhines are often influenced by a large concave DNE signal that could lead researchers to misinterpret dental sharpness in a dietary context. Whether or not sharp occlusal sulci serve a direct functional purpose (see Introduction) or are a developmental byproduct of selective processes acting on cusps (e.g., Butler, 1956) is unclear without additional dedicated study of these features, including their expression, development, and biomechanical effects. The present analysis documents this pattern in early Oligocene anthropoids, demonstrating its antiquity and underscoring the need to focus on analyzing vexDNE (as opposed to surface-wide DNE) when drawing dietary inferences for anthropoid primates.

Table 3
Summary statistics for all six wear series (all variables untransformed).

Genus	Variable	Mean	SD	Min	Max	Range
Alouatta	DNE	239.842	54.006	139.696	318.413	178.716
	vexDNE	200.757	51.628	116.730	289.546	172.816
	DNE-R	0.205	0.081	0.03	0.34	0.31
	SA-R	0.499	0.14	0.327	0.87	0.543
	DER	0.414	0.248	0.040	0.883	0.843
	RFI	0.352	0.053	0.200	0.455	0.255
	OR	1.501	0.152	1.310	1.846	0.536
Ateles	DNE	146.194	21.458	115.376	201.157	85.781
	vexDNE	124.147	18.140	100.264	167.503	67.239
	DNE-R	0.179	0.056	0.065	0.3	0.235
	SA-R	0.351	0.075	0.267	0.504	0.237
	DER	0.162	0.195	0.017	0.727	0.710
	RFI	0.423	0.050	0.335	0.502	0.167
	OR	1.594	0.169	1.247	1.862	0.614
Plecturocebus	DNE	163.098	14.454	148.916	190.226	41.31
	vexDNE	128.873	8.975	118.336	147.328	28.992
	DNE-R	0.265	0.051	0.173	0.315	0.143
	SA-R	0.308	0.037	0.262	0.411	0.149
	DER	0.085	0.113	0.003	0.423	0.420
	RFI	0.526	0.029	0.456	0.567	0.111
	OR	1.634	0.150	1.346	1.874	0.529
Sapajus	DNE	128.233	19.807	96.857	175.699	78.841
	vexDNE	109.871	13.111	91.705	148.068	56.363
	DNE-R	0.165	0.085	0.056	0.329	0.273
	SA-R	0.254	0.035	0.192	0.360	0.168
	DER	0.049	0.100	0	0.413	0.413
	RFI	0.460	0.039	0.401	0.546	0.146
	OR	1.495	0.168	1.261	1.883	0.622
Aegyptopithecus[a]	DNE	140.655	26.559	99.855	194.660	94.805
	vexDNE	105.397	18.623	76.017	139.382	63.364
	DNE-R	0.334	0.094	0.120	0.535	0.415
	SA-R	0.253	0.051	0.198	0.410	0.212
	DER	0.089	0.179	0	0.714	0.714
	RFI	0.434	0.038	0.321	0.490	0.169
	OR	1.409	0.114	1.214	1.656	0.442
Apidium[a]	DNE	156.878	57.466	77.010	285.960	208.950
	vexDNE	97.886	23.918	65.739	156.651	90.911
	DNE-R	0.567	0.284	0.112	1.032	0.92
	SA-R	0.215	0.058	0.160	0.477	0.317
	DER	0.047	0.142	0	0.634	0.634
	RFI	0.465	0.048	0.339	0.523	0.184
	OR	1.441	0.186	1.143	1.832	0.690

Abbreviations: SD = standard deviation; Min = minimum; Max = maximum; DNE = total surface Dirichlet normal energy; vexDNE = convex Dirichlet normal energy; DNE-R = ratio of concave to convex Dirichlet normal energy; SA-R = ratio of concave to convex surface area; DER = dentine exposure ratio; RFI = relief index; OR = occlusal relief.
[a] Extinct genus.

[2] With respect to *Propliopithecus*, Gregory (1916:284) writes, "The furrows formed by the intersection of the bases of the cusps make a pattern that foreshadows the '*Dryopithecus* pattern' …".

4.2. Changes in convex Dirichlet normal energy with wear among extant platyrrhines

A robust history of study has demonstrated that macroscopic dental wear (as distinct from microscopic wear features) results from the complex interaction between occluding teeth and the physical and chemical properties of ingested materials and the oral environment, and can therefore also be informative of jaw movements (Butler, 1952, 1956, 1973; Crompton and Hiiemäe, 1969; Molnar, 1971; Kay and Hiiemäe, 1974; Elgart, 2010; Benazzi et al., 2013; Lucas et al., 2013; Ungar, 2015; Kullmer et al., 2020). However, despite an extensive literature exploring intraspecific macrowear in humans (see review in Larsen, 2015), consensus on how macrowear should be quantified has yet to emerge. In particular,

Table 4
Kruskal–Wallis tests for mean differences between taxa (all variables untransformed).

Variable	χ^2	Df	*p*-value
DNE	44.871	5	<0.001
vexDNE	64.692	5	<0.001
DER	58.066	5	<0.001
RFI	64.692	5	<0.001
OR	21.400	5	<0.001

Abbreviations: Df = degrees of freedom; DNE = total surface Dirichlet normal energy; vexDNE = convex Dirichlet normal energy; DER = dentine exposure ratio; RFI = relief index; OR = occlusal relief.

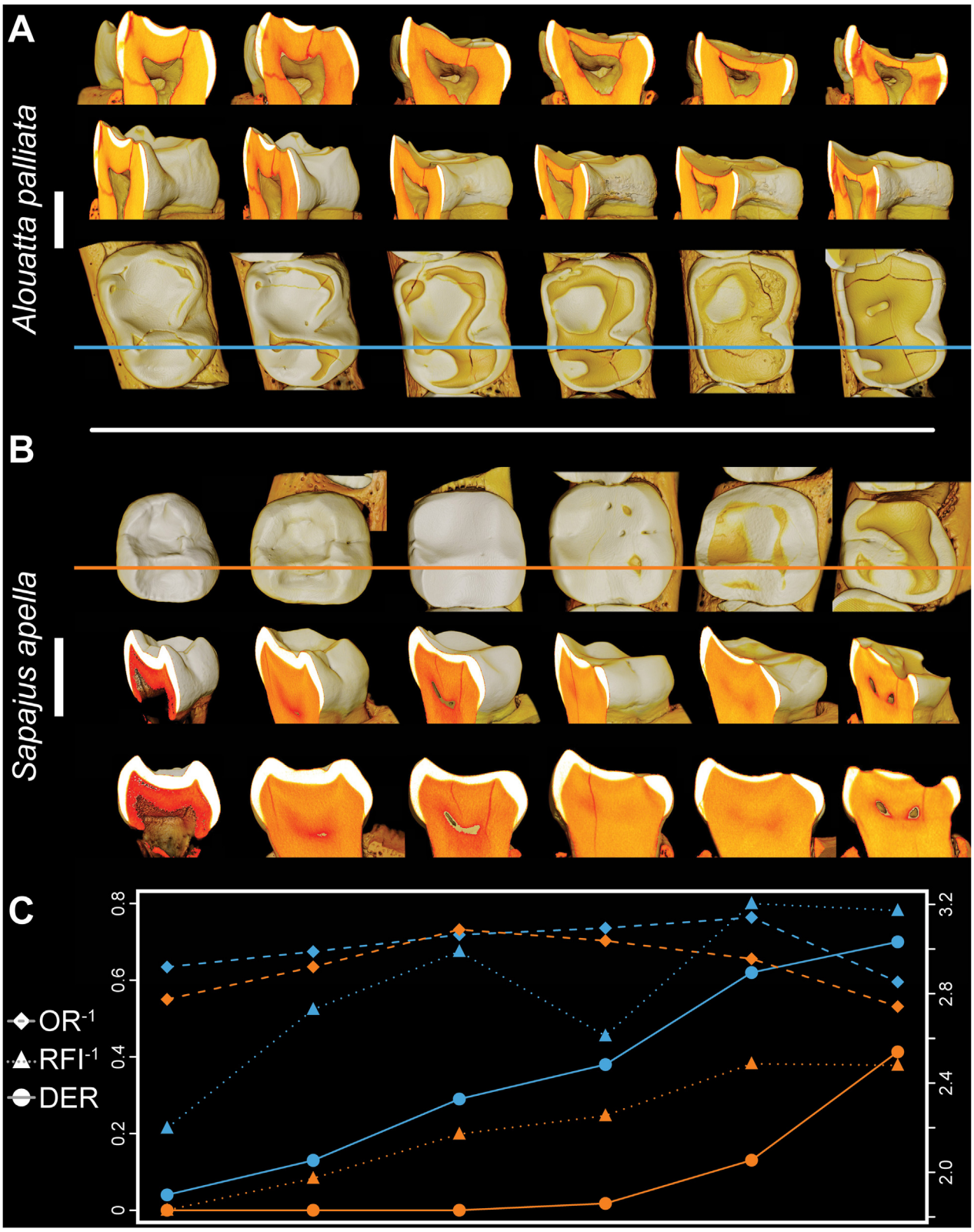

Figure 6. Three-dimensional renderings and cross sections through the protoconid and metaconid (estimated in cases where these cusps are worn away) of digitized specimens of (A) *Al. palliata* and (B) *S. apella*, illustrating differences in relative enamel thickness and how enamel distribution is altered during wear, with progressively more worn specimens to the right. False coloration ramp illustrates differences in density, with most dense elements in white and least dense in red. Lines in occlusal views indicate locations of cross sections. (C) Plot of values of dentine exposure ratio (DER), inverse of relief index (RFI^{-1}), and inverse of occlusal relief (OR^{-1}) for each of the illustrated specimens, indicating how these change across the wear series, with *Al. palliata* plotted in blue and *S. apella* plotted in orange. Left y-axis is for DER and OR^{-1}, right y-axis is for RFI^{-1}. Included specimens of *Al. palliata* are from the Duke University Department of Evolutionary Anthropology collection (DU-LP); from left to right: DU-LP-09 (R); DU-LP-25 (R); DU-LP-06; DU-LP-05 (R); DU-LP-26; DU-LP-07 (R). Included specimens of *S. apella* from left to right: AMNH 10571 (unerupted M_2 isolated from its crypt), AMNH 61786, AMNH 211578 (R), AMNH 80403 (R), AMNH 133600 (R), AMNH 133578 (R). Scale bars = 3 mm. R = reversed. (For interpretation of the references to color in this figure legend, the reader is referred to the Web version of this article).

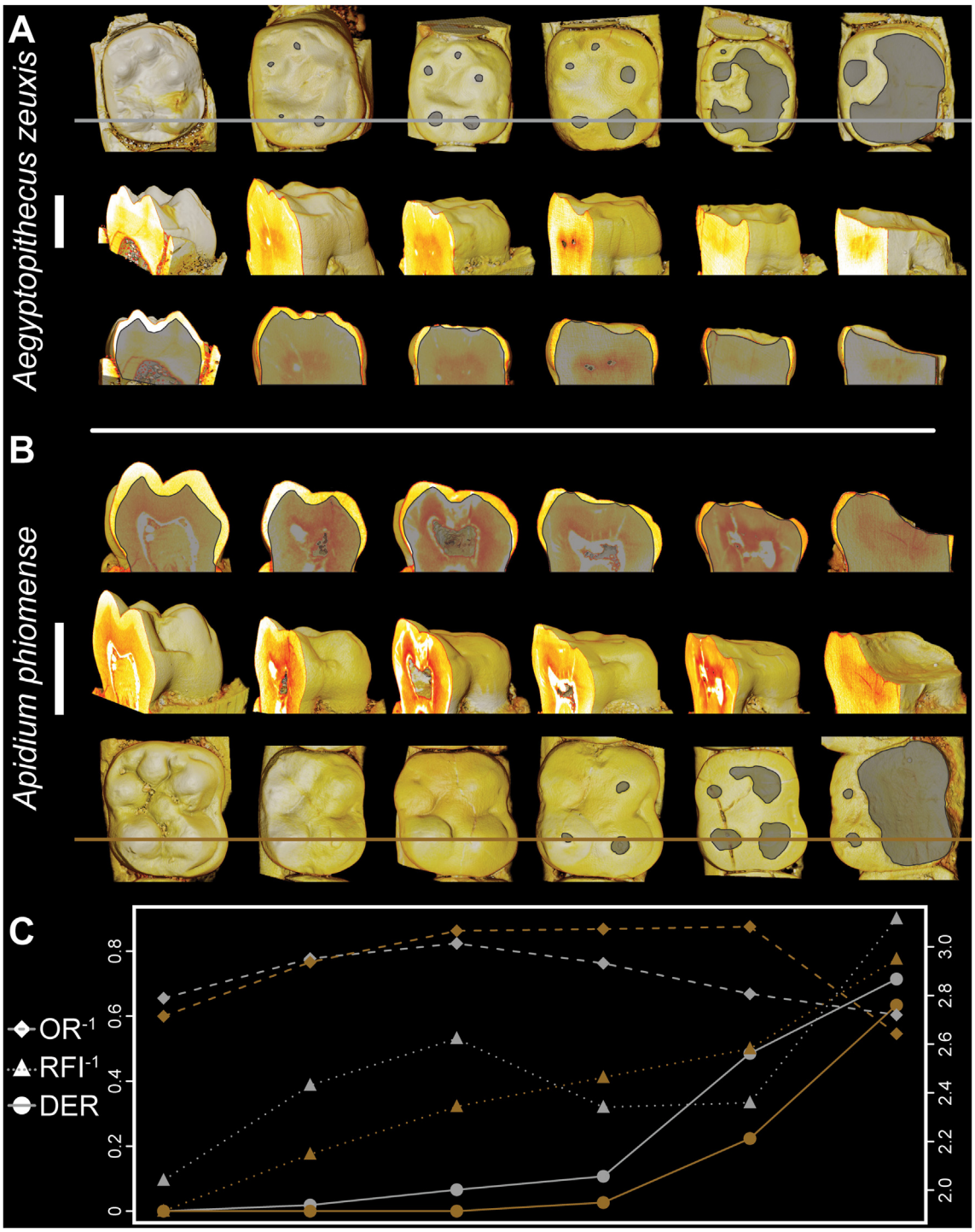

Figure 7. Three-dimensional renderings and cross sections through the protoconid and metaconid (estimated in cases where these cusps are worn away) of digitized specimens of (A) *Ae. zeuxis* and (B) *Ap. phiomense*, illustrating differences in relative enamel thickness and how enamel distribution is altered during wear, with progressively more worn specimens to the right. False coloration ramp illustrates differences in density, with most dense elements in white and least dense in red. As density values do not always clearly distinguish dentine and enamel due to fossilization, areas of dentine exposure are outlined in occlusal views and the enamel-dentine boundary is traced in cross sections, highlighting non-enamel regions. Lines in occlusal views indicate locations of cross sections. C) Plot of values of dentine exposure ratio (DER), inverse of relief index (RFI^{-1}), and inverse of occlusal relief (OR^{-1}) for each of the illustrated specimens, indicating how these change across the wear series, with *Ae. zeuxis* plotted in silver and *Ap. phiomense* plotted in gold. Left y-axis is for DER and OR^{-1}, right y-axis is for RFI^{-1}. Included specimens of *Ae. zeuxis* from left to right: DPC 23231 (R), DPC 2332, DPC 7258, DPC 8797, DPC 5258 (R), DPC 24208. Included specimens of *Ap. phiomense* from left to right: DPC 12645, DPC 6253 (R), DPC 3133, DPC 2059 (R), DPC 1115, DPC 1041. Scale bars = 3 mm. R = reversed. (For interpretation of the references to color in this figure legend, the reader is referred to the Web version of this article).

Table 5
Ordinary least-squares regression results comparing RFI^{-1} and OR^{-1} against DER for specimens with DER > 0 in all six taxa. Variables are not normalized. Significant *p*-values are listed in bold. Note that while the regression coefficient is positive for all regressions of RFI^{-1} against DER, the coefficient sign is inconsistent among taxa for regressions of OR^{-1} against DER. Significant *p*-values are listed in bold.

Genus	Variable	Coefficient	F-statistic	Df	r^2	*p*-value
Alouatta	RFI^{-1}	1.699	21.218	1, 18	0.54	**<0.001**
	OR^{-1}	0.039	0.428	1, 18	0.02	0.521
Ateles	RFI^{-1}	1.199	20.347	1, 14	0.59	**<0.001**
	OR^{-1}	0.280	19.151	1, 14	0.58	**0.001**
Plecturocebus	RFI^{-1}	0.792	20.916	1, 11	0.66	**0.001**
	OR^{-1}	0.384	12.894	1, 11	0.54	**0.004**
Sapajus	RFI^{-1}	0.758	15.395	1, 11	0.58	**0.002**
	OR^{-1}	−0.413	8.217	1, 11	0.43	**0.015**
Aegyptopithecus[a]	RFI^{-1}	0.892	17.794	1, 16	0.53	**0.001**
	OR^{-1}	−0.153	5.959	1, 16	0.27	**0.027**
Apidium[a]	RFI^{-1}	1.029	14.728	1, 12	0.55	**0.002**
	OR^{-1}	−0.155	1.350	1, 12	0.10	0.268

Abbreviations: DER = dentine exposure ratio; Df = degrees of freedom; RFI^{-1} = inverse of relief index; OR^{-1} = inverse of occlusal relief.
[a] Extinct genus.

Table 6
Ordinary least-squares regression results comparing vexDNE against normalized values of RFI^{-1} and OR^{-1} for only specimens with DER = 0 in *S. apella* and *Ap. phiomense*. Significant *p*-values are listed in bold.

Genus	Variable	Coefficient	F-statistic	Df	r^2	*p*-value
Sapajus	RFI^{-1}	−9.564	10.233	1, 7	0.59	**0.015**
	OR^{-1}	−8.215	4.949	1, 7	0.41	0.061
Apidium[a]	RFI^{-1}	−22.050	41.520	1, 16	0.72	**<0.001**
	OR^{-1}	−23.895	180.655	1, 16	0.92	**<0.001**

Abbreviations: DER = dentine exposure ratio; Df = degrees of freedom; RFI^{-1} = inverse of relief index; OR^{-1} = inverse of occlusal relief.
[a] Extinct genus.

Table 7
Ordinary least-squares regression results comparing vexDNE with three normalized wear proxies for all six taxa. Significant *p*-values are listed in bold.

Variable	Genus	Coefficient	F-statistic	Df	r^2	*p*-value
DER	*Alouatta*	41.422	31.443	1, 18	0.64	**<0.001**
	Ateles	10.918	7.771	1, 14	0.36	**0.015**
	Plecturocebus	−3.185	1.553	1, 11	0.12	0.239
	Sapajus	5.551	3.279	1, 20	0.14	0.085
	Aegyptopithecus[a]	−4.019	0.867	1, 19	0.04	0.363
	Apidium[a]	1.014	0.037	1, 30	<0.01	0.849
RFI^{-1}	*Alouatta*	28.297	7.596	1, 18	0.30	**0.013**
	Ateles	7.797	3.115	1, 14	0.18	0.099
	Plecturocebus	−0.537	0.039	1, 11	<0.01	0.848
	Sapajus	2.337	0.649	1, 20	0.03	0.430
	Aegyptopithecus[a]	−6.385	2.498	1, 19	0.12	0.130
	Apidium[a]	−10.962	7.898	1, 30	0.21	**0.009**
OR^{-1}	*Alouatta*	−4.124	0.114	1, 18	0.01	0.739
	Ateles	5.115	1.19	1, 14	0.08	0.294
	Plecturocebus	0.334	0.015	1, 11	<0.01	0.905
	Sapajus	−8.832	16.282	1, 20	0.45	**<0.001**
	Aegyptopithecus[a]	−15.18	36.348	1, 19	0.66	**<0.001**
	Apidium[a]	−20.365	76.857	1, 30	0.72	**<0.001**

Abbreviations: vexDNE = convex Dirichlet normal energy; Df = degrees of freedom; DER = dentine exposure ratio; RFI^{-1} = inverse of relief index; OR^{-1} = inverse of occlusal relief.
[a] Extinct genus.

the problem of how to account for interspecific differences in enamel thickness and other variables has yet to be established. The most commonly used approaches involve either qualitative ordination of degree of wear based on an observer's perception of dental tissue loss (Molnar, 1971; Scott, 1979), or quantification of dentine exposure on the surface of the molar crown as a proportion of crown area (Kay and Cant, 1988; Elgart, 2010; Morse et al., 2013; Galbany et al., 2014, 2020), such as the DER metric employed in this study. More sophisticated 3D techniques such as occlusal fingerprint analysis have been developed for identifying regular molar wear facets and applied to taxonomic questions (Kullmer et al., 2009, 2020), but have thus far shown little success in corresponding to general dietary strategies among extant great apes (Fiorenza et al., 2022). These methods have not been applied to—and may not be appropriate for—wear series that include unworn specimens (in which planar attrition wear facets are not yet

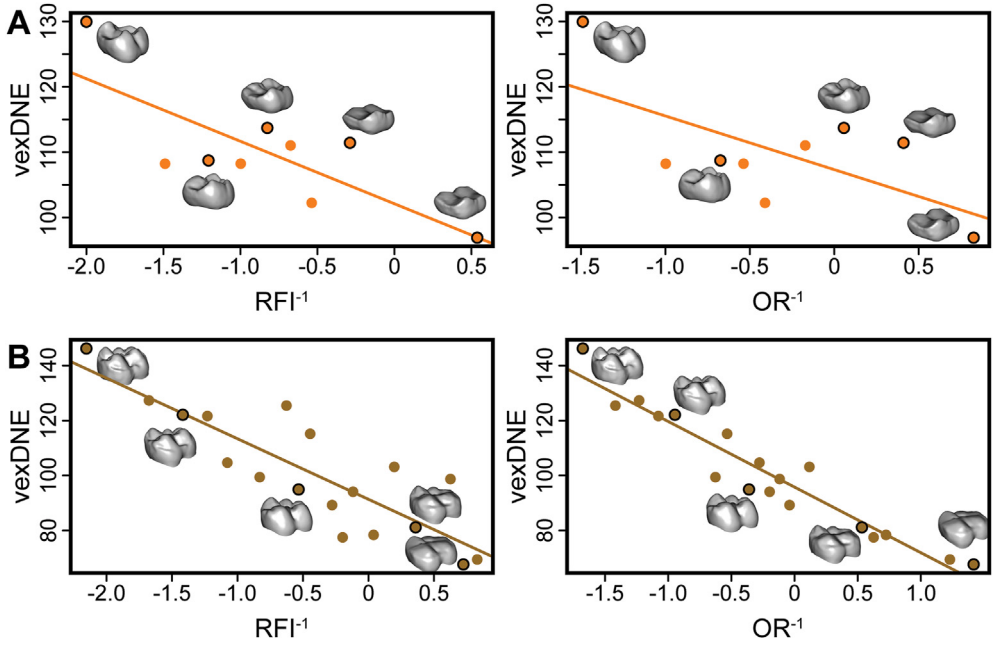

Figure 8. Bivariate plots of ordinary least-squares regressions showing negative correlation of convex Dirichlet normal energy (vexDNE) against normalized inverse of relief index (RFI^{-1}) and inverse of occlusal relief (OR^{-1}) for specimens with dentine exposure ratio = 0 in (A) *S. apella* and (B) *Ap. phiomense*. Five specimens of each taxon are illustrated (not to scale) to indicate changes in crown morphology with increasing RFI^{-1} and OR^{-1}, with point circled in black to indicate displayed specimen. Included specimens of *S. apella* from left to right: AMNH 10571, AMNH 80404, AMNH 133878, AMNH 211578, AMNH 6319. Included specimens of *Ap. phiomense* from left to right: DPC 8808, DPC 5046, DPC 3871 (R), DPC 6251 (R), DPC 3133. R = reversed. (For interpretation of the references to color in this figure legend, the reader is referred to the Web version of this article).

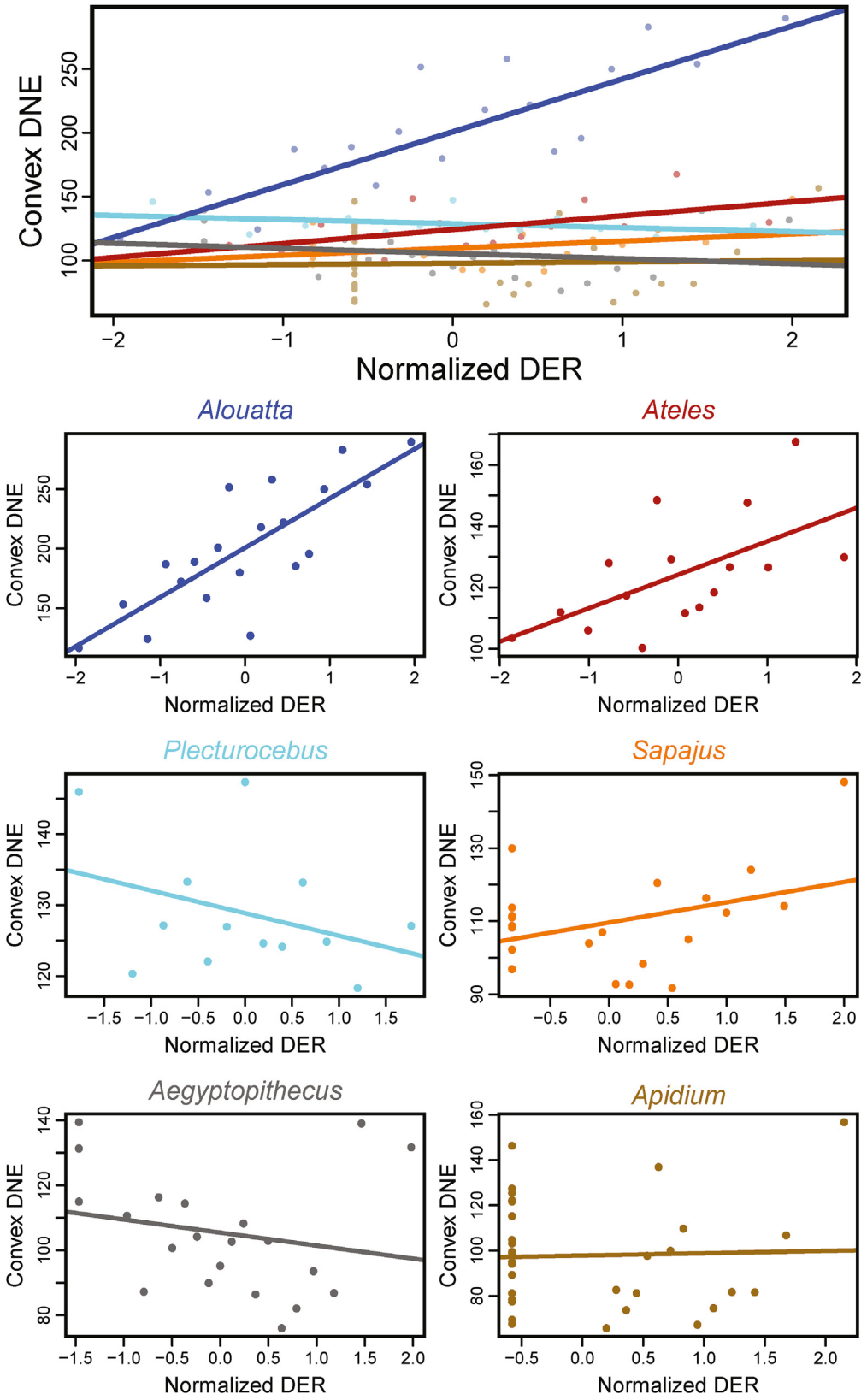

Figure 9. Bivariate plots of ordinary least-squares regressions of convex Dirichlet normal energy (vexDNE) against normalized dentine exposure ratio (DER) for all wear series. Upper plot shows all data, with regressions colored by genus and individual data points faded to improve visualization of regression lines. Lower six plots show the regression for each individual taxon with data points unfaded. Note that values and ranges of Y-axes differ among the lower six plots. Ordinary least-squares regression results are listed in Table 7. (For interpretation of the references to color in this figure legend, the reader is referred to the Web version of this article).

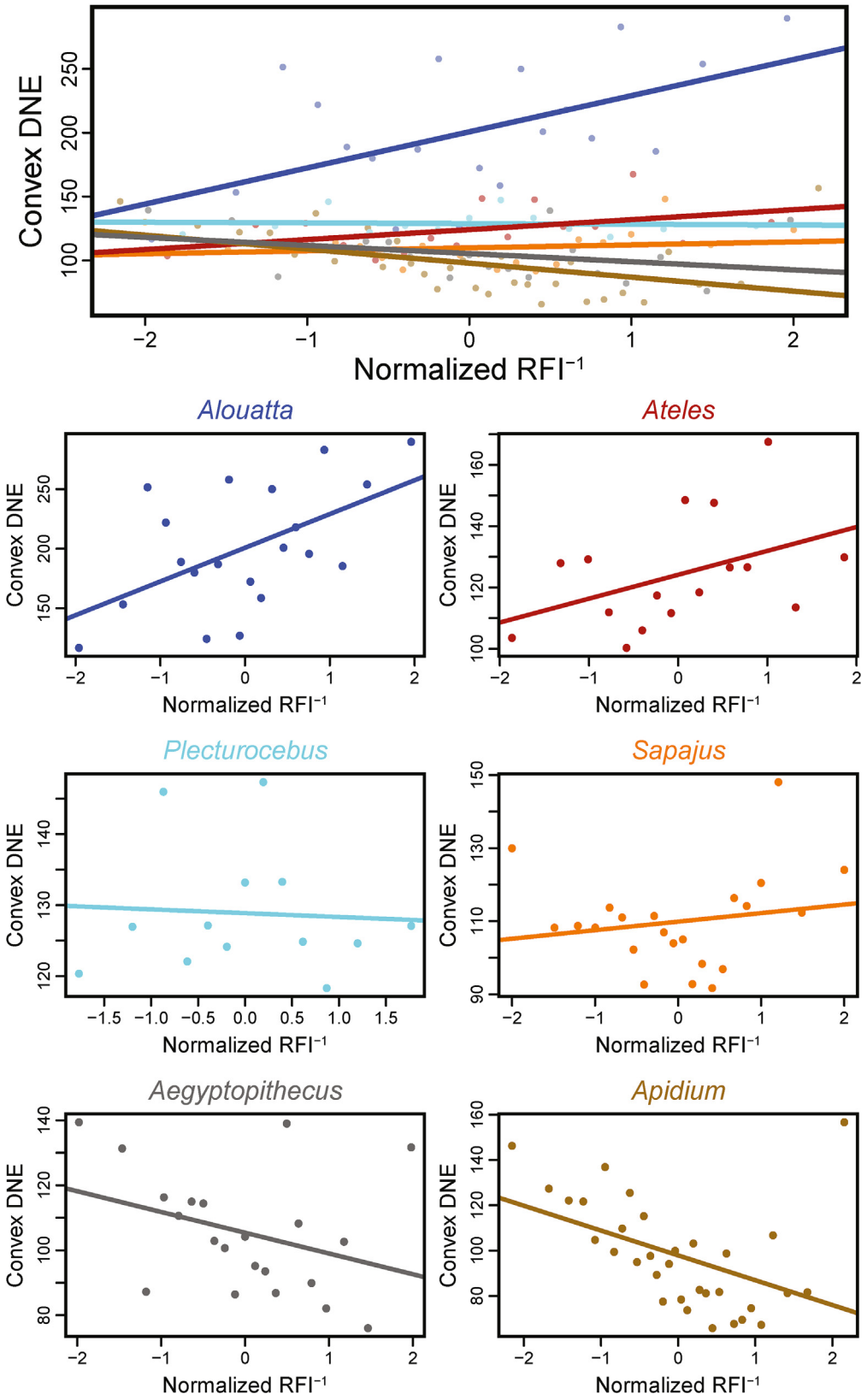

Figure 10. Bivariate plots of ordinary least-squares regressions of convex Dirichlet normal energy (vexDNE) against normalized inverse of relief index (RFI^{-1}) for all wear series. Upper plot shows all data, with regressions colored by genus and individual data points faded to improve visualization of regression lines. Lower six plots show the regression for each individual taxon with data points unfaded. Note that values and ranges of Y-axes differ among the lower six plots. Ordinary least-squares regression results are listed in Table 7. (For interpretation of the references to color in this figure legend, the reader is referred to the Web version of this article).

Table 8
Significance (p) values for interaction terms between vexDNE and wear variables in pairwise analyses of covariance employing genus as an independent factor (covariate). Those significant at the $\alpha = 0.05$ level are shown in bold.

Wear variable	Genus	*Alouatta*	*Ateles*	*Plecturocebus*	*Sapajus*	*Aegyptopithecus*[a]
DER	*Ateles*	**0.002**	–			
	Plecturocebus	**<0.001**	**0.009**	–		
	Sapajus	**<0.001**	0.278	0.051	–	
	Aegyptopithecus[a]	**<0.001**	**0.018**	0.888	0.080	–
	Apidium[a]	**<0.001**	0.186	0.590	0.501	0.479
RFI^{-1}	*Ateles*	0.104	–			
	Plecturocebus	**0.037**	0.144	–		
	Sapajus	**0.015**	0.289	0.516	–	
	Aegyptopithecus[a]	**0.003**	**0.025**	0.310	0.085	–
	Apidium[a]	**<0.001**	**0.005**	0.199	**0.016**	0.438
OR^{-1}	*Ateles*	0.526	–			
	Plecturocebus	0.778	0.417	–		
	Sapajus	0.693	**0.006**	**0.015**	–	
	Aegyptopithecus[a]	0.369	**<0.001**	**<0.001**	0.064	–
	Apidium[a]	0.109	**<0.001**	**<0.001**	**0.001**	0.149

Abbreviations: vexDNE = convex Dirichlet normal energy; DER = dentine exposure ratio; RFI^{-1} = inverse of relief index; OR^{-1} = inverse of occlusal relief.
[a] Extinct genus.

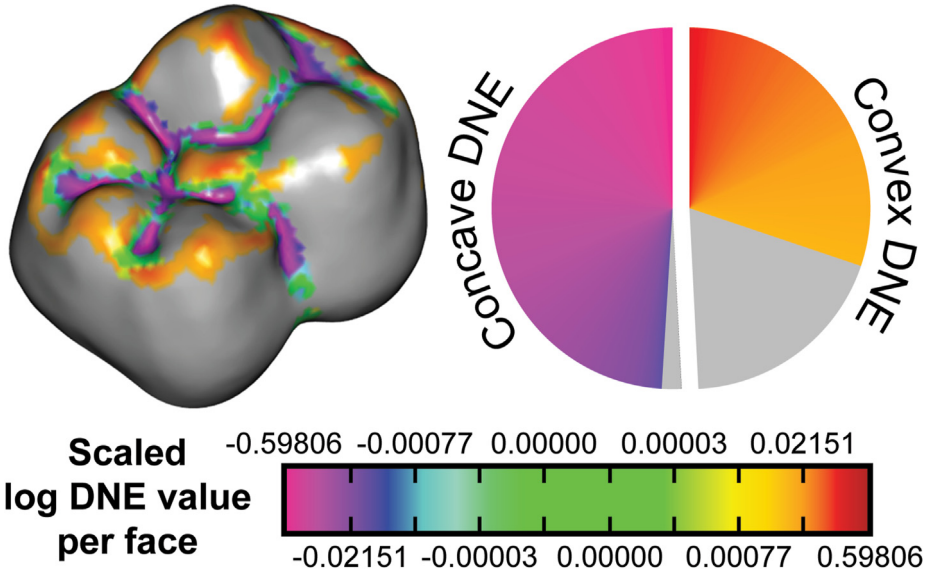

Figure 11. Distribution of the top quartile of Dirichlet normal energy (DNE) values across the right M_2 of DPC 3871, *Ap. phiomense*. Pie chart distinguishes convex and concave contributions to total surface DNE, with contribution from the top quartile of DNE values colored (contribution from the bottom three quartiles in gray). Color scale differentiates sharp convex features (in red) from sharp concave features (in magenta). Note that a majority of the surface DNE comes from convex portions of the surface, and the top quartile of DNE is dominated by that contributed from sharp furrows (in magenta). Coloration is natural log-transformed to improve visualization. (For interpretation of the references to color in this figure legend, the reader is referred to the Web version of this article).

Table 9
Quadratic regression results with vexDNE as response variable to the two predictor values RFI^{-1} and $(RFI^{-1})^2$. Convex DNE is modeled as: vexDNE = Intercept + (Coefficient 1 × RFI^{-1}) + (Coefficient 2 × $(RFI^{-1})^2$) for each taxon. Significant p-values are listed in bold.

Genus	Intercept	Coefficient 1	Coefficient 2	F-statistic	Df	r^2	p-value
Alouatta	−112.506	148.056	−13.500	4.451	2, 17	0.34	0.465
Ateles	−253.666	286.781	−53.090	1.513	2, 13	0.19	0.352
Plecturocebus	−309.981	448.999	−114.419	0.218	2, 10	0.04	0.537
Sapajus	1194.239	−1014.930	235.805	10.169	2, 19	0.52	**<0.001**
Aegyptopithecus[a]	929.551	−653.797	127.478	5.820	2, 18	0.39	**0.003**
Apidium[a]	1457.203	−1169.61	247.389	40.284	2, 29	0.74	**<0.001**

Abbreviations: vexDNE = convex Dirichlet normal energy; DNE = Dirichlet normal energy; RFI^{-1} = inverse of relief index; Df = degrees of freedom.
[a] Extinct genus.

fully developed) and extremely worn specimens (in which enamel and its associated attrition facets have been entirely removed). A potential solution to this issue lies in the implementation of 'pachymetric profiles' that measure the distance between a surface defining the EDJ and another defining the outer occlusal surface of an individual tooth (Thiery et al., 2017b). These distance profiles can be compared among individuals or taxa to characterize their relative evenness in enamel thickness. However, additional

methodological refinement will be required before thickness in homologous regions across teeth can be directly compared (see Bondioli et al., 2010; Zanolli et al., 2017).

In this study, DER and two additional metrics (RFI^{-1}, and OR^{-1}) were used as proxies for wear, with the latter two requiring validation to prove they consistently increase across the entire wear series. Figure 6 illustrates how each proxy changes across a wear series for *Al. palliata* and *S. apella*. Inverse RFI changes with wear according to expectations—increasing across the wear series for all taxa—indicating that overall crown height is reduced with wear regardless of whether or not enamel has been perforated. For specimens with DER > 0, RFI^{-1} is significantly positively correlated with DER across all six analyzed taxa (Table 5), in agreement with past studies (Ungar and M'Kirera, 2003; Ungar, 2004; Glowacka et al., 2016; Pampush et al., 2016a, 2018; Li et al., 2020; Cuesta-Torralvo et al., 2021). The same cannot be said for OR^{-1}. Prior analysis found no change in OR with DER in *Alouatta* (Pampush et al., 2018), which is unsurprisingly also true of OR^{-1} in this study (Fig. 6; Table 5). Both *Ateles* and *Plecturocebus* exhibit significant positive correlations between OR^{-1} and DER, as was expected, yet in *S. apella* specimens with exposed dentine, OR^{-1} and DER are significantly negatively correlated (Table 5). This latter finding is noteworthy, as OR^{-1} increase appears to correspond to wear in *S. apella* specimens that have not yet perforated their enamel (Figs. 6 and 8A), implying that the proxy performs as expected, reflecting loss of tissue in terms of relative cusp height—but only while DER = 0. These results raise serious concerns about the use of OR^{-1} as a proxy for wear across the entire wear series. While it may be an indicator of wear prior to enamel perforation in some taxa (Fig. 8), the finding that OR^{-1} behaves inconsistently with increasing wear among taxa with different diets (Table 5) and that it might in fact initially increase only to decrease after the enamel cap is perforated, as appears to be the case with *S. apella* (Fig. 6), indicates that OR^{-1} is an unreliable proxy of wear for considering how vexDNE changes across full wear series. In particular, this latter finding calls into question the significant negative correlation between vexDNE and OR^{-1} in *S. apella* (Table 7), as the lowest values of OR^{-1} (corresponding to the highest vexDNE values in this taxon) likely represent a combination of the least worn and most worn specimens.

Differences in the relationship between RFI^{-1} and OR^{-1} to macrowear likely derive from the distinct ways the 2D planometric footprint area reflect dental morphology. Both 2D footprints are planometric areas of the 3D dental surface above some point. In the RFI calculation, this point is the lowest point on the enamel cervix (Boyer, 2008), meaning the dental sidewalls contribute to both the 3D surface area and the 2D planometric area, whereas in the OR calculation, this point is the lowest point on the occlusal table (M'Kirera and Ungar, 2003). Inclusion of the dental sidewalls means the 2D footprint should be stable through advanced stages of wear, as the widest part of primate teeth is typically below the occlusal table where most wear takes place. In contrast, using the lowest point on the occlusal table as the cutoff for defining the 2D footprint creates issues if wear causes the position of that point—and thus the area of the tooth that will be projected into a plane for 2D area calculation—to change. This issue could potentially become even more exaggerated if the slope of the sidewalls of the taxa being compared differs, such that the rate at which the planometric area changes with wear is also different (Pampush et al., 2018). These issues likely explain why a good relationship between OR^{-1} and wear appears to hold prior to enamel perforation—at least for some taxa (Fig. 8)—but that OR^{-1} is variably, and often poorly, correlated with more advanced wear as measured by DER (Table 5). The finding that OR^{-1} decreases with wear in its later stages among some taxa (Fig. 6C) reflects the earlier finding that OR increases with wear among heavily worn specimens of *Pan troglodytes* and *Gorilla gorilla* (M'Kirera and Ungar, 2003). Despite the robust results relating vexDNE to OR^{-1} in OLS regressions for some taxa (Table 7), we find these issues with how OR^{-1} appears to reflect wear to be too great for it to be considered a suitable proxy of wear across the full wear series for all taxa in this study.

The ways in which vexDNE varies (or doesn't) with wear depends on whether DER or RFI^{-1} is used as wear proxy (Figs. 9 and 10; Table 7). Previous studies have utilized DER as the independent wear metric against which to measure change in DNE through wear series (Pampush et al., 2016a, 2018; Li et al., 2020). The choice of DER as an independent variable against which to compare a measurement of surface sharpness has a clear rationale—the exposed interface between harder enamel and softer dentine is argued to create 'compensatory blades' that replace the original crests and are further sharpened with more wear (Kay, 1981; Fortelius, 1985; Lanyon and Sanson, 1986; Lucas and Teaford, 1994; King et al., 2005; Ungar, 2015; Pampush et al., 2018). In support of this hypothesis, the DNE of molars with thin enamel, such as howling monkeys (*Alouatta*), increases with DER, as does the length of the exposed EDJ (Pampush et al., 2016a). In contrast, the DNE levels of closely related but more thickly enameled spider monkeys (*Ateles*) are maintained with increasing DER, retaining the presumed functional attributes of the primary occlusal morphology despite wear (Pampush et al., 2016a, 2018).

This study reanalyzed the wear series of *Alouatta* and *Ateles* previously described by Pampush et al. (2016a, 2018) by measuring vexDNE, rather than total surface DNE as in their earlier publications. Intriguingly, both atelid genera are found to have a significant positive relationship between vexDNE and DER (Fig. 9). This likely reflects the fact that the relationship between DNE and DER was already near significance for *Ateles* (Pampush et al., 2018: table 3). However, the relationship is considerably stronger and the coefficient (slope) much higher in *Alouatta* than in *Ateles* (Table 7), resulting in a much more dramatic increase in vexDNE with increasing macrowear in the former. Indeed, the range of vexDNE values in the macrowear series of *Alouatta* is more than 2.5 times that in *Ateles* (Table 3). Based on the much stronger relationship with DER and greater magnitude of change in vexDNE for *Alouatta* relative to *Ateles*, as well as the much higher absolute vexDNE values in *Alouatta* compared to *Ateles* (Fig. 5), the distinctions between these taxa observed by Pampush et al. (2018) hold.

Yet it is apparent that DER is not an ideal metric for measuring wear among all the species included in this study—particularly the thickly enameled taxa like *S. apella* (Figs. 6 and 9). Despite efforts to sample the broadest possible wear series for *S. apella*, only 13 of the 22 study specimens (~60%) exhibit any perforation of the enamel cap at all (Table 1), with the median DER value in *S. apella* equal to only 0.005, compared to 0.39 in *Alouatta* (Fig. 5). This finding results from the very thick enamel of *S. apella* (Dumont, 1995; Martin et al., 2003; Wright, 2005), where considerable crown wear occurs before the enamel is perforated (Fig. 6), and highlights a central question in investigation of DT change with wear: Is EDJ exposure, as a potential source of sharpness and/or loss of structural crown integrity (Lucas, 2006; Ungar, 2015) the only relevant feature to measure in dental wear, or does tissue loss prior to EDJ exposure influence functional properties such as crown sharpness?

Unlike the single-tailed, positively-skewed distribution of DER in *S. apella*, caused by the large number of specimens with DER = 0, RFI has a broader, double-tailed distribution (Fig. 5). Furthermore, RFI^{-1} is significantly positively correlated with DER in all taxa (Table 5) and increases with wear even prior to enamel perforation (Fig. 6C), making it an ideal proxy for comparing among differentially worn specimens with different enamel thicknesses. The OLS

regressions resulted in few significant correlations between vexDNE and RFI^{-1}. Among the extant taxa, only *Alouatta* has a significant, positive correlation between vexDNE and RFI^{-1} (Fig. 10; Table 7), indicating an increase in the sharpness of convex crown features with wear and mirroring past findings that used DER as a wear proxy (Pampush et al., 2016a, 2018). The lack of significant findings for the other extant taxa indicates that a linear regression of vexDNE against RFI^{-1} does not distinguish the effects of wear on convex dental sharpness in frugivorous *Ateles* and *Plecturocebus* from that of seed-predator *S. apella* (Table 7).

However, close inspection of the relationship between vexDNE and RFI^{-1} in *S. apella* (Fig. 10) reveals an interesting pattern not shared with the other extant taxa: Those specimens with the highest vexDNE values occur at either the lowest values of RFI^{-1}—e.g., American Museum of Natural History (AMNH) specimen 10571, the leftmost *S. apella* rendering in Figure 6—or among the highest values of RFI^{-1}—e.g., AMNH 133578, the rightmost *S. apella* rendering in Figure 6. Meanwhile, specimens around median values of RFI^{-1} exhibit the lowest vexDNE values. These findings strongly indicate that the relationship between convex crown sharpness and wear in *S. apella* is not linear, but rather curvilinear. To test this hypothesis, we performed post-hoc curvilinear regression analyses that examined a polynomial fit between vexDNE as the response variable and RFI^{-1} and $(RFI^{-1})^2$ as the predictor variables (a quadratic regression). Among extant taxa, a significant curvilinear relationship between vexDNE and wear as quantified through RFI^{-1} is only found for *S. apella* (Table 9). This relationship is characterized by an r^2 value greater than that of any of the linear relationships between vexDNE and either DER or RFI^{-1} for all taxa, with the exception of DER in *Alouatta* (Table 7).

The finding that vexDNE increases from moderately worn to heavily worn specimens of *S. apella* raises the possibility that a dental sculpting process, like that suggested to increase occlusal sharpness with wear in *Alouatta* (Pampush et al., 2018), also characterizes *S. apella*. However, this hypothesis suffers from several flaws that make it quite unlikely. First, crown sharpness increases consistently (linearly) in *Alouatta* as its teeth wear, whether that wear is measured with DER or RFI^{-1} (Figs. 9 and 10; Table 7). This finding fits with the expectations of dental sculpting as a process that shapes teeth continuously as they wear and that—importantly—alters some attribute of crown morphology that may ostensibly improve mastication (Ungar, 2015). The results for *S. apella* clearly do not support any such continuous increase in crown sharpness (assessed here as vexDNE) for the majority of their wear series. Whereas the moderately worn teeth of *Alouatta* are sharper than its unworn teeth, the moderately worn teeth of *S. apella* are blunt relative to its unworn morphology (Figs. 6 and 10). If the subsequent increase in vexDNE in *S. apella* wear series represented dental sculpting, this would imply that its teeth operate with a suboptimal morphology for the majority of its reproductive life. Second, the absolute values of vexDNE differ strongly between *Alouatta* and *S. apella* (Table 3), such that their ranges only overlap for the least worn specimens of *Alouatta* and either the least worn or most heavily worn specimens in *S. apella*. Third, the magnitude of difference between lowest and highest vexDNE values in *Alouatta* dwarfs that of the other taxa in this study (Table 3), emphasizing the dramatic change in this crown morphology attribute with wear. Finally, the majority of the diet in *Alouatta* is comprised of leaves (Glander, 1981) and—while vexDNE (like all DT metrics) lacks formal validation in studies of actual masticating primates—an increase in crown sharpness with wear to improve shearing capacity fits with the expectations of dental sculpting for this taxon (Ungar, 2015; Pampush et al., 2018). It is much less clear how an increase in crown sharpness would be of benefit to *S. apella*, which focuses on hard seed predation (Peres, 1991; Galetti and Pedroni, 1994; Fragaszy et al., 2004) and regularly employs crushing, rather than shearing, to access its primary food resources. Rather, the increase in vexDNE in the final wear stages of this hard-object feeder indicate to us a senescent decline in its dental morphology.

Relief index captures the relative height of the occlusal crown (Boyer, 2008). In *S. apella*, vexDNE declines with increasing RFI^{-1} before the enamel cap is perforated (Fig. 8), indicating that the cusps of these surfaces become lower, blunter, and more gently curving as enamel is removed through wear. Enamel loss on the lower molars of *S. apella* advances more rapidly on the buccal cusps and crests, producing low, rounded protoconids and hypoconids before enamel is perforated and before enamel loss progresses to the lingual cusps and crests (Fig. 6B). This pattern of wear may be the result of compressive, crushing forces during initial puncture-

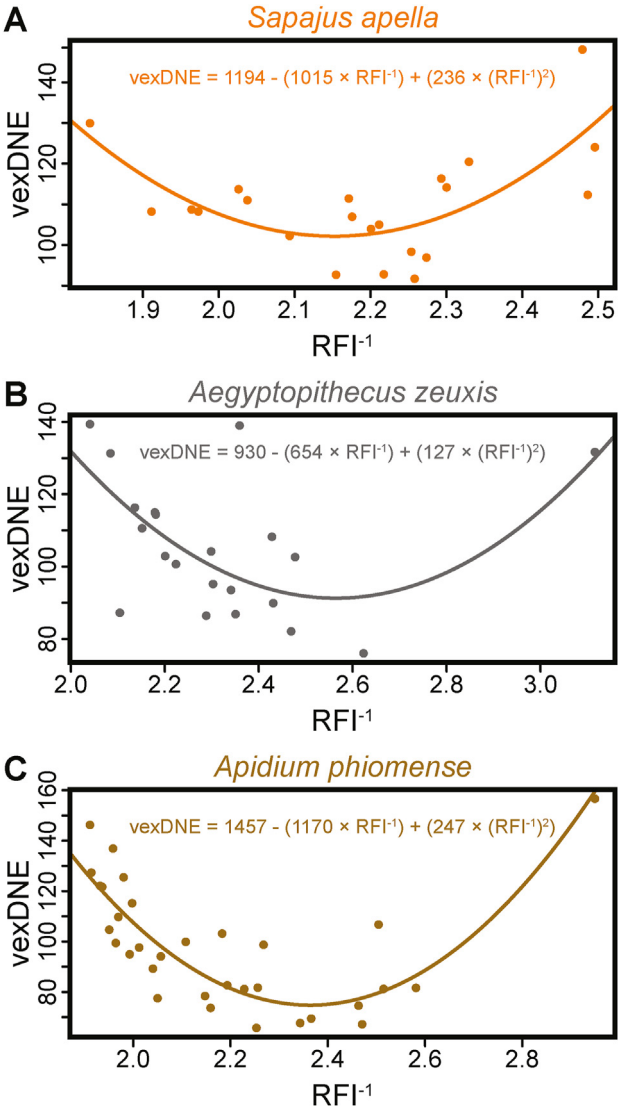

Figure 12. Bivariate plots of convex Dirichlet normal energy (vexDNE) against the inverse of relief index (RFI^{-1}) in A) *S. apella*, B) *Ae. zeuxis*, and C) *Ap. phiomense*. Lines indicate the best fit of quadratic regression models of vexDNE against RFI^{-1} (equations provided; see Table 9 for details). Note that for all three taxa, the majority of specimens have lower vexDNE than the least worn specimen (particularly moderately worn specimens where vexDNE is lowest), but that a single, heavily worn specimen corresponds to both high inverse of relief index and high vexDNE. These specimens are also illustrated as the rightmost specimens in figures of wear series: AMNH 133578 (*S. apella*) in Figure 6, DPC 24208 (*Ae. zeuxis*) and DPC 1041 (*Ap. phiomense*) in Figure 7.

crushing and Phase I of mastication. In contrast, relatively thinly enameled mantled howling monkeys (*Al. palliata*) appear to experience enamel loss on the lingual and buccal sides at nearly equal rate, and enamel perforation occurs even while cusps and crests are still high and sharp (Fig. 6A). For *Al. palliata*, this arrangement effectively adds sharpness to the surface by introducing a sharp EDJ interface at early stages of wear, rapidly increasing vexDNE with dentine exposure (Fig. 9). Unlike the atelids, and more like the pattern exhibited by *Plecturocebus*, the vexDNE of *S. apella* does not begin to increase with exposure of EDJ edges (Fig. 9). Furthermore, enamel perforation does not occur until later stages of wear in *S. apella*, when it rapidly spreads across the tooth and appears to represent a near surface-wide thinning of the enamel cap (Fig. 6B). Among worn *S. apella* specimens, only that with the greatest dentine exposure and one of the highest RFI^{-1} values—AMNH 133578—has a correspondingly high vexDNE value (Fig. 6; Table 1). This specimen represents the only *S. apella* M_2 in the sample for which dentine has been significantly excavated, resulting in higher vexDNE and helping to drive the curvilinear relationship between it and RFI^{-1} (Fig. 12A). Given these morphological extremes relative to other specimens in our *S. apella* sample, we interpret this individual as having reached a stage at which this tooth no longer functions or wears as it did throughout most of its lifespan (dental senescence), and not an adaptive improvement in shearing capacity. Convex DNE in *Plecturocebus* is uncorrelated with wear, no matter how wear is quantified (Table 7). This genus is further distinguished by having the narrowest range of DNE and vexDNE values of any in the study (Table 3). These findings add support to the conclusions reached by Li et al. (2020) that this small-bodied platyrrhine, with a diet consisting mostly of fruit alongside seasonally important leaves and insects (Kinzey, 1992; DeLuycker, 2021), has a dental morphology that resists wear and conserves its functional properties across the dental lifespan. Similarly, the frugivore *Ateles* shows limited evidence for change in occlusal sharpness with wear: Although a significant positive relationship was recovered between vexDNE and DER in *Ateles* (Table 7), the relationship is weak ($r^2 = 0.36$), it is not reflected in either the linear or quadratic regressions of vexDNE on RFI^{-1}, and the magnitude of change in vexDNE is relatively small compared to *Alouatta* (Table 3). The available evidence suggests that, like *Plecturocebus*, dental macrowear in *Ateles* introduces minimal change in occlusal sharpness and the presumed ability to process tough dietary items.

The contrasting patterns of change between vexDNE and wear proxies for *Alouatta* and *S. apella* highlight how these metrics differ between primate molars with vastly different relative enamel thicknesses. *Alouatta* has very thin enamel, whereas *Sapajus* has among the relatively thickest molar enamel caps in platyrrhines (Dumont, 1995; Shellis et al., 1998; Martin et al., 2003; Wright, 2005; Olejniczak et al., 2008; Pampush et al., 2013; see Fig. 6). The results reported here indicate that enamel thickness and distribution may be highly influential on how DT changes with wear. Dental sculpting appears to be dependent on perforation of the enamel cap (Fortelius, 1985; Popowics and Fortelius, 1997; Ungar, 2015; Pampush et al., 2018), and therefore enamel thickness will necessarily impact the production and magnitude of this phenomenon. Thus, it is essential that enamel thickness be considered during future interspecific studies of macrowear (e.g., when examining a frugivore with relatively thin enamel versus one with thicker enamel). They further demonstrate that different wear proxies may be appropriate for analysis of different primate taxa, with implications for interpreting diet in the fossil record. Finally, these results underscore the importance of developing methodologies for comparing enamel thickness distributions (Bondioli et al., 2010; Zanolli et al., 2017) across the occlusal surface among different taxa and individuals at different stages of wear.

In summary, the linear OLS regression results of vexDNE against DER and vexDNE against RFI^{-1} for *Alouatta*, *Ateles*, *Plecturocebus*, and *S. apella* are largely in agreement (Table 7). Inverse RFI is the preferred proxy for wear in drawing comparisons among these taxa as it is significantly positively correlated with DER for all taxa once enamel is perforated (Table 5), but also permits the inclusion of thickly-enameled specimens of *S. apella* that experience modification in crown morphology before the enamel is perforated (Table 6; Fig. 8A). Convex DNE responds distinctly to increasing RFI^{-1} based on the primary diet of the taxon in question: In folivorous *Alouatta*, vexDNE has a significant, linear positive correlation with RFI^{-1} (Table 7; Fig. 10). In frugivorous, seed-ingesting *Ateles* and *Plecturocebus* (Russo et al., 2005; González-Zamora et al., 2009), there is no correlation between vexDNE and RFI^{-1} (Tables 7 and 9; Fig. 10). In *S. apella*, vexDNE has a significant curvilinear relationship with RFI^{-1}, initially declining and staying low through moderate stages of wear, then increasing in the most worn specimens (Table 9; Fig. 12). These differences likely arise from distinctions in the constructional morphology of the molars of these primates with distinct dietary strategies.

4.3. Enamel thickness and wear dynamics

Several different physiological mechanisms, including the salivatory response and interdental sensory feedback during chewing, trigger the avoidance of biting down too hard on particles that may damage teeth (either through wear or fracture) during mastication (Lucas, 2006). Additionally, several intrinsic factors of hard dental tissues have evolved to further resist wear. These primarily include increasing tooth height (hypsodonty: Simpson, 1944; Stirton, 1947; Van Valen, 1960; Fortelius, 1985; Janis and Fortelius, 1988; Williams and Kay, 2001), evolving complex enamel microstructure patterns (decussation: Maas, 1993; Maas and Dumont, 1999; Chai et al., 2009; Yang et al., 2022), and increasing enamel thickness (Molnar and Gantt, 1977; Kay, 1981; Dumont, 1995; Lucas et al., 2008; Vogel et al., 2008; McGraw et al., 2012; Pampush et al., 2013). No primates in our sample exhibit hypsodonty, but enamel microstructure and thickness do vary considerably among the taxa in this study, and likely play a role both in macrowear expression and how wear affects DT (Pampush et al., 2018; Foster and Constantino, 2020; Yang et al., 2022).

Alouatta, *Ateles*, *S. apella*, and *Ae. zeuxis* all have molar enamel decussation (Teaford et al., 1996; Martin et al., 2003; Darnell et al., 2010). In the case of *Alouatta*, enamel decussation is more pronounced closer to the EDJ, like the pattern observed in humans (Darnell et al., 2010). Decussation seems more developed in the latter three taxa, with Martin et al. (2003) describing the decussating prisms of both *Ateles* and *S. apella* as composing the inner 2/3 of enamel and simple, radial enamel composing the outer 1/3, while enamel decussation is visible even closer to the outer enamel surface in *Ae. zeuxis* (Teaford et al., 1996). In contrast, both *Plecturocebus* and *Ap. phiomense* are characterized by simple, radial enamel prisms oriented from the internal EDJ to the outer enamel surface (Teaford et al., 1996; Martin et al., 2003). While the importance of enamel decussation has been emphasized for dissipating crack propagation and therefore aiding in resistance to enamel failure under high load conditions (von Koenigswald et al., 1987; Maas and Dumont, 1999; Rensberger, 2000; Shimizu et al., 2005; Lucas et al., 2008), the patterns of enamel decussation exhibited by extant taxa with relatively well-characterized diets do not map simply onto the hardness of commonly eaten foods. For example, although both *Ateles* and *S. apella* have similar patterns of enamel microstructure, *Ateles* is a seed disperser—it has a relatively

soft, fruit-dominated diet (González-Zamora et al., 2009) and either spits seeds out or ingests them whole, passing them through the digestive tract (Russo et al., 2005). In contrast, *S. apella* is a seed predator—it regularly feeds on hard, brittle seeds that are crushed before swallowing (Terborgh, 1983; Peres, 1991; Galetti and Pedroni, 1994; Fragaszy et al., 2004). *Plecturocebus*—which, like *Ateles*, occasionally ingests hard seeds (Kinzey, 1992) but then expels them or swallows them whole without chewing (DeLuycker, 2021)—has only radial enamel that would seemingly be poor at resisting the tensile forces produced in enamel at the EDJ under compressive load from a structural biomaterials standpoint (Lucas, 2006; Lucas et al., 2008). In short, enamel microstructure is not a straightforward predictor of whether a primate frugivore is a seed disperser or a seed predator that would be anticipated to produce high occlusal crushing forces. Comparisons between molar enamel microstructure patterns and body size among mammals broadly (von Koenigswald et al., 1987), and in primates particularly (Maas and Dumont, 1999), indicate a body size threshold of about 1.5 kg above which enamel decussation is common and below which it is absent. *Plecturocebus* and *Ap. phiomense* fall below this body size threshold (Conroy, 1987; Smith and Jungers, 1997; Perry et al., 2018) and, unsurprisingly, do not exhibit enamel decussation (Teaford et al., 1996; Martin et al., 2003).

The uniquely thick enamel of *Ap. phiomense* among living and fossil primates of its size has sparked a variety of competing interpretations as to its purpose in diet and/or oral processing (Fleagle and Kay, 1985; Teaford et al., 1996; Fleagle, 1999; Maas and Dumont, 1999). A natural extant comparison to *Ap. phiomense* based on small body size and thick molar enamel is *S. apella*, though its body mass is still approximately double that estimated for *Ap. phiomense* (Smith and Jungers, 1997; Martin et al., 2003; Wright, 2005). This difference in body size will influence maximal bite force production (Deutsch et al., 2020), with the larger *S. apella* capable of producing greater absolute force. Factors such as gape and its influence on object positioning along the toothrow also change with body size and will thus influence muscle architecture (Laird et al., 2020) and bite force production to insure against distraction at the temporomandibular joint (Spencer, 1998). *Sapajus apella* also has enlarged chewing muscle physiologic cross-sectional areas relative to other capuchins in the genus *Cebus*, permitting large bite force production without creating excursion at the temporomandibular joint (Taylor and Vinyard, 2009). As a result of these factors, *Ap. phiomense* was almost certainly not capable of producing the same amount of bite force as *S. apella*. However, this does not preclude it from producing bite forces that are large for its body size or appropriate for brittle fracture of smaller hard objects (Lucas et al., 2008).

Sapajus apella and *Ap. phiomense* exhibit several additional similarities, including single-tailed DER distributions with median values of ~0 (Fig. 5), decline in vexDNE with increasing RFI^{-1} prior to enamel perforation (Table 6; Fig. 8), and a significant quadratic relationship between vexDNE and RFI^{-1} (Table 9; Fig. 12), although these characteristics are also found (to a degree) in *Ae. zeuxis*, which has relatively thinner enamel. Cross-sections through the M_2s of *S. apella* (Fig. 6) illustrate that with tooth wear, the molar cusps of *S. apella* become generally blunter and more rounded. This process begins early in the wear sequence, before the thick enamel of *S. apella* is perforated (Fig. 8). When its molars are thus worn, the angle at which radial enamel prisms intersect the occlusal surface is altered. This generally has the effect of lowering the angle at which radially-oriented enamel prisms (the outermost 1/3 of enamel in *S. apella*; Martin et al., 2003) approach the surface, which improves resistance to tensile stresses created when a particle is dragged across the occlusal surface during abrasive wear (Shimizu et al., 2005; Foster and Constantino, 2020). Differences in enamel prism orientation have been shown to affect the rate at which enamel wears; when distinct enamel textures abut, opportunities are created to develop a self-sharpening enamel edge (Hunt et al., 2023). In *S. apella*, significant dental tissue loss can occur before enamel is perforated (Fig. 6), and once this does occur, the dentine is not rapidly excavated into sharp borders with enamel, but rather contributes to a low-crowned, blunt surface topography. These trends resemble those found in human molars, which decline in a variety of DT metrics with age (Cuesta-Torralvo et al., 2021). Humans are also characterized by very thick enamel, which has been suggested to have been inherited from a previous ecology focused on hard-object consumption (Jolly, 1970; Walker, 1981) or to be a result of long lifespan (Pampush et al., 2013). The mineral composition of the enamel prisms and interprismatic enamel has been shown to differ in humans, with the properties of the enamel crystallites being reflected in the lattice organization of enamel tissue (Free et al., 2022). This indicates an intermediate scale (larger than crystallites, and smaller than bundles of enamel prisms) at which enamel microstructure may influence its performance and wear, which may be particularly pronounced in thickly-enameled taxa.

The enamel properties of *S. apella* are well-suited to fracture hard (but brittle) food objects: Breaking down increasingly smaller food particles requires an expanded occlusal surface (Lucas, 2006; Lucas and Omar, 2012), and the molars of *S. apella* are apparently effective at reducing large, brittle palm nuts to a size sufficient for swallowing (Terborgh, 1983), potentially through an occlusal surface expansion relative to its sister genus *Cebus* (Wright, 2005). They have low, bulbous cusps with wide bases that increase their zone of action and reduce particle slippage, which is beneficial when crushing brittle objects (Lucas, 2006). Finally, the thickly-enameled molars of *S. apella* incorporate radial prisms in the outer 1/3 and decussating zones of differentially-oriented prisms in the inner 2/3—an arrangement that should be highly resistant both to abrasive (shearing) forces at the occlusal surface, as well as tensile forces that can initiate radial crack propagation from the EDJ (Maas, 1993; Teaford et al., 1996; Maas and Dumont, 1999; Lucas et al., 2008; Ungar, 2015).

In terms of molar shape, *Ap. phiomense* bears a striking resemblance to *S. apella*, but with even greater relative enamel thickness (Fleagle and Kay, 1985; Teaford et al., 1996), permitting considerable wear before enamel is breached (Figs. 7 and 8; Kay and Simons, 1983). It does, however, lack enamel prism decussation, consistent with its small body size (Teaford et al., 1996; Maas and Dumont, 1999). Although this lack of decussation theoretically makes the molars of *Ap. phiomense* more susceptible to crack initiation at the EDJ, crack initiation is also compensated by increasing the relative thickness of enamel (Lucas et al., 2008). This relocates stress concentration toward the outer occlusal surface where damage may occur in the form of pitting or chipping. These complex factors are all likely to affect how DT changes with wear, as well as how teeth interact with food items, and must therefore be considered when generating dietary interpretations of extinct taxa such as *Ae. zeuxis* and *Ap. phiomense*.

4.4. *Paleodietary interpretations for* Aegyptopithecus zeuxis *and* Apidium phiomense

Previous analyses have measured the SQs of unworn teeth, incidence and size of microwear features, and enamel microstructure of *Ae. zeuxis* and *Ap. phiomense* in order to draw dietary inferences (Kay and Simons, 1980a, 1980b; Teaford et al., 1996). Our analysis of dental topographic change across a macrowear series offers an additional dimension for dietary inference from those previously employed—extracting information about a property presumed to influence dental masticatory efficiency (i.e., the influence of sharpness on the

ability of molars to comminute food) as teeth wear. Here we evaluate and contextualize these findings with the results of prior work and additional paleobiological and ecological data for *Ae. zeuxis* and *Ap. phiomense* in order to make dietary interpretations that are supported by multiple lines of evidence.

Based on unworn teeth, Kay and Simons (1980a, 1980b) found that the SQs of *Ae. zeuxis* and *Ap. phiomense* were most similar to extant frugivorous anthropoids (sensu lato, including consumers of hard-objects such as *Sapajus* and/or soft fruits such as *Hylobates* and *Pan*). This accords with the analysis of unworn teeth in this study, in which the vexDNE of the two Fayum taxa most closely resembles that of extant platyrrhine seed predators (Fig. 3; Table 2). These findings are also in agreement with the molar surface microwear data of Teaford et al. (1996), who reported that the irregular sizing of microwear pits in *Ae. zeuxis* was like the pattern observed in their group of extant 'mixed feeders' (including taxa such as *Cebus capucinus* and *Ateles* sp.) and hard-object feeders (*S. apella*). The frequency of microwear features (pits and scratches) Teaford and colleagues observed in *Ap. phiomense* was statistically indistinguishable from that of *Ae. zeuxis*, although the pattern of regular, small pits in *Ap. phiomense* did not appear in any of the extant taxa they evaluated.

Three broad patterns have been observed to date for how occlusal sharpness changes with macrowear (Figs. 9, 10 and 12): 1) an increase in sharpness with wear in *Alouatta*, linked to its thin enamel and folivorous diet (Pampush et al., 2016a, 2018); 2) no (or minor) change in sharpness with wear in *Ateles* and *Plecturocebus* (Pampush et al., 2018; Li et al., 2020); and 3) an initial decline in sharpness with wear followed by a return to the level of sharpness exhibited by unworn teeth in the most worn specimens of *S. apella* (this study). The relationships between vexDNE and wear in the two Fayum taxa investigated here resemble one another (Tables 7 and 8). Neither shows any evidence of correlation between vexDNE and DER (Fig. 9), which is unsurprising given the large proportion of individuals lacking dentine exposure (DER = 0), particularly in *Ap. phiomense* (Fig. 5; Tables 1 and 3). *Apidium phiomense* has a significant negative linear correlation between vexDNE and RFI^{-1}, although the relationship between these variables is weak ($r^2 = 0.21$; Table 7). Finally, both genera exhibit a significant quadratic correlation between vexDNE and RFI^{-1} (Table 9), with a greater strength than nearly all of linear correlations between vexDNE and wear (Table 7). These data indicate that the two Fayum species measured here have a different relationship between occlusal sharpness and wear than that exhibited by either extant soft-fruit eater—*Ateles* or *Plecturocebus*. Whereas these two extant taxa show little or no correlation between vexDNE and any wear proxy (i.e., a maintenance of primary occlusal shearing ability), the extinct taxa decline in vexDNE and maintain lower sharpness values through moderate wear stages—a trend that is particularly apparent in *Ap. phiomense* (Fig. 12C), as well as stronger ($r^2 = 0.74$; Table 9) than the linear relationship of vexDNE to any wear proxy for any taxon (Table 7). This finding implies either that the diets of *Ae. zeuxis* and *Ap. phiomense* emphasized shearing so little that its maintenance was subject to minimal selection acting on molar sharpness, or that these taxa exhibited dietary flexibility and/or compensatory feeding behaviors (such as shifting to softer food items) as their teeth wore down, as has been observed in ring-tailed lemurs (Cuozzo and Sauther, 2006; Millette et al., 2009). Overall, changes in vexDNE with wear in *Ae. zeuxis* and *Ap. phiomense* bear the greatest resemblance with the trends exhibited by the extant hard-object specialist *S. apella* (Table 9; Fig. 12).

However, these results cannot be used to simply infer that the diets of *Ae. zeuxis* and *Ap. phiomense* were therefore analogous to that of *S. apella* (i.e., frequently feeding on relatively large, hard seeds) without further evaluation of their known paleobiology and ecology. For instance, *Ae. zeuxis* was a much larger animal than is *S. apella*, with relatively thinner enamel (Teaford et al., 1996; Martin et al., 2003). A similar constellation of traits has been observed in other extant hard-object feeders, notably the pitheciine platyrrhines *Cacajao*, *Chiropotes*, and *Pithecia* (Martin et al., 2003; Kay et al., 2013). Like extant pitheciines, *Ae. zeuxis* also exhibits molar enamel decussation throughout most of its thickness and a high incidence of irregular-sized microwear pitting, which has been considered a hallmark of hard-object feeding (Teaford et al., 1996). The robust incisor and canine morphology of *Ae. zeuxis* (Kay and Simons, 1980b; Simons et al., 2007) may also have been well-suited to sclerocarpic foraging, a feeding strategy of pitheciines (Van Roosmalen et al., 1988; Kinzey and Norconk, 1990; Kinzey, 1992). While extant pitheciines have been analyzed in terms of their unworn DT (Ledogar et al., 2013), future studies should consider how their topography (particularly vexDNE) varies with wear when measured by RFI^{-1} and compare them with *S. apella* and *Ae. zeuxis*. The findings of low molar relief and total surface DNE values as well as high microwear complexity in the Miocene colobine *Mesopithecus* have similarly been inferred to have been indicative of hard-object consumption and/or seed predation (Thiery et al., 2017a, 2021).

Apidium phiomense possessed very thick enamel for its size—a similarity with *S. apella*. Indeed, on the basis of this characteristic, *Ap. phiomense* has been compared to *S. apella* as a potential hard-object feeder (Fleagle and Kay, 1985). Analogous to the most worn *S. apella* specimen (AMNH 133578, see above), the most worn specimen of *Ap. phiomense* (DPC 1041; Fig. 7; Table 1) is the only individual to exhibit significant dentine excavation. Like AMNH 133578 for *S. apella*, DPC 1041 has high vexDNE compared to moderately worn specimens, helping to drive the significant curvilinear relationship with RFI^{-1} (Fig. 12). Indeed, without inclusion of this heavily-worn specimen, the change in sharpness and wear would be strongly linearly negative—a relationship still recovered as significant for *Ap. phiomense* even despite inclusion of DPC 1041 (Table 7). However, these taxa do differ in terms of their microwear traits: *S. apella* has microwear features that include many heterogeneous pits, as do other hard-object feeders (Teaford, 1985; Scott et al., 2006; Teaford et al., 2020), whereas the microwear in *Ap. phiomense* is characterized by a large number of small, regularly proportioned pits—a characteristic unique in the dataset of Teaford et al. (1996). Based on these results and the regularity of radially oriented enamel crystallites, Teaford and colleagues argued that the enamel of *Ap. phiomense* would have been better suited to resisting large amounts of abrasion. Yet it is difficult to envision an ecology that would incur such high abrasion in a primate that was likely arboreal (Kay and Simons, 1980b; Fleagle and Simons, 1995) with a low-crowned, blunt dentition ill-suited for slicing tough plant materials (Kay and Simons, 1980b; this study). This is bolstered by data showing that arboreal primates in dry environments exposed to novel potential grit sources such as ashfall do not appear to wear their molars at a faster rate (Spradley et al., 2016). Frequent dental processing of tough seed pods such as that of *Tamarindus indica*, which is frequently consumed by frugivorous *Lemur catta* in Madagascar and influences their DT (Yamashita et al., 2016) may present a potential source of dietary abrasives for a low-crowned taxon such as *Ap. phiomense*.

Microwear interpretations have traditionally followed a model whereby mastication of tough foods produces more scratches and greater surface texture anisotropy due to the lengthened shearing chew stroke and ductility of consumed foods, while harder, more brittle foods produce a greater ratio of pits to scratches and greater surface complexity during high magnitude crushing actions (Teaford et al., 1996; Scott et al., 2006; Ungar and Sponheimer, 2011; Grine et al., 2012; Borrero-Lopez et al., 2015; Ungar et al., 2017). While Teaford et al. (1996) interpreted their microwear

findings within this framework, recent feeding trials with living animals indicate that microwear texture is generated through a much more complex interaction among food material properties, grit load, and oral processing behaviors (Teaford et al., 2021; Mihlbachler et al., 2022). Furthermore, in vitro wear experiments have failed to replicate the enamel pitting proposed to be indicative of hard, woody seed consumption (van Casteren et al., 2020), with the frequent observation that microwear texture is not highly complex in many robust hominins or in the Miocene ape *Sivapithecus* that possess derived craniodental traits commonly interpreted as indicative of hard-object feeding (Teaford and Walker, 1984; Ungar and Sponheimer, 2011; Lucas et al., 2013).

The multitude of small microwear pits observed in *Ap. phiomense* is also consistent with damage caused by stress limited to the outer enamel surface as a result of the thick enamel in this taxon (Lucas et al., 2008). The regularity of the dimensions of those pits described by Teaford et al. (1996) implies the frequent consumption of a commonly available dietary resource with a reliable pattern of fracture. The small size of the pits is consistent with contacting small hard objects that cause localized plastic deformation of the outer enamel coat, unlike larger hard objects that would cause flexing of the enamel cap (Lucas, 2006; Lucas et al., 2008). Such microcontacts have been proposed to occur between enamel and hard consumed items, or even potentially between the enamel of occluding teeth, possibly leading to fracturing at enamel prism boundaries (Teaford and Runestad, 1992). If the brittle component of the food (e.g., the endocarp of a fruit or the seed itself) were surrounded by fluid-expressing mesocarp, its increased hydration should result in a reduced work of fracture with more consistent fracturing patterns (Williamson and Lucas, 1995). The low, mortar-and-pestle shape of *Ap. phiomense* molars, as well as the presence of its centroconid, would be advantageous for efficient consumption of such small, brittle, hydrated materials (Lucas, 2006).

The Egyptian Jebel Qatrani Fm. that has produced fossils of *Ae. zeuxis* and *Ap. phiomense* has also yielded many specimens of fossil fruits (Bown et al., 1982), including several with large, likely durable seeds. These include seeds of the genus *Canarium*, which produces a variety of edible, widely consumed nuts. *Canarium* consumption has been observed in several species of Malagasy lemurs, including the aye–aye for whom it is the second-most common food type, which it crushes with its low-crowned, bunodont molars (Randimbiharinirina et al., 2018). Larger seeds of the family Annonaceae (with a variety of extant members that are consumed by living primates) are also reported from the Jebel Qatrani Fm. (Bown et al., 1982), although they have not been reported from the same stratigraphic level as *Ae. zeuxis* and *Ap. phiomense*. The seeds of these fruits would have been covered in fleshy rinds. The most common fossil fruit of the Jebel Qatrani Fm. is that of the extant Australasian taxon *Epipremnum*, a vine with a compound fruit infructescence that incorporates several small, kidney-shaped seeds into each berry, likely within a juicy mesocarp surrounded by a potentially abrasive pericarp (Bown et al., 1982). The berry-like fruits of this genus are consumed by extant primates such as macaques (Lucas and Corlett, 1991), and it has been suggested as a potential dietary resource for *Ae. zeuxis* by previous authors (Simons, 1987). Another fruit from the Jebel Qatrani Fm. is *Pyrenacantha*—drupes with a fleshy exocarp and mesocarp surrounding a single pit of hardened endocarp encasing the seed. There is no direct evidence for consumption of any particular fruit by either *Ae. zeuxis* or *Ap. phiomense*, nor direct evidence for the co-occurrence of any plant fossils with Fayum primates. Nevertheless, *Epipremnum* and *Pyrenacantha* are found at the level of Fossil Quarry G, where a different species of *Apidium* (*Ap. moustafai* Simons 1962) and *Propliopithecus*, a close relative of *Aegyptopithecus* (Seiffert, 2007) are also present. The dietary strategies developed by these earlier taxa in association with contemporaneous flora may have influenced the diets and dental morphology of the fossil taxa analyzed in this study. It is clear that the Oligocene Rupelian flora of the Fayum contained a variety of robust fruits with durable seeds, the relatives of which are consumed by many extant primates.

The finding of a quadratic relationship between vexDNE and tooth wear in *S. apella* and both fossil primate taxa analyzed here (Fig. 12), as well as the similar pattern of decline in sharpness with wear prior to enamel perforation observed in *S. apella* and *Ap. phiomense* (Fig. 8), support the interpretation that *Ae. zeuxis* and *Ap. phiomense* would have commonly encountered brittle, mechanically challenging foods like those frequently consumed by *S. apella*. We consider the drupes and arronaceous fruits with their hard seeds to be good examples of the kinds of dietary resources that would likely explain the constellation of dental traits observed in *Ae. zeuxis*. Likewise, the smaller, but common seeds possibly suspended in a liquid-expressing mesocarp of *Epipremnum* are a good fit for the various dental traits found in the molars of *Ap. phiomense*.

These findings lend support to the hypothesis that tough, leafy diets were relatively uncommon among early anthropoids. Given that *Ae. zeuxis* craniofacial morphology is broadly similar to that of the younger Miocene hominoid *Afropithecus* (Leakey et al., 1991) and cercopithecoid *Victoriapithecus* (Benefit and McCrossin, 1993), its feeding strategy must be carefully considered as potentially relevant for understanding that of the last common ancestor of catarrhine primates. Change in DT with wear is a ripe topic for additional research, particularly within primate taxa that are well suited for tough diets, such as bilophodont cercopithecoids, which to date have received limited attention in DT studies (Bunn and Ungar, 2009; Winchester, 2016). In particular, DT analysis of the Oligocene-Miocene fossil radiation that produced cercopithecoids (Miller et al., 2009; Stevens et al., 2013) may shed light on the dietary material properties for which their teeth were best suited. This is particularly relevant given the apparently mosaic fashion in which bilophodonty arose, including being completely absent from the primitive cercopithecoid *Alophia metios* (Rasmussen et al., 2019). The dental topography of *Ae. zeuxis* and *Ap. phiomense* and its dietary implications provide useful grounding for such investigations.

5. Conclusions

Here we examine occlusal sharpness in M_2 wear series of two fossil Oligocene anthropoids (*Ae. zeuxis* and *Ap. phiomense*), ranging from unworn to heavily worn, with four extant platyrrhine primates serving as extant models (*Alouatta*, *Ateles*, *Plecturocebus*, and *S. apella*). Comparison of DNE and vexDNE in a subset of lightly worn *Ae. zeuxis* and *Ap. phiomense* M_2s against a large, diverse sample of unworn platyrrhine M_2s indicates that the sharp occlusal sulci present in the fossil taxa influence total surface DNE—producing values that resemble those of extant platyrrhine insectivores in the case of *Ap. phiomense*—while their vexDNE is more in line with frugivores that predate on hard seeds. We regard the convex component of crown sharpness associated with cusps and ridges to be more functionally relevant in mastication than are sharp sulci between the cusps, and therefore advocate for quantification of occlusal sharpness using only vexDNE when making dietary investigations.

When evaluating the various proxies available to quantify tissue loss across wear series, RFI^{-1} increases consistently with wear regardless of enamel perforation and is therefore preferred for making comparisons between taxa with different enamel thicknesses. Convex DNE increases with RFI^{-1} in the folivorous, thinly enameled *Alouatta* and has a quadratic relationship that initially decreases with RFI^{-1} in the hard-object feeding, thickly enameled

species *S. apella*. Both Oligocene anthropoids exhibit a quadratic relationship between vexDNE and RFI^{-1} that resembles that of *S. apella*. The findings of change in molar sharpness with wear in *Ae. zeuxis* and *Ap. phiomense* reported here, in addition to previous qualitative and quantitative studies of their morphology that evaluated shearing crest development, enamel thickness and microwear, permit a reinterpretation of diet in these taxa. Based on the totality of this evidence, we interpret *Ae. zeuxis* as having likely fed on soft fruits encased in a tough pericarp and potentially pursuing a foraging strategy akin to extant pitheciine platyrrhines like *Pithecia*. We interpret *Ap. phiomense* as having a diet that incorporated more hard materials, perhaps the seeds of several fruits with small hard seeds encased in a soft mesocarp and, aided by its thick molar enamel, likely consuming objects with relatively consistent fracture mechanics. Future work should include examination of a wider range of extant primates, including pitheciines, cercopithecoids, and hominoids. As research on the effects of macrowear on dental topography progresses, the relevance of enamel thickness and its properties for dietary inference continues to be crucial. The phenomenon of dental sculpting may well be dependent on enamel cap perforation, and therefore enamel thickness (both overall, and its distribution on a single tooth crown) likely dictates in which primate taxa it is able to manifest. Additional study of the changes in enamel thickness distribution, enamel prism orientation, and the chemical properties of enamel across the occlusal surface in wear series bears promise for revealing how wear influences dental topography.

Acknowledgments

We thank Matthew Borths and Steven Heritage of the Duke Lemur Center Museum of Natural History for curating and providing access to μCT scans of Fayum primates hosted on MorphoSource. Hesham Sallam of The American University in Cairo and Mansoura University Vertebrate Paleontology Center was instrumental in collecting much of the original fossil scan data. Scott Wing of the National Museum of Natural History, Smithsonian Institution, provided helpful insight on the diversity and morphology of fossil Fayum fruits. The authors also thank Sara Ketelsen and the other collections staff of the American Museum of Natural History for their gracious loan of *Sapajus apella* specimens. This manuscript was improved by the insightful comments and critiques of two anonymous reviewers, Michael Berthaume (London South Bank University), Erik Seiffert (University of Southern California), and Mark Teaford (Touro University California), Associate Editor, to all of whom the authors are grateful for their significant time and effort. This work was supported by the National Science Foundation (grant numbers BCS 2018769, BCS 2018779).

Supplementary Online Material

Supplementary Online Material related to this article can be found at https://doi.org/10.1016/j.jhevol.2023.103387.

References

Allen, K.L., Cooke, S.B., Gonzales, L.A., Kay, R.F., 2015. Dietary inference from upper and lower molar morphology in platyrrhine primates. PLoS One 10, e0118732.
Almécija, S., Tallman, M., Sallam, H.M., Fleagle, J.G., Hammond, A.S., Seiffert, E.R., 2019. Early anthropoid femora reveal divergent adaptive trajectories in catarrhine hind-limb evolution. Nat. Commun. 10, 4778.
Anapol, F., Lee, S., 1994. Morphological adaptation to diet in platyrrhine primates. Am. J. Phys. Anthropol. 94, 239–261.
Andrews, P., 1981. Species diversity and diet in monkeys and apes during the Miocene. In: Stringer, C.B. (Ed.), Aspects of Human Evolution. Taylor & Francis, London, pp. 25–61.
Andrews, P., Aiello, L.C., 1984. An evolutionary model for feeding and positional behaviour. In: Chivers, D.J., Wood, B.A., Bilsborough, A. (Eds.), Food Acquisition and Processing in Primates. Plenum, New York, pp. 429–466.
Benazzi, S., Nguyen, H.N., Kullmer, O., Hublin, J.-J., 2013. Unravelling the functional biomechanics of dental features and tooth wear. PLoS One 8, e69990.
Benefit, B.R., McCrossin, M.L., 1993. Facial anatomy of *Victoriapithecus* and its relevance to the ancestral cranial morphology of Old World monkeys and apes. Am. J. Phys. Anthropol. 92, 329–370.
Berthaume, M.A., 2014. Tooth cusp sharpness as a dietary correlate in great apes. Am. J. Phys. Anthropol. 153, 226–235.
Berthaume, M.A., Schroer, K., 2017. Extant ape dental topography and its implications for reconstructing the emergence of early *Homo*. J. Hum. Evol. 112, 15–29.
Berthaume, M.A., Delezene, L.K., Kupczik, K., 2018. Dental topography and the diet of *Homo naledi*. J. Hum. Evol. 118, 14–26.
Berthaume, M.A., Winchester, J., Kupczik, K., 2019. Effects of cropping, smoothing, triangle count, and mesh resolution on 6 dental topographic metrics. PLoS One 14, e0216229.
Berthaume, M.A., Lazzari, V., Guy, F., 2020. The landscape of tooth shape: Over 20 years of dental topography in primates. Evol. Anthropol. 29, 245–262.
Bondioli, L., Bayle, P., Dean, C., Mazurier, A., Puymerail, L., Ruff, C., Stock, J.T., Volpato, V., Zanolli, C., Macchiarelli, R., 2010. Morphometric maps of long bone shafts and dental roots for imaging topographic thickness variation. Am. J. Phys. Anthropol. 142, 328–334.
Borrero-Lopez, O., Pajares, A., Constantino, P.J., Lawn, B.R., 2015. Mechanics of microwear traces in tooth enamel. Acta Biomater. 14, 146–153.
Borries, C., Lu, A., Ossi-Lupo, K., Larney, E., Koenig, A., 2011. Primate life histories and dietary adaptations: A comparison of Asian colobines and macaques. Am. J. Phys. Anthropol. 144, 286–299.
Bown, T.M., Kraus, M.J., Wing, S.L., Fleagle, J.G., Tiffney, B.H., Simons, E.L., Vondra, C.F., 1982. The Fayum primate forest revisited. J. Hum. Evol. 11, 603–632.
Boyer, D.M., 2008. Relief index of second mandibular molars is a correlate of diet among prosimian primates and other euarchontan mammals. J. Hum. Evol. 55, 1118–1137.
Boyer, D.M., Winchester, J., Kay, R.F., 2015. The effect of differences in methodology among some recent applications of shearing quotients. Am. J. Phys. Anthropol. 156, 166–178.
Boyer, D.M., Gunnell, G.F., Kaufman, S., McGeary, T.M., 2016. MorphoSource: Archiving and sharing 3-D digital specimen data. Paleontol. Soc. Pap. 22, 157–181.
Bunn, J.M., Ungar, P.S., 2009. Dental topography and diets of four old world monkey species. Am. J. Primatol. 71, 466–477.
Bunn, J.M., Boyer, D.M., Lipman, Y., St Clair, E.M., Jernvall, J., Daubechies, I., 2011. Comparing Dirichlet normal surface energy of tooth crowns, a new technique of molar shape quantification for dietary inference, with previous methods in isolation and in combination. Am. J. Phys. Anthropol. 145, 247–261.
Bush, E.C., Simons, E.L., Allman, J.M., 2004. High-resolution computed tomography study of the cranium of a fossil anthropoid primate, *Parapithecus grangeri*: New insights into the evolutionary history of primate sensory systems. Anat. Rec. 281A, 1083–1087.
Butler, P.M., 1952. The milk molars of Perissodactyla with remarks on molar occlusion. Proc. Zool. Soc. Lond. 121, 777–817.
Butler, P.M., 1956. The ontogeny of molar pattern. Biol. Rev. 31, 30–69.
Butler, P.M., 1973. Molar wear facets of Early Tertiary North American primates. In: Montagna, W., Zingeser, M.R. (Eds.), Craniofacial Biology of Primates. Karger, Basel, pp. 1–27.
Byrne, H., Rylands, A.B., Carneiro, J.C., Alfaro, J.W.L., Bertuol, F., da Silva, M.N.F., Messias, M., Groves, C.P., Mittermeier, R.A., Farias, I., Hrbek, T., Schneider, H., Sampaio, I., Boubli, J.P., 2016. Phylogenetic relationships of the New World titi monkeys (*Callicebus*): First appraisal of taxonomy based on molecular evidence. Front. Zool. 13, 10.
Chai, H., Lee, J.J.-W., Constantino, P.J., Lucas, P.W., Lawn, B.R., 2009. Remarkable resilience of teeth. Proc. Natl. Acad. Sci. USA 106, 7289–7293.
Cignoni, P., Callieri, M., Corsini, M., Dellepiane, M., Ganovelli, F., Ranzuglia, G., 2008. MeshLab: An open-source mesh processing tool. In: Scarano, V., De Chiara, R., Erra, U. (Eds.), Eurographics Italian Chapter Conference, Salerno, Italy, pp. 129–136.
Conroy, G.C., 1987. Problems of body-weight estimations in fossil primates. Int. J. Primatol. 8, 115–137.
Crompton, A.W., Hiiemäe, K.M., 1969. Functional occlusion in tribosphenic molars. Nature 222, 678–679.
Cuesta-Torralvo, E., Pacheco, D., Martínez, L.M., Romero, A., Umbelino, C., Avià, Y., Pérez-Pérez, A., 2021. Three-dimensional proxies to dental wear characterization in a known age-at-death skeletal collection. J. Archaeol. Method Theory 28, 1261–1275.
Cuozzo, F.P., Head, B.R., Sauther, M.L., Ungar, P.S., O'Mara, M.T., 2014. Sources of tooth wear variation early in life among known-aged wild ring-tailed lemurs (*Lemur catta*) at the Bezà Mahafaly Special Reserve, Madagascar. Am. J. Primatol. 76, 1037–1048.
Cuozzo, F.P., Sauther, M.L., 2006. Severe wear and tooth loss in wild ring-tailed lemurs (*Lemur catta*): A function of feeding ecology, dental structure, and individual life history. J. Hum. Evol. 51, 490–505.
Daegling, D.J., 1992. Mandibular morphology and diet in the genus *Cebus*. Int. J. Primatol. 13, 545–570.

Darnell, L.A., Teaford, M.F., Livi, K.J.T., Weihs, T.P., 2010. Variations in the mechanical properties of *Alouatta palliata* molar enamel. Am. J. Phys. Anthropol. 141, 7–15.
Davis, M., Pineda-Munoz, S., 2016. The temporal scale of diet and dietary proxies. Ecol. Evol. 6, 1883–1897.
DeLuycker, A.M., 2021. Diet and feeding ecology of the critically endangered San Martín titi monkey (*Plecturocebus oenanthe*) in Peru. Int. J. Primatol. https://doi.org/10.1007/s10764-021-00256-w.
Dennis, J.C., Ungar, P.S., Teaford, M.F., Glander, K.E., 2004. Dental topography and molar wear in *Alouatta palliata* from Costa Rica. Am. J. Phys. Anthropol. 125, 152–161.
Deutsch, A.R., Dickinson, E., Leonard, K.C., Pastor, F., Muchlinski, M.N., Hartstone-Rose, A., 2020. Scaling of anatomically derived maximal bite force in primates. Anat. Rec. 303, 2026–2035.
Dumont, E.R., 1995. Enamel thickness and dietary adaptation among extant primates and chiropterans. J. Mammal. 76, 1127–1136.
Elgart, A.A., 2010. Dental wear, wear rate, and dental disease in the African apes. Am. J. Primatol. 72, 481–491.
Evans, A.R., Hunter, J., Fortelius, M., Sanson, G.D., 2005. The scaling of tooth sharpness in mammals. Ann. Zool. Fenn. 42, 603–613.
Evans, A.R., Janis, C.M., 2014. The evolution of high dental complexity in the horse lineage. Ann. Zool. Fenn. BioOne 73–79.
Evans, A.R., Sanson, G.D., 1998. The effect of tooth shape on the breakdown of insects. J. Zool. 246, 391–400.
Evans, A.R., Wilson, G.P., Fortelius, M., Jernvall, J., 2007. High-level similarity of dentitions in carnivorans and rodents. Nature 445, 78–81.
Fiorenza, L., Harty, T., Janocha, M.M., Kullmer, O., Nguyen, H.N., Bortolini, E., Benazzi, S., 2022. Understanding dietary ecology in great apes from dental macrowear analysis. Am. J. Biol. Anthropol. 178, 605–616.
Fleagle, J.G., 1999. Primate Adaptation and Evolution, 2nd ed. Academic Press, New York.
Fleagle, J.G., Kay, R.F., 1985. The paleobiology of catarrhines. In: Delson, E. (Ed.), Ancestors: The Hard Evidence. Alan R. Liss, Inc., New York, pp. 23–36.
Fleagle, J.G., Kay, R.F., 1987. The phyletic position of the Parapithecidae. J. Hum. Evol. 16, 483–532.
Fleagle, J.G., Simons, E.L., 1982. The humerus of *Aegyptopithecus zeuxis*: A primitive anthropoid. Am. J. Phys. Anthropol. 59, 175–193.
Fleagle, J.G., Simons, E.L., 1995. Limb skeleton and locomotor adaptations of *Apidium phiomense*, an Oligocene anthropoid from Egypt. Am. J. Phys. Anthropol. 97, 235–289.
Fleagle, J.G., Simons, E.L., Conroy, G.C., 1975. Ape limb bone from the Oligocene of Egypt. Science 189, 135–137.
Fleagle, J.G., Kay, R.F., Simons, E.L., 1980. Sexual dimorphism in early anthropoids. Nature 287, 328–330.
Fortelius, M., 1985. Ungulate cheek teeth: Developmental, functional, and evolutionary interrelations. Acta Zool. Fenn. 180, 1–76.
Fortelius, M., Solounias, N., 2000. Functional characterization of ungulate molars using the abrasion-attrition wear gradient: A new method for reconstructing paleodiets. Am. Mus. Novit. New York NY 3301, 1–36.
Foster, F.R., Constantino, P.J., 2020. Macrowear and the mechanical behavior of enamel. In: Schmidt, C.W., Watson, J.T. (Eds.), Dental Wear in Evolutionary and Biocultural Contexts. Academic Press, pp. 73–97.
Fragaszy, D.M., Visalberghi, E., Fedigan, L.M., 2004. The Complete Capuchin: The Biology of the Genus *Cebus*. Cambridge University Press, New York.
Free, R., DeRocher, K., Cooley, V., Xu, R., Stock, S.R., Joester, D., 2022. Mesoscale structural gradients in human tooth enamel. Proc. Natl. Acad. Sci. USA 119, e2211285119.
Fulwood, E.L., Shan, S., Winchester, J.M., Gao, T., Kirveslahti, H., Daubechies, I., Boyer, D.M., 2021. Reconstructing dietary ecology of extinct strepsirrhines (Primates, Mammalia) with new approaches for characterizing and analyzing tooth shape. Paleobiology 47, 612–631.
Galbany, J., Altmann, J., Pérez-Pérez, A., Alberts, S.C., 2011. Age and individual foraging behavior predict tooth wear in Amboseli baboons. Am. J. Phys. Anthropol. 144, 51–59.
Galbany, J., Romero, A., Mayo-Alesón, M., Itsoma, F., Gamarra, B., Pérez-Pérez, A., Willaume, E., Kappeler, P.M., Charpentier, M.J.E., 2014. Age-related tooth wear differs between forest and savanna primates. PLoS One 9, e94938.
Galbany, J., Imanizabayo, O., Romero, A., Vecellio, V., Glowacka, H., Cranfield, M.R., Bromage, T.G., Mudakikwa, A., Stoinski, T.S., McFarlin, S.C., 2016. Tooth wear and feeding ecology in mountain gorillas from Volcanoes National Park, Rwanda. Am. J. Phys. Anthropol. 159, 457–465.
Galbany, J., Twahirwa, J.C., Baiges-Sotos, L., Kane, E.E., Tuyisingize, D., Kaleme, P., Rwetsiba, A., Bitariho, R., Cranfield, M.R., Bromage, T.G., Mudakikwa, A., Stoinski, T.S., Robbins, M.M., McFarlin, S.C., 2020. Dental macrowear in catarrhine primates: Variability across species. In: Schmidt, C.W., Watson, J.T. (Eds.), Dental Wear in Evolutionary and Biocultural Contexts. Academic Press, Cambridge, pp. 11–37.
Galetti, M., Pedroni, F., 1994. Seasonal diet of capuchin monkeys (*Cebus apella*) in a semideciduous forest in south-east Brazil. J. Trop. Ecol. 10, 27–39.
Gingerich, P.D., 1978. The Stuttgart collection of Oligocene primates from the Fayum province of Egypt. Paläontol. Z. 52, 82–92.
Glander, K.E., 1981. Feeding patterns in mantled howling monkeys. In: Kamil, A.C., Sargent, T.D. (Eds.), Foraging Behavior: Ecological, Ethological, and Psychological Approaches. Garland Press, New York, pp. 231–257.
Glowacka, H., McFarlin, S.C., Catlett, K.K., Mudakikwa, A., Bromage, T.G., Cranfield, M.R., Stoinski, T.S., Schwartz, G.T., 2016. Age-related changes in molar topography and shearing crest length in a wild population of mountain gorillas from Volcanoes National Park, Rwanda. Am. J. Phys. Anthropol. 160, 3–15.
Godfrey, L.R., Samonds, K.E., Jungers, W.L., Sutherland, M.R., 2001. Teeth, brains, and primate life histories. Am. J. Phys. Anthropol. 114, 192–214.
Godfrey, L.R., Winchester, J.M., King, S.J., Boyer, D.M., Jernvall, J., 2012. Dental topography indicates ecological contraction of lemur communities. Am. J. Phys. Anthropol. 148, 215–227.
González-Zamora, A., Arroyo-Rodríguez, V., Chaves, Ó.M., Sánchez-López, S., Stoner, K.E., Riba-Hernández, P., 2009. Diet of spider monkeys (*Ateles geoffroyi*) in Mesoamerica: Current knowledge and future directions. Am. J. Primatol. 71, 8–20.
Gregory, W.K., 1916. Studies on the evolution of the primates. Part I. The Cope-Osborn "Theory of Tritubercularity" and the ancestral molar patterns of the primates. Bull. Am. Mus. Nat. Hist. 35, 239–257.
Grine, F.E., Daegling, D.J., 2017. Functional morphology, biomechanics and the retrodiction of early hominin diets. C. R. Palevol 16, 613–631.
Grine, F.E., Ungar, P.S., Teaford, M.F., 2002. Error rates in dental microwear quantification using scanning electron microscopy. Scanning 24, 144–153.
Grine, F.E., Sponheimer, M., Ungar, P.S., Lee-Thorp, J., Teaford, M.F., 2012. Dental microwear and stable isotopes inform the paleoecology of extinct hominins. Am. J. Phys. Anthropol. 148, 285–317.
Hainsworth, S.V., Delaney, R.J., Rutty, G.N., 2008. How sharp is sharp? Towards quantification of the sharpness and penetration ability of kitchen knives used in stabbings. Int. J. Legal Med. 122, 281–291.
Harty, T., Berthaume, M.A., Bortolini, E., Evans, A.R., Galbany, J., Guy, F., Kullmer, O., Lazzari, V., Romero, A., Fiorenza, L., 2022. Dental macrowear reveals ecological diversity of *Gorilla* spp. Sci. Rep. 12, 9203.
Hespenheide, H.A., 1973. Ecological inferences from morphological data. Ann. Rev. Ecol. Syst. 4, 213–229.
Hunt, T.C., Grejtak, T., Kodangal, D., Varma, S., Rinaldi, C.E., Pathak, S., Krick, B.A., Erickson, G.M., 2023. Microstructurally driven self-sharpening mechanism in beaver incisor enamel facilitates their capacity to fell trees. Acta Biomater. 158, 412–422.
Jaeger, J.-J., Soe, U.A.N., Aung, U.A.K., Benammi, M., Chaimanee, Y., Ducrocq, R.-M., Tun, T., Thein, U.T., Ducrocq, S., 1998. New Myanmar middle Eocene anthropoids. An Asian origin for catarrhines? C. R. Acad. Sci. 321, 953–959.
Jaeger, J.-J., Beard, K.C., Chaimanee, Y., Salem, M., Benammi, M., Hlal, O., Coster, P., Bilal, A.A., Duringer, P., Schuster, M., Valentin, X., Marandat, B., Marivaux, L., Métais, E., Hammuda, O., Brunet, M., 2010. Late middle Eocene epoch of Libya yields earliest known radiation of African anthropoids. Nature 467, 1095–1098.
Janis, C.M., 1984. Prediction of primate diets from molar wear patterns. In: Chivers, D.J., Wood, B.A., Bilsborough, A. (Eds.), Food Acquisition and Processing in Primates. Springer, New York, pp. 331–340.
Janis, C.M., Fortelius, M., 1988. On the means whereby mammals achieve increased functional durability of their dentitions, with special reference to limiting factors. Biol. Rev. 63, 197–230.
Janzen, D.H., 1970. Herbivores and the number of tree species in tropical forests. Am. Nat. 104, 501–528.
Jernvall, J., Selänne, L., 1999. Laser confocal microscopy and geographic information systems in the study of dental morphology. Paleontol. Electron. 2, 1–18.
Jolly, C.J., 1970. The seed-eaters: A new model of hominid differentiation based on a baboon analogy. Man 5, 5–26.
Kay, R.F., 1975. The functional adaptations of primate molar teeth. Am. J. Phys. Anthropol. 43, 195–216.
Kay, R.F., 1977. The evolution of molar occlusion in Cercopithecidae and early catarrhines. Am. J. Phys. Anthropol. 46, 327–352.
Kay, R.F., 1981. The nut-crackers: A new theory of the adaptations of the Ramapithecinae. Am. J. Phys. Anthropol. 55, 141–152.
Kay, R.F., Cant, J.G.H., 1988. Age assessment using cementum annulus counts and tooth wear in a free-ranging population of *Macaca mulatta*. Am. J. Primatol. 15, 1–15.
Kay, R.F., Covert, H.H., 1984. Anatomy and behaviour of extinct primates. In: Chivers, D.J., Wood, B.A., Bilsborough, A. (Eds.), Food Acquisition and Processing in Primates. Plenum Press, New York, pp. 467–508.
Kay, R.F., Hiiemäe, K.M., 1974. Jaw movement and tooth use in recent and fossil primates. Am. J. Phys. Anthropol. 40, 227–256.
Kay, R.F., Kirk, E.C., 2000. Osteological evidence for the evolution of activity pattern and visual acuity in primates. Am. J. Phys. Anthropol. 113, 235–262.
Kay, R.F., Simons, E.L., 1980a. Comments on the adaptive strategy of the first African anthropoids. Z. Morphol. Anthropol. 71, 143–148.
Kay, R.F., Simons, E.L., 1980b. The ecology of Oligocene African Anthropoidea. Int. J. Primatol. 1, 21–37.
Kay, R.F., Simons, E.L., 1983. Dental formulae and dental eruption patterns in Parapithecidae (Primates, Anthropoidea). Am. J. Phys. Anthropol. 62, 363–375.
Kay, R.F., Fleagle, J.G., Simons, E.L., 1981. A revision of the African Oligocene apes of the Fayum Province, Egypt. Am. J. Phys. Anthropol. 55, 293–322.
Kay, R.F., Williams, B.A., Ross, C.F., Takai, M., Shigehara, N., 2004. Anthropoid origins: A phylogenetic analysis. In: Ross, C.F., Kay, R.F. (Eds.), Anthropoid Origins: New Visions. Kluwer/Plenum, New York, pp. 91–135.
Kay, R.F., Meldrum, D.J., Takai, M., 2013. Pitheciidae and other platyrrhine seed predators. In: Veiga, L.M., Barnett, A.A., Ferrari, S.F., Norconk, M.A. (Eds.), Evolutionary Biology and Conservation of Titis, Sakis and Uacaris. Cambridge University Press, Cambridge, pp. 3–12.
King, S.J., Arrigo-Nelson, S.J., Pochron, S.T., Semprebon, G.M., Godfrey, L.R., Wright, P.C., Jernval, J., 2005. Dental senescence in a long-lived primate links infant survival to rainfall. Proc. Natl. Acad. Sci. USA 102, 16579–16583.

Kinzey, W.G., 1992. Dietary and dental adaptations in the Pitheciinae. Am. J. Phys. Anthropol. 88, 499–514.
Kinzey, W.G., Norconk, M.A., 1990. Hardness as a basis of fruit choice in two sympatric primates. Am. J. Phys. Anthropol. 81, 5–15.
Kirk, E.C., Kay, R.F., 2004. The evolution of high visual acuity in the Anthropoidea. In: Ross, C.F., Kay, R.F. (Eds.), Anthropoid Origins: New Visions. Kluwer/Plenum Publishing, New York, pp. 539–602.
Kirk, E.C., Simons, E.L., 2001. Diet of fossil primates from the Fayum depression of Egypt: A quantitative analysis of molar shearing. J. Hum. Evol. 40, 203–229.
Klukkert, Z.S., Teaford, M.F., Ungar, P.S., 2012. A dental topographic analysis of chimpanzees. Am. J. Phys. Anthropol. 148, 276–284.
Kruskal, W.H., Wallis, W.A., 1952. Use of ranks in one-criterion variance analysis. J. Am. Stat. Assoc. 47, 583–621.
Kullmer, O., Benazzi, S., Fiorenza, L., Schulz, D., Bacso, S., Winzen, O., 2009. Occlusal fingerprint analysis: Quantification of tooth wear pattern. Am. J. Phys. Anthropol. 139, 600–605.
Kullmer, O., Menz, U., Fiorenza, L., 2020. Occlusal Fingerprint Analysis (OFA) reveals dental occlusal behavior in primate molars. In: Martin, T., von Koenigswald, W. (Eds.), Mammalian Teeth – Form and Function. Verlag, München, Germany, pp. 25–43.
Laird, M.F., Granatosky, M.C., Taylor, A.B., Ross, C.F., 2020. Muscle architecture dynamics modulate performance of the superficial anterior temporalis muscle during chewing in capuchins. Sci. Rep. 10, 6410.
Lanyon, J.M., Sanson, G.D., 1986. Koala (*Phascolarctos cinereus*) dentition and nutrition. II. Implications of tooth wear in nutrition. J. Zool. 209, 169–181.
Larsen, C.S., 2015. Masticatory and nonmasticatory functions: Craniofacial adaptation to mechanical loading. Bioarchaeology: Interpreting Behavior from the Human Skeleton, 2 ed. Cambridge University Press, Cambridge, pp. 256–300.
Leakey, M.G., Leakey, R.E., Richtsmeier, J.T., Simons, E.L., Walker, A.C., 1991. Similarities in *Aegyptopithecus* and *Afropithecus* facial morphology. Folia Primatol. 56, 65–85.
Ledogar, J.A., Winchester, J.M., St Clair, E.M., Boyer, D.M., 2013. Diet and dental topography in pitheciine seed predators. Am. J. Phys. Anthropol. 150, 107–121.
Li, P., Morse, P.E., Kay, R.F., 2020. Dental topographic change with macrowear and dietary inference in *Homunculus patagonicus*. J. Hum. Evol. 144, 102786.
López-Torres, S., Selig, K.R., Prufrock, K.A., Lin, D., Silcox, M.T., 2018. Dental topographic analysis of paromomyid (Plesiadapiformes, Primates) cheek teeth: More than 15 million years of changing surfaces and shifting ecologies. Hist. Biol. 30, 76–88.
Lucas, P.W., 2006. Dental Functional Morphology: How Teeth Work, 2nd ed. Cambridge University Press, Cambridge.
Lucas, P.W., Corlett, R.T., 1991. Relationship between the diet of *Macaca fascicularis* and forest phenology. Folia Primatol. 57, 201–215.
Lucas, P.W., Omar, R., 2012. New perspectives on tooth wear. Int. J. Dent. 2012, 1–6.
Lucas, P.W., Teaford, M.F., 1994. Functional morphology of colobine teeth. In: Davies, A.G., Oates, J.F. (Eds.), Colobine Monkeys: Their Ecology, Behaviour and Evolution. Cambridge University Press, Cambridge, UK, pp. 173–203.
Lucas, P.W., Constantino, P., Wood, B.A., Lawn, B., 2008. Dental enamel as a dietary indicator in mammals. BioEssays 30, 374–385.
Lucas, P.W., Omar, R., Al-Fadhalah, K., Almusallam, A.S., Henry, A.G., Michael, S., Thai, L.A., Watzke, J., Strait, D.S., Atkins, A.G., 2013. Mechanisms and causes of wear in tooth enamel: Implications for hominin diets. J. R. Soc. Interface 10, 20120923.
M'Kirera, F., Ungar, P.S., 2003. Occlusal relief changes with molar wear in *Pan troglodytes troglodytes* and *Gorilla gorilla gorilla*. Am. J. Primatol. 60, 31–41.
Maas, M.C., 1993. Enamel microstructure and molar wear in the greater galago, *Otolemur crassicaudatus* (mammalia, primates). Am. J. Phys. Anthropol. 92, 217–233.
Maas, M.C., Dumont, E.R., 1999. Built to last: The structure, function, and evolution of primate dental enamel. Evol. Anthropol. 8, 133–152.
Macho, G.A., 2001. Primate molar crown formation times and life history evolution revisited. Am. J. Primatol. 55, 189–201.
Martin, L.B., Olejniczak, A.J., Maas, M.C., 2003. Enamel thickness and microstructure in pitheciin primates, with comments on dietary adaptations of the middle Miocene hominoid *Kenyapithecus*. J. Hum. Evol. 45, 351–367.
McGraw, W.S., Pampush, J.D., Daegling, D.J., 2012. Brief communication: Enamel thickness and durophagy in mangabeys revisited. Am. J. Phys. Anthropol. 147, 326–333.
Melstrom, K.M., Wistort, Z.P., 2021. The application of dental complexity metrics on extant saurians. Herpetologica 77, 279–288.
Mihlbachler, M.C., Rusnack, F., Beatty, B.L., 2022. Experimental approaches to assess the effect of composition of abrasives in the cause of dental microwear. R. Soc. Open Sci. 9, 211549.
Miller, E.R., Simons, E.L., 1997. Dentition of *Proteopithecus sylviae*, an archaic anthropoid from the Fayum, Egypt. Proc. Natl. Acad. Sci. USA 94, 13760–13764.
Miller, E.R., Gunnell, G.F., Martin, R.D., 2005. Deep time and the search for anthropoid origins. Yearb. Phys. Anthropol. 48, 60–95.
Miller, E.R., Benefit, B.R., McCrossin, M.L., Plavcan, J.M., Leakey, M.G., El-Barkooky, A.N., Hamdan, M.A., Abdel Gawad, M.K., Hassan, M.S.H., Simons, E.L., 2009. Systematics of early and middle Miocene Old World monkeys. J. Hum. Evol. 57, 195–211.
Miller, E.R., Gunnell, G.F., Seiffert, E.R., Sallam, H., Schwartz, G.T., 2018. Patterns of dental emergence in early anthropoid primates from the Fayum Depression, Egypt. Hist. Biol. 30, 157–165.
Millette, J.B., Sauther, M.L., Cuozzo, F.P., 2009. Behavioral responses to tooth loss in wild ring-tailed lemurs (*Lemur catta*) at the Beza Mahafaly Special Reserve, Madagascar. Am. J. Phys. Anthropol. 140, 120–134.
Molnar, S., 1971. Human tooth wear, tooth function and cultural variability. Am. J. Phys. Anthropol. 34, 175–189.
Molnar, S., Gantt, D.G., 1977. Functional implications of primate enamel thickness. Am. J. Phys. Anthropol. 46, 447–454.
Morse, P.E., Daegling, D.J., McGraw, W.S., Pampush, J.D., 2013. Dental wear among cercopithecid monkeys of the Taï forest, Côte d'Ivoire. Am. J. Phys. Anthropol. 150, 655–665.
Morse, P.E., Pampush, J.D., Kay, R.F., 2019. Junk DNE: How surface simplification and scanning resolution affect measures of dental crown sharpness. Am. J. Phys. Anthropol. 168, 169.
Napier, J.R., Napier, P.H. (Eds.), 1970. Old World Monkeys: Evolution, Systematics and Behavior. Academic Press, New York.
Olejniczak, A.J., Tafforeau, P., Feeney, R.N.M., Martin, L.B., 2008. Three-dimensional primate molar enamel thickness. J. Hum. Evol. 54, 187–195.
Osborn, H.F., 1908. New fossil mammals from the Fayûm Oligocene, Egypt. Bull. Am. Mus. Nat. Hist. 24, 265–272.
Pampush, J.D., Duque, A.C., Burrows, B.R., Daegling, D.J., Kenney, W.F., McGraw, W.S., 2013. Homoplasy and thick enamel in primates. J. Hum. Evol. 64, 216–224.
Pampush, J.D., Spradley, J.P., Morse, P.E., Harrington, A.R., Allen, K.L., Boyer, D.M., Kay, R.F., 2016a. Wear and its effects on dental topography measures in howling monkeys (*Alouatta palliata*). Am. J. Phys. Anthropol. 161, 705–721.
Pampush, J.D., Winchester, J.M., Morse, P.E., Vining, A.Q., Boyer, D.M., Kay, R.F., 2016b. Introducing molaR: A new R package for quantitative topographic analysis of teeth (and other topographic surfaces). J. Mammal. Evol. 23, 397–412.
Pampush, J.D., Spradley, J.P., Morse, P.E., Griffith, D., Gladman, J.T., Gonzales, L.A., Kay, R.F., 2018. Adaptive wear-based changes in dental topography associated with atelid (Mammalia: Primates) diets. Biol. J. Linn. Soc. 124, 584–606.
Pampush, J.D., Crowell, J., Karme, A., Macrae, S.A., Kay, R.F., Ungar, P.S., 2019. Comparing dental topography software using platyrrhine molars. Am. J. Phys. Anthropol. 169, 179–185.
Pampush, J.D., Morse, P.E., Fuselier, E.J., Skinner, M.M., Kay, R.F., 2022. Sign-oriented Dirichlet normal energy: Aligning dental topography and dental function in the R-package molaR. J. Mammal. Evol. 29, 713–732.
Peres, C.A., 1991. Seed predation of *Cariniana micrantha* (Lecythidaceae) by brown capuchin monkeys in Central Amazônia. Biotropica 23, 262–270.
Perry, J.M.G., Cooke, S.B., Runestad Connour, J.A., Burgess, M.L., Ruff, C.B., 2018. Articular scaling and body mass estimation in platyrrhines and catarrhines: Modern variation and application to fossil anthropoids. J. Hum. Evol. 115, 20–35.
Peterson, R.A., Cavanaugh, J.E., 2020. Ordered quantile normalization: A semi-parametric transformation built for the cross-validation era. J. Appl. Stat. 47, 2312–2327.
Pineda-Munoz, S., Lazagabaster, I.A., Alroy, J., Evans, A.R., 2017. Inferring diet from dental morphology in terrestrial mammals. Methods Ecol. Evol. 8, 481–491.
Polly, P.D., Mock, O.B., 2018. Heritability: The link between development and the microevolution of molar tooth form. Hist. Biol. 30, 53–63.
Popowics, T.E., Fortelius, M., 1997. On the cutting edge: Tooth blade sharpness in herbivorous and faunivorous mammals. Ann. Zool. Fenn. 34, 73–88.
Prufrock, K.A., Boyer, D.M., Silcox, M.T., 2016a. The first major primate extinction: An evaluation of paleoecological dynamics of North American stem primates using a homology free measure of tooth shape. Am. J. Phys. Anthropol. 159, 683–697.
Prufrock, K.A., López-Torres, S., Silcox, M.T., Boyer, D.M., 2016b. Surfaces and spaces: Troubleshooting the study of dietary niche space overlap between North American stem primates and rodents. Surf. Topogr. Metrol. Prop. 4, 024005.
R Core Team, 2022. R: A language and environment for statistical computing. R Foundation for Statistical Computing, Vienna.
Randimbiharinirina, D.R., Raharivololona, B.M., Hawkins, M.T.R., Frasier, C.L., Culligan, R.R., Sefczek, T.M., Randriamampionona, R., Louis, E.E., 2018. Behaviour and ecology of male aye-ayes (*Daubentonia madagascariensis*) in the Kianjavato Classified Forest, south-eastern Madagascar. Folia Primatol. 89, 123–137.
Rasmussen, D.T., Simons, E.L., 1992. Paleobiology of the oligopithecines, the earliest known anthropoid primates. Int. J. Primatol. 13, 477–508.
Rasmussen, D.T., Friscia, A.R., Gutierrez, M., Kappelman, J., Miller, E.R., Muteti, S., Reynoso, D., Rossie, J.B., Spell, T.L., Tabor, N.J., Gierlowski-Kordesch, E., Jacobs, B.F., Kyongo, B., Macharwas, M., Muchemi, F., 2019. Primitive Old World monkey from the earliest Miocene of Kenya and the evolution of cercopithecoid bilophodonty. Proc. Natl. Acad. Sci. USA 116, 6051–6056.
Rensberger, J.M., 2000. Pathways to functional differentiation in mammalian enamel. In: Teaford, M.F., Ferguson, M.W.J., Meredith Smith, M. (Eds.), Development, Function and Evolution of Teeth. Cambridge University Press, Cambridge, pp. 252–268.
Robinson, Beren W., Wilson, David S., 1998. Optimal foraging, specialization, and a solution to Liem's paradox. Am. Nat. 151, 223–235.
Russo, S.E., Campbell, C.J., Dew, J.L., Stevenson, P.R., Suarez, S.A., 2005. A multi-forest comparison of dietary preferences and seed dispersal by *Ateles* spp. Int. J. Primatol. 26, 1017–1037.
Schindelin, J., Arganda-Carreras, I., Frise, E., Kaynig, V., Longair, M., Pietzsch, T., Preibisch, S., Rueden, C., Saalfeld, S., Schmid, B., Tinevez, J.-Y., White, D.J., Hartenstein, V., Eliceiri, K., Tomancak, P., Cardona, A., 2012. Fiji: An open-source platform for biological-image analysis. Nat. Methods 9, 676–682.

Schlosser, M., 1910. Über einige fossile Säugetiere aus dem Oligocän von Ägypten. Zool. Anz. 35, 500–508.
Scott, E.C., 1979. Dental wear scoring technique. Am. J. Phys. Anthropol. 51, 213–217.
Scott, R.S., Ungar, P.S., Bergstrom, T.S., Brown, C.A., Childs, B.E., Teaford, M.F., Walker, A., 2006. Dental microwear texture analysis: Technical considerations. J. Hum. Evol. 51, 339–349.
Scott, R.S., Teaford, M.F., Ungar, P.S., 2012. Dental microwear texture and anthropoid diets. Am. J. Phys. Anthropol. 147, 551–579.
Seiffert, E.R., 2006. Revised age estimates for the later Paleogene mammal faunas of Egypt and Oman. Proc. Natl. Acad. Sci. USA 103, 5000–5005.
Seiffert, E.R., 2007. Evolution and extinction of Afro-Arabian primates near the Eocene-Oligocene boundary. Folia Primatol. 78, 314–327.
Seiffert, E.R., 2012. Early primate evolution in Afro-Arabia. Evol. Anthropol. 21, 239–253.
Seiffert, E.R., Simons, E.L., 2001. Astragalar morphology of late Eocene anthropoids from the Fayum Depression (Egypt) and the origin of catarrhine primates. J. Hum. Evol. 41, 577–606.
Seiffert, E.R., Simons, E.L., Clyde, W.C., Rossie, J.B., Attia, Y., Bown, T.M., Chatrath, P., Mathison, M.E., 2005. Basal anthropoids from Egypt and the antiquity of Africa's higher primate radiation. Science 310, 300–304.
Seiffert, E.R., Simons, E.L., Boyer, D.M., Perry, J.M.G., Ryan, T.M., Sallam, H.M., 2010. A fossil primate of uncertain affinities from the earliest late Eocene of Egypt. Proc. Natl. Acad. Sci. USA 107, 9712–9717.
Seiffert, E.R., Tejedor, M.F., Fleagle, J.G., Novo, N.M., Cornejo, F.M., Bond, M., de Vries, D., Campbell, K.E., 2020. A parapithecid stem anthropoid of African origin in the Paleogene of South America. Science 368, 194–197.
Selig, K.R., Sargis, E.J., Silcox, M.T., 2019. The frugivorous insectivores? Functional morphological analysis of molar topography for inferring diet in extant treeshrews (Scandentia). J. Mammal. 100, 1901–1917.
Selig, K.R., Khalid, W., Silcox, M.T., 2021. Mammalian molar complexity follows simple, predictable patterns. Proc. Natl. Acad. Sci. USA 118, e2008850118.
Shapiro, S.S., Wilk, M.B., 1965. An analysis of variance test for normality (complete samples). Biometrika 52, 591–611.
Shellis, R.P., Beynon, A.D., Reid, D.J., Hiiemae, K.M., 1998. Variations in molar enamel thickness among primates. J. Hum. Evol. 35, 507–522.
Shimizu, D., Macho, G.A., Spears, I.R., 2005. Effect of prism orientation and loading direction on contact stresses in prismatic enamel of primates: Implications for interpreting wear patterns. Am. J. Phys. Anthropol. 126, 427–434.
Simons, E.L., 1962. Two new primate species from the African Oligocene. Postilla 64, 1–12.
Simons, E.L., 1965. New fossil apes from Egypt and the initial differentiation of Hominoidea. Nature 205, 135–139.
Simons, E.L., 1971. Relationships of *Amphipithecus* and *Oligopithecus*. Nature 232, 489–491.
Simons, E.L., 1974. *Parapithecus grangeri* (Parapithecoidea, Old World Higher Primates): New species from the Oligocene of Egypt and the initial differentiation of the Cercopithecoidea. Postilla Yale Peabody Museum 166, 1–12.
Simons, E.L., 1987. New faces of *Aegyptopithecus* from the Oligocene of Egypt. J. Hum. Evol. 16, 273–289.
Simons, E.L., 1995. Crania of *Apidium*: Primitive Anthropoidean (Primates, Parapithecidae) from the Egyptian Oligocene, vol. 3124. Am. Mus. Novit., New York NY, pp. 1–10.
Simons, E.L., 2001. The cranium of *Parapithecus grangeri*, an Egyptian Oligocene anthropoidean primate. Proc. Natl. Acad. Sci. USA 98, 7892–7897.
Simons, E.L., Bown, T.M., 1985. *Afrotarsius chatrathi*, first tarsiiform primate (? Tarsiidae) from Africa. Nature 313, 475–477.
Simons, E.L., Kay, R.F., 1983. *Qatrania*, new basal anthropoid primate from the Fayum, Oligocene of Egypt. Nature 304, 624–626.
Simons, E.L., Seiffert, E.R., Ryan, T.M., Attia, Y., 2007. A remarkable female cranium of the early Oligocene anthropoid *Aegyptopithecus zeuxis* (Catarrhini, Propliopithecidae). Proc. Natl. Acad. Sci. USA 104, 8731–8736.
Simpson, G.G., 1944. Tempo and Mode in Evolution. Columbia University Press, New York.
Smith, R.J., Jungers, W.L., 1997. Body mass in comparative primatology. J. Hum. Evol. 32, 523–559.
Spencer, M.A., 1998. Force production in the primate masticatory system: Electromyographic tests of biomechanical hypotheses. J. Hum. Evol. 34, 25–54.
Spradley, J.P., Glander, K.E., Kay, R.F., 2016. Dust in the wind: How climate variables and volcanic dust affect rates of tooth wear in Central American howling monkeys. Am. J. Phys. Anthropol. 159, 210–222.
Spradley, J.P., Pampush, J.D., Morse, P.E., Kay, R.F., 2017. Smooth operator: The effects of different 3D mesh retriangulation protocols on the computation of Dirichlet normal energy. Am. J. Phys. Anthropol. 163, 94–109.
Stevens, N.J., Seiffert, E.R., O'Connor, P.M., Roberts, E.M., Schmitz, M.D., Krause, C., Gorscak, E., Ngasala, S., Hieronymus, T.L., Temu, J., 2013. Palaeontological evidence for an Oligocene divergence between Old World monkeys and apes. Nature 497, 611–614.
Stirton, R.A., 1947. Observations on evolutionary rates in hypsodonty. Evolution 1, 32–41.
Taylor, A.B., Vinyard, C.J., 2009. Jaw-muscle fiber architecture in tufted capuchins favors generating relatively large muscle forces without compromising jaw gape. J. Hum. Evol. 57, 710–720.
Teaford, M.F., 1982. Differences in molar wear gradient between juvenile macaques and langurs. Am. J. Phys. Anthropol. 57, 323–330.
Teaford, M.F., 1985. Molar microwear and diet in the genus *Cebus*. Am. J. Phys. Anthropol. 66, 363–370.
Teaford, M.F., 1994. Dental microwear and dental function. Evol. Anthropol. 3, 17–30.
Teaford, M.F., Oyen, O.J., 1989a. In vivo and in vitro turnover in dental microwear. Am. J. Phys. Anthropol. 80, 447–460.
Teaford, M.F., Oyen, O.J., 1989b. Differences in the rate of molar wear between monkeys raised on different diets. J. Dent. Res. 68, 1513–1518.
Teaford, M.F., Runestad, J.A., 1992. Dental microwear and diet in Venezuelan primates. Am. J. Phys. Anthropol. 88, 347–364.
Teaford, M.F., Walker, A., 1984. Quantitative differences in dental microwear between primate species with different diets and a comment on the presumed diet of *Sivapithecus*. Am. J. Phys. Anthropol. 64, 191–200.
Teaford, M.F., Maas, M.C., Simons, E.L., 1996. Dental microwear and microstructure in early Oligocene primates from the Fayum, Egypt: Implications for diet. Am. J. Phys. Anthropol. 101, 527–543.
Teaford, M.F., Ungar, P.S., Taylor, A.B., Ross, C.F., Vinyard, C.J., 2017. *In vivo* rates of dental microwear formation in laboratory primates fed different food items. Biosurf. Biotribol. 3, 166–173.
Teaford, M.F., Ungar, P.S., Taylor, A.B., Ross, C.F., Vinyard, C.J., 2020. The dental microwear of hard-object feeding in laboratory *Sapajus apella* and its implications for dental microwear formation. Am. J. Phys. Anthropol. 171, 439–455.
Teaford, M.F., Ross, C.F., Ungar, P.S., Vinyard, C.J., Laird, M.F., 2021. Grit your teeth and chew your food: Implications of food material properties and abrasives for rates of dental microwear formation in laboratory *Sapajus apella* (Primates). Palaeogeogr. Palaeoclimatol. Palaeoecol. 583, 110644.
Temerin, L.A., Cant, J.G.H., 1983. The evolutionary divergence of Old World monkeys and apes. Am. Nat. 122, 335–351.
Terborgh, J., 1983. Five New World Primates: A Study in Comparative Ecology. Princeton University Press, Princeton.
Thiery, G., Gibert, C., Guy, F., Lazzari, V., Geraads, D., Spassov, N., Merceron, G., 2021. From leaves to seeds? The dietary shift in late Miocene colobine monkeys of southeastern Europe. Evolution 75, 1983–1997.
Thiery, G., Gillet, G., Lazzari, V., Merceron, G., Guy, F., 2017a. Was *Mesopithecus* a seed eating colobine? Assessment of cracking, grinding and shearing ability using dental topography. J. Hum. Evol. 112, 79–92.
Thiery, G., Lazzari, V., Ramdarshan, A., Guy, F., 2017b. Beyond the map: Enamel distribution characterized from 3D dental topography. Front. Physiol. 8, 524.
Thiery, G., Guy, F., Lazzari, V., 2019. A comparison of relief estimates used in three-dimensional dental topography. Am. J. Phys. Anthropol. 170, 260–274.
Ungar, P.S., 1995. A semiautomated image analysis procedure for the quantification of dental microwear II. Scanning 17, 57–59.
Ungar, P.S., 2004. Dental topography and diets of *Australopithecus afarensis* and early *Homo*. J. Hum. Evol. 46, 605–622.
Ungar, P.S., 2015. Mammalian dental function and wear: A review. Biosurf. Biotribol. 1, 25–41.
Ungar, P.S., M'Kirera, F., 2003. A solution to the worn tooth conundrum in primate functional anatomy. Proc. Natl. Acad. Sci. USA 100, 3874–3877.
Ungar, P.S., Sponheimer, M., 2011. The diets of early hominins. Science 334, 190–193.
Ungar, P.S., Williamson, M.D., 2000. Exploring the effects of tooth wear on functional morphology: A preliminary study using dental topographic analysis. Paleontol. Electron. 3, 1–18.
Ungar, P.S., Hartgrove, C.L., Wimberly, A.N., Teaford, M.F., 2017. Dental topography and microwear texture in *Sapajus apella*. Biosurf. Biotribol. 3, 124–134.
Ungar, P.S., Healy, C., Karme, A., Teaford, M.F., Fortelius, M., 2018. Dental topography and diets of platyrrhine primates. Hist. Biol. 30, 64–75.
van Casteren, A., Strait, D.S., Swain, M.V., Michael, S., Thai, L.A., Philip, S.M., Saji, S., Al-Fadhalah, K., Almusallam, A.S., Shekeban, A., McGraw, W.S., Kane, E.E., Wright, B.W., Lucas, P.W., 2020. Hard plant tissues do not contribute meaningfully to dental microwear: Evolutionary implications. Sci. Rep. 10, 582.
Van Roosmalen, G.M., Mittermeier, R.A., Fleagle, J.G., 1988. Diet of the Northern Bearded Saki (*Chiropotes satanas chiropotes*): A neotropical seed predator. Am. J. Primatol. 14, 11–35.
Van Valen, L., 1960. A functional index of hypsodonty. Evolution 14, 531–532.
Vogel, E.R., van Woerden, J.T., Lucas, P.W., Utami Atmoko, S.S., van Schaik, C.P., Dominy, N.J., 2008. Functional ecology and evolution of hominoid molar enamel thickness: *Pan troglodytes schweinfurthii* and *Pongo pygmaeus wurmbii*. J. Hum. Evol. 55, 60–74.
Vogel, E.R., Zulfa, A., Hardus, M., Wich, S.A., Dominy, N.J., Taylor, A.B., 2014. Food mechanical properties, feeding ecology, and the mandibular morphology of wild orangutans. J. Hum. Evol. 75, 110–124.
von Koenigswald, W., Rensberger, J.M., Pretzschner, H.U., 1987. Changes in the tooth enamel of early Paleocene mammals allowing increased diet diversity. Nature 328, 150–152.
Walker, A., 1981. Diet and teeth: Dietary hypotheses and human evolution. Philos. Trans. R. Soc. Lond. B Biol. Sci. 292, 57–64.
Watts, D.P., Potts, K.B., Lwanga, J.S., Mitani, J.C., 2012. Diet of chimpanzees (*Pan troglodytes schweinfurthii*) at Ngogo, Kibale National Park, Uganda, 1. Diet composition and diversity. Am. J. Primatol. 74, 114–129.
Williams, S.H., Kay, R.F., 2001. A comparative test of adaptive explanations for hypsodonty in ungulates and rodents. J. Mammal. Evol. 8, 207–229.
Williamson, L., Lucas, P.W., 1995. The effect of moisture content on the mechanical properties of a seed shell. J. Mater. Sci. 30, 162–166.
Wilson, G.P., Evans, A.R., Corfe, I.J., Smits, P.D., Fortelius, M., Jernvall, J., 2012. Adaptive radiation of multituberculate mammals before the extinction of dinosaurs. Nature 483, 457–460.

Winchester, J.M., 2016. MorphoTester: An open source application for morphological topographic analysis. PLoS One 11, e0147649.
Winchester, J.M., Boyer, D.M., St Clair, E.M., Gosselin-Ildari, A.D., Cooke, S.B., Ledogar, J.A., 2014. Dental topography of platyrrhines and prosimians: Convergence and contrasts. Am. J. Phys. Anthropol. 153, 29–44.
Wrangham, R.W., Conklin, N.L., Chapman, C.A., Hunt, K.D., 1991. The significance of fibrous foods for Kibale Forest chimpanzees. Philos. Trans. R. Soc. B Biol. Sci. 334, 171–178.
Wright, B.W., 2005. Craniodental biomechanics and dietary toughness in the genus *Cebus*. J. Hum. Evol. 48, 473–492.
Yamashita, N., Cuozzo, F.P., Sauther, M.L., Fitzgerald, E., Riemenschneider, A., Ungar, P.S., 2016. Mechanical food properties and dental topography differentiate three populations of *Lemur catta* in southwest Madagascar. J. Hum. Evol. 98, 66–75.
Yang, D., Bharatiya, M., Grine, F.E., 2022. Hunter-Schreger Band configuration in human molars reveals more decussation in the lateral enamel of 'functional' cusps than 'guiding' cusps. Arch. Oral Biol. 142, 105524.
Zachos, J.C., Pagani, M., Sloan, L., Thomas, E., Billups, K., 2001. Trends, rhythms, and aberrations in global climate 65 Ma to present. Science 292, 686–693.
Zanolli, C., Bayle, P., Bondioli, L., Dean, M.C., Le Luyer, M., Mazurier, A., Morita, W., Macchiarelli, R., 2017. Is the deciduous/permanent molar enamel thickness ratio a taxon-specific indicator in extant and extinct hominids? C. R. Palevol 16, 702–714.
Zelentsov, V.B., Sadyrin, E.V., Mitrin, B.I., Swain, M.V., 2023. Mathematical tools for recovery of the load on the fissure according to the micro-CT results. J. Mech. Behav. Biomed. Mater. 138, 105625.
Zuccotti, L.F., Williamson, M.D., Limp, W.F., Ungar, P.S., 1998. Modeling primate occlusal topography using geographic information systems technology. Am. J. Phys. Anthropol. 107, 137–142.